Toward an improved understanding of the global biogeochemical cycle of mercury

Toward an improved understanding of the global biogeochemical cycle of mercury

A dissertation presented

by

Helen Marie Amos

to

The Department of Earth and Planetary Sciences

in partial fulfillment of the requirements

for the degree of

Doctor of Philosophy

in the subject of

Earth and Planetary Sciences

Harvard University

Cambridge, Massachusetts

May 2014

Dissertation Advisors: Professors Daniel Jacob & Elsie Sunderland Helen Marie Amos

Toward an improved understanding of the global biogeochemical cycle of mercury

Abstract

Mercury (Hg) is a potent neurotoxin, has both natural and anthropogenic sources to the environment, and is globally dispersed. Humans have been using Hg since antiquity and continue its use in large quantities, mobilizing Hg from stable long-lived geologic reservoirs to actively cycling surface terrestrial and aquatic ecosystems. Human activities, such as mining and coal combustion, have perturbed the natural biogeochemical cycle of Hg. However, the distribution of natural versus anthropogenic Hg in the environment today and the extent of anthropogenic perturbation (i.e., enrichment) are uncertain. Previous model estimates of anthropogenic enrichment have been limited by a lack of information about historical emissions, examined only near-term effects, or have not accounted for the full coupling between biogeochemical reservoirs. Presented here is a framework that integrates recently available historical emission inventories and overcomes these barriers, providing an improved quantitative understanding of global Hg cycling.

This dissertation aims to advance our understanding of the global biogeochemical cycle of Hg by synthesizing observations together with state-of-the-science global Hg models. The objectives of this work are: (1) Develop an empirical relationship for gas-particle partitioning of atmospheric Hg and quantify the impact on global Hg deposition; (2) quantify the present-day enrichment of Hg levels in the ocean, atmosphere, and terrestrial ecosystems resulting from all-time anthropogenic emissions; and

(3) explore the impact of riverine discharges of Hg on the marine environment and the biogeochemical implications of burial of riverine Hg in ocean margin sediments.

The first dissertation chapter concludes that atmospheric Hg partitions between gas and particle-phases as a function of temperature and that inclusion of this process improves our ability to simulate observed deposition. In the second chapter, global anthropogenic enrichment is shown to be larger than previously estimated. It is also found that the legacy of past anthropogenic emissions plays a central role in influencing future trajectories of environmental Hg concentrations. Lastly, it is demonstrated that although coastal waters occupy only a few percent of the ocean surface, the effect of Hg burial in sediments at ocean margins propagates globally and affects anthropogenic Hg enrichment in all geochemical reservoirs.

Table of Contents

Appendix

List of Tables

List of Figures

Acknowledgements:

First and foremost I would like to thank my PhD advisors, Daniel Jacob and Elsie Sunderland, whose guidance has been fundamental in shaping me as a scientist. Each is unique in their approach to advising and I have learned so much from both. I have nothing but the most genuine gratitude for the many hours they have dedicated to challenging, discussing, and improving the body of work that has gone into this dissertation.

The work here was also made possible by the many generous collaborators, co-authors, and members of Harvard who have provided observations, code, critical feedback, and thoughtful discussion. Alphabetically, this includes: Mark Brigham, Claire Carouge, Long Chen, Bess Corbitt, Steph Dutkeiwcz, Eric Edgerton, Jenny Fisher, Elisabeth Galarneau, Amanda Giang, Jenny Graydon, Mae Gustin, Chris Holmes, Ian Hedgecock, Hannah Horowitz, Milena Horvat, Dan Jaffe, Oliver Jahn, Christoph Keller, David Kocman, Dave Krabbenhoft, Carl Lamborg, Leonard Levin, Miling Li, Mike Long, Rob Mason, Lee Murray, Daniel Obrist, Melissa Payer, Asif Quereshi, Andy Rutter, Amina Schartup, Noelle Selin, Anne Soerensen, Shaojie Song, Jeroen Sonke, Sandy Steffen, Vince St. Louis, David Streets, Ruoyu Sun, Bob Talbot, Chad Vecitis, Qiaoqiao Wang, Peter Weiss-Penzias, Simon Wilson, Melanie Witt, Bob Yantosca, Lin Zhang, and Yanxu Zhang.

Thank you to the Harvard Atmospheric Chemistry Modeling Group and Department of Earth and Planetary Sciences for bringing me into your communities. Your spirit and support has defined my time at Harvard. It has been a privilege.

Thank you Sarah Colgan, Brenda Matheiu, Chenoweth Moffat, Cindy Marsh, Maryorie Grande, Bridget Mastandrea, Isabelle Altman, and Alice Smythe for making the administration of this whole operation happen. I would also like to express my gratitude to the American Metrological Society, NASA Earth & Space Science Program, and National Science Foundation for funding my dissertation work.

Lastly, I would like to thank my friends and family for all their help along the way and for keeping me sane. An enormous thanks goes to my sisters, Emily and Grace, for their unflinching support. Thank you Christoph for your companionship day in and day out. The sun shines a little brighter when you're around.

This thesis is dedicated to my grandparents, Doug and Nancy Morningstar, whose generosity has made so many educational opportunities possible.

Chapter 1. Overview

Mercury (Hg) poses a global threat to human and wildlife health due to its toxicity and ubiquitous presence in the environment. Humans have used and released Hg to the environment for millennia [*Cooke et al*., 2009], resulting in an enrichment of terrestrial and aquatic ecosystems globally. Hg is distributed globally through long-range atmospheric transport [*Swartzendruber et al.*, 2006; *Corbitt et al*., 2011] and large-scale oceanographic circulation [*Sunderland et al.,* 2009]. Continued anthropogenic releases of Hg from activities such as coal combustion is worrisome because modern background levels are already close to toxicological thresholds [*Scheuhammer et al.*, 2007]. Anthropogenic enrichment in the oceans is of particular concern because Hg exposure for many human populations is through consumption of marine fish [*Johansen et al.*, 2004; *Sunderland*, 2007; *Kim et al.,* 2010]. Determining the current distributions of anthropogenic and natural Hg in the environment requires knowledge of the past history of anthropogenic Hg releases as well as understanding of Hg cycling within and between the ocean, atmosphere, and terrestrial ecosystems. The work presented in this dissertation aims to collectively improve the understanding of global Hg cycling by addressing three major themes: (1) the effect of gas-particle on partitioning global atmospheric Hg deposition; (2) the extent of anthropogenic enrichment in the present-day global biogeochemical cycle of Hg as a result of all-time anthropogenic emissions; and (3) the impact of rivers and burial in ocean margin sediments on Hg trends the marine environment and on Hg biogeochemical cycling.

Atmospheric deposition of Hg(II) represents a major input of Hg to surface environments. The phase of Hg(II) (gas or particle) has important implications for deposition. Here I use long-term observations of reactive gaseous mercury (RGM, the gaseous component of Hg(II)), particle-bound

mercury (PBM, the particulate component of Hg(II)), fine particulate matter ($PM_{2.5}$), and temperature (T) at five sites in North America to derive an empirical gas-particle partitioning relationship. I implement this empirical relationship in the GEOS-Chem global 3-D Hg model to partition Hg(II) between the gas and particle phases. The resulting gas-phase fraction of Hg(II) ranges from over 90% in warm air with little aerosol to less than 10% in cold air with high aerosol. Model comparison to Hg observations at the North American surface sites suggests that subsidence from the free troposphere (warm air, low aerosol) is a major factor driving the seasonality of RGM, while elevated PBM is mostly associated with high aerosol loads. Simulation of RGM and PBM at these sites is improved by including fast in-plume reduction of Hg(II) emitted from coal combustion and by assuming that anthropogenic particulate Hg(P) behaves as semi-volatile Hg(II) rather than as a refractory particulate component. The simulation of Hg wet deposition fluxes in the US is also improve relative to a previous version of GEOS-Chem; this largely reflects updates made to the washout algorithm. The observed wintertime minimum in wet deposition fluxes is attributed to inefficient snow scavenging of gas-phase Hg(II).

Second, I present a global biogeochemical model with fully coupled atmospheric, terrestrial and oceanic Hg reservoirs to better understand human influence on Hg cycling and timescales for responses. The model is driven with a historical inventory of anthropogenic emissions from 2000 BC to present. Results show that anthropogenic perturbations introduced to surface reservoirs (atmosphere, ocean, or terrestrial) accumulate and persist in the subsurface ocean for decades to centuries. The simulated present-day atmosphere is enriched by a factor of 2.6 relative to 1840 levels, consistent with sediment archives, and by a factor of 7.5 relative to natural levels (2000 BC). Legacy anthropogenic Hg re-emitted from surface reservoirs accounts for 60% of present-day atmospheric deposition, compared to 27% from primary anthropogenic

emissions, and 13% from natural sources. I find that only 17% of the present-day Hg in the surface ocean is natural, and that half of its anthropogenic enrichment originates from pre-1950 emissions. Although Asia is presently the dominant contributor to primary anthropogenic emissions, only 17% of the surface ocean reservoir is of Asian anthropogenic origin, as compared to 30% of North American and European origin. The accumulated burden of legacy anthropogenic Hg means that future deposition will increase even if primary anthropogenic emissions are held constant. Aggressive global Hg emissions reductions will be necessary just to maintain oceanic Hg concentrations at present levels.

Lastly, I examine rivers and associated burial of riverborne Hg in ocean margin sediments on the global biogeochemical cycle of Hg. Rivers link anthropogenic Hg releases on land to marine ecosystems. I estimate global present-day Hg discharges from rivers to ocean margins of 5400 ± 2700 Mg a^{-1}, of which 28% reaches the open ocean and the rest is deposited to ocean margin sediments. This is larger than previously estimated due to our accounting for elevated concentrations in Asian rivers and variability in offshore transport across different types of estuaries. Inputs from rivers to the North Atlantic have decreased several-fold since the 1970s but increased to the North Pacific. The analysis shows these trends have large effects at ocean margins but are small offshore and thus do not explain observed declines in vertical seawater profiles in the North Atlantic or increases in the North Pacific. Burial in nearshore marine sediments represents a major sink in the global Hg biogeochemical cycle that has not previously been considered. Its inclusion in a fully coupled global biogeochemical box model helps to accommodate new findings of a large historical anthropogenic Hg source from commercial use. It implies that natural environmental Hg levels are lower than previously estimated, suggesting a larger relative impact from human activity and a potentially faster timescale (centuries instead of

millennia) for resequestration of anthropogenic Hg into the lithosphere.

The work presented here quantitatively demonstrates anthropogenic activity has resulted in the enrichment of all geochemical reservoirs (ocean, atmosphere, and land) and that the enrichment is larger than previously estimated. It also advances the understanding of the fundamental couplings between global geochemical reservoirs and the timescales of those interactions.

References:

Cooke, C. A., et al. (2009), Over three millennia of mercury pollution in the Peruvian Andes, Proc. Natl. Acad. Sci. U. S. A., 106(22), 8830-8834.

Corbitt, E. S., et al. (2011), Global source-receptor relationships for mercury deposition under present-day and 2050 emissions scenarios, *Environ. Sci. Technol.*, *45*(24), 10477-10484.

Johansen, P., et al. (2004), Human exposure to contaminants in the traditional Greenland diet, Sci. Total Environ., 331(1-3), 189-206.

Kim, N. S., and B. K. Lee (2010), Blood total mercury and fish consumption in the Korean general population in KNHANES III, 2005, Sci. Total Environ., 408(20), 4841-4847.

Scheulhammer, A. M., et al. (2007), Effects of environmental methylmercury on the health of wild birds, mammals, and fish, Ambio, 36(1), 12-18.

Sunderland, E. M. (2007), Mercury exposure from domestic and imported estuarine and marine fish in the US seafood market, Environ. Health Perspect., 115(2), 235-242.

Sunderland, E. M., et al. (2009), Mercury sources, distribution, and bioavailability in the North Pacific Ocean: Insights from data and models, *Glob. Biogeochem. Cycle*, *23*, 14.

Swartzendruber, P. C., et al. (2006), Observations of reactive gaseous mercury in the free troposphere at the Mount Bachelor Observatory, J. Geophys. Res.-Atmos., 111(D24), 12.

Chapter 2. Gas-particle partitioning of atmospheric Hg(II) and its effect on global mercury deposition

[Amos, H. M., Jacob, D. J., Holmes, C. D., Fisher, J. A., Wang, Q., Yantosca, R. M. , Corbitt, E. S., Galarneau, E. , Rutter, A. P. , Gustin, M. S., Steffen, A., Schauer, J. J., Graydon, J. A., St. Louis, V. L., Talbot, R. W., Edgerton, E. S., Zhang, Y. , Sunderland, E. M., 2012. Gas-particle partitioning of atmospheric Hg(II) and its effect on global mercury deposition. Atmospheric Chemistry and Physics, 12, 591-603.

Abstract

Atmospheric deposition of Hg(II) represents a major input of mercury to surface environments. The phase of Hg(II) (gas or particle) has important implications for deposition. We use long-term observations of reactive gaseous mercury (RGM, the gaseous component of Hg(II)), particle-bound mercury (PBM, the particulate component of Hg(II)), fine particulate matter ($PM_{2.5}$), and temperature (T) at five sites in North America to derive an empirical gas-particle partitioning relationship $\log_{10}(K^{-1}) = (10\pm1) - (2500\pm300)/T$ where $K = (PBM/PM_{2.5})/RGM$ with PBM and RGM in common mixing ratio units, $PM_{2.5}$ in $\mu g\ m^{-3}$, and T in Kelvin. This relationship is within the range of previous work but is based on far more extensive data from multiple sites. We implement this empirical relationship in the GEOS-Chem global 3-D Hg model to partition Hg(II) between the gas and particle phases. The resulting gas-phase fraction of Hg(II) ranges from over 90% in warm air with little aerosol to less than 10% in cold air with high aerosol. Hg deposition to high latitudes increases because of more efficient

scavenging of particulate Hg(II) by precipitating snow. Model comparison to Hg observations at the North American surface sites suggests that subsidence from the free troposphere (warm air, low aerosol) is a major factor driving the seasonality of RGM, while elevated PBM is mostly associated with high aerosol loads. Simulation of RGM and PBM at these sites is improved by including fast in-plume reduction of Hg(II) emitted from coal combustion and by assuming that anthropogenic particulate Hg(P) behaves as semi-volatile Hg(II) rather than as a refractory particulate component. We improve the simulation of Hg wet deposition fluxes in the US relative to a previous version of GEOS-Chem; this largely reflects independent improvement of the washout algorithm. The observed wintertime minimum in wet deposition fluxes is attributed to inefficient snow scavenging of gas-phase Hg(II).

2.1 Introduction

Mercury (Hg) is a naturally occurring metal that can cause adverse health effects on humans and wildlife [*Clarkson and Magos*, 2006; *Mergler et al.*, 2007; *Scheulhammer et al.*, 2007]. Human exposure in developed countries is mainly through contaminated fish consumption [*Mahaffey et al.*, 2004; 2009]. As a result of anthropogenic emissions, deposition to the oceans has increased roughly threefold since the pre-industrial era [*Mason and Sheu*, 2002; *Sunderland and Mason*, 2007]. Mercury is released to the atmosphere mainly as elemental mercury (Hg(0)), though combustion processes also emit divalent mercury (Hg(II)). Hg(0) in the atmosphere can eventually be oxidized to Hg(II). Hg(II) compounds have low vapor pressure ($HgCl_2$ 8.99×10^{-3} Pa at 20°C, HgO 9.20×10^{-12} Pa at 25°C), partition between the gas and particle phases, and are thus readily removed by removed by wet and dry deposition [*Schroeder and Munthe*, 1998; *Lin et al.*, 2006]. The phase partitioning of Hg(II) has important implications for deposition because gases and particles are

deposited by different physical processes and at different rates [*Seinfeld and Pandis*, 2006]. Hg(0) has a high vapor pressure (0.18 Pa at 20°C [*Schroeder and Munthe*, 1998]) and its sorption to particles is thought to be negligible [*Seigneur et al.*, 1998]. Limited measurements suggest Hg(0) may be present in particulate Hg in heavily polluted urban areas [*Sakata and Marumoto*, 2002; *Xiu et al.*, 2009]. Here we use long-term observational records of speciated Hg to develop a mechanistic parameterization of Hg(II) gas-particle partitioning, and apply it to a simulation of Hg deposition using the GEOS-Chem global 3-D chemical transport model (CTM).

There is considerable uncertainty regarding the atmospheric chemistry of Hg [*Hynes et al.*, 2009] and atmospheric measurement methods [*Gustin and Jaffe*, 2010]. Despite these uncertainties, atmospheric Hg(II) compounds are thought to be semi-volatile and hence partition between the gas phase and particulate matter (PM) [*Petersen et al.*, 1995; *Seigneur et al.*, 1998]. Current measurements use an operationally defined method for quantifying reactive gaseous mercury (RGM) and fine fraction (<2.5 μm) particle-bound mercury (PBM) [*Lamborg et al.*, 1995; *Keeler et al.*, 1995; *Landis et al.*, 2002]. *Rutter and Schauer* [2007b] investigated the mechanism of Hg partitioning in the air by fitting urban and laboratory data for RGM and PBM to a temperature-dependent expression for Hg(II) sorption onto PM smaller than 2.5 μm in diameter ($PM_{2.5}$). This approach is similar to parameterizations previously developed for other semi-volatile species including polycyclic aromatic hydrocarbons [*Yamasaki et al.*, 1982; *Pankow*, 1987] and secondary organic compounds [*Pankow*, 1994; *Odum et al.*, 1996; *Chung and Seinfeld*, 2002].

Little was known about Hg(II) gas-particle partitioning prior to the work of *Rutter and Schauer et al.* [2007a,b]. Earlier models of atmospheric Hg included parameterizations for the sorption of dissolved Hg species to soot particles suspended in cloud water [*Petersen et al.*, 1998; *Seigneur et al.*, 2001; *Bullock and Brehme*, 2002; *Dastoor and Larocque*, 2004] based on experimental results from

Petersen et al. [1995] and *Seigneur et al.* [1998]. In more recent years, models of atmospheric Hg have taken various approaches to treating Hg(II) gas-particle partitioning. *Vijayaraghavan et al.* [2008] implemented the temperature-dependent Hg(II) gas-particle partitioning formulation of *Rutter and Schauer* [2007b] into a regional model over the United States for a two-month (August-September) simulation. *Vijayaraghavan et al.* [2008] found that including Hg(II) gas-particle partitioning was most important in regions of high PM. Previous versions of GEOS-Chem have either assumed atmospheric Hg(II) to be entirely gas-phase [*Selin et al.*, 2007; *Selin et al.*, 2008] or assumed 50/50 gas-particle [*Holmes et al.*, 2010; *Soerensen et al.*, 2010; *Corbitt et al.*, 2011].

Here we use long-term RGM and PBM observations at five sites in North America to derive an empirical gas-particle Hg(II) partitioning coefficient as a function of $PM_{2.5}$ and temperature, following the approach of *Rutter and Schauer* [2007b] but with a much larger data set. We show that a single parameterization can describe the Hg(II) partitioning across sites, and compare the resulting GEOS-Chem simulation to observations. The implications for global Hg deposition are discussed.

2.2 Hg(II) gas-particle partitioning

Data sets of RGM and PBM were obtained from five sites: Reno, Thompson Farm, Outlying Landing Field (Pensacola), Experimental Lakes Area, and Milwaukee (**Table 2.1**). The Experimental Lakes site includes 4 years of data, the Reno site 2 years and the others one year or slightly less. **Figures 2.1** and **2.2** show the spatial and seasonal (monthly) distributions of the data and are discussed in Section 2.4.

All Hg measurements were collected with Tekran mercury analyzers (2537A, 1130, and 1135 units). Air is drawn through a heated (50°C) impactor which removes coarse (>2.5μm) particles from the air stream, then through a KCl-coated annual denuder to collect RGM,

followed by a quartz fiber filter to collect PBM [*Landis et al.*, 2002]. The filter and denuder are sequentially heated to 800°C and 500°C, respectively, to thermally desorb the collected RGM and PBM. The desorbed RGM and PBM are sequentially reduced to Hg(0) as they pass through an 800°C pyrolyzer and are finally analyzed as Hg(0) by cold vapor atomic fluorescence spectroscopy (CVAFS). Previous work has suggested that there are artifacts associated with PBM collection and there are interferences with the collection of RGM on the denuders, and surrogate methods suggest that the annular denuders do not have 100% collection efficiency [*Lynam and Keeler*, 2005; *Lyman et al*., 2007; *Malcolm and Keeler*, 2007; *Rutter et al*., 2008a; *Gustin and Jaffe*, 2010; *Lyman et al.*, 2010]. *Lyman and Gustin* [2009] reported that two Tekran instruments sampling side-by-side disagreed by 8±40% for RGM and 71±41% for PBM.

Keeping the limitations of the Tekran instrument in mind, we use them in the absence of other information. We parameterize the partitioning of Hg(II) between the gas and particle phases with a partitioning coefficient K [*Rutter and Schauer*, 2007a,b]

$$K = (\mathrm{PBM}/\ \mathrm{PM}_{2.5}) / \mathrm{RGM} \qquad (2.1)$$

where RGM and PBM are atmospheric mixing ratios (ppq) and $PM_{2.5}$ is the dry mass concentration ($\mu g\ m^{-3}$). It is assumed that Eq. 1 represents equilibrium between the gas and particle phases of atmospheric Hg(II), and that the major Hg(II) compounds measured as RGM and PBM have similar volatilities so that a single equilibrium constant is applicable. Normalization by $PM_{2.5}$ makes the additional assumption that uptake is proportional to the aerosol mass concentration, although adsorption to a solid aerosol phase would be equivalent if a fixed scaling is assumed between the volume and area of the aerosol [*Yamasaki et al.*, 1982;

Table 2.1 Measurement sites for RGM and PBM

Site	Location	Record	$PM_{2.5}$ data[a]	Reference
Experimental Lakes, Ontario, Canada	49.7°N, 93.7°W	May 2005 – Dec 2009	*b*	Graydon et al., 2008
Milwaukee, Wisconsin	43.1°N, 87.8°W	Jul 2004 – May 2005	*c*	Rutter and Schauer, 2007b
Outlying Landing Field, Pensacola, Florida	30.6°N, 87.4°W	Jan 2009 – Dec 2009	*c*	Edgerton et al., 2006
Reno, Nevada	39.3°N, 119.5°W	Feb 2007 – Jan 2009	*d*	Lyman and Gustin, 2009
Thompson Farm, New Hampshire	43.1°N, 71.0°W	Jan 2009 – Jun 2010	*d*	Sigler et al., 2009

[a] All $PM_{2.5}$ data are 24-h averages.
[b] $PM_{2.5}$ from nearby Voyageurs National Park IMPROVE site (http://vista.cira.colostate.edu/IMPROVE/).
[c] $PM_{2.5}$ collocated with Hg measurements.
[d] $PM_{2.5}$ for Reno and Thompson Farm were obtained from the Environmental Protection Agency Air Quality System (http://www.epa.gov/ttn/airs/airsaqs).

Pankow, 1987; *Rutter and Schauer*, 2007a,b]. Restriction to fine aerosol ($PM_{2.5}$) in Eq. (2.1) is consistent with the size cut-off of the Tekran instrument used to measure these Hg species.

Previous applications of Eq. (2.1) to PAHs and SOA have found a van't Hoff type of relationship between K and the local temperature T [*Yamasaki et al.*, 1982; *Pankow*, 1987]

$$\log_{10}(K^{-1}) = a + \frac{b}{T} \qquad (2.2)$$

where a and b are coefficients. **Figure 2.3** shows the daily data from the sites in **Table 1.1** fit to Eq. (2.2). Confidence intervals (95%) for the slope and intercept are constructed using a bootstrap method. All RGM and PBM observations are averaged over midday hours (10:00-16:00 local time) when vertical mixing is strongest and the air mass being sampled is more likely to be homogenous. $PM_{2.5}$ data are 24-h averages as no higher temporal resolution is available. Use of 24-h average RGM and PBM data, as compared to daytime averages, does not significantly change the results. *Pankow et al.* [1993] suggested that relative humidity (RH)

affected gas-particle partitioning of semi-volatile organic compounds. We tested this by performing a multivariate regression, $\log_{10}(K^{-1}) = a + b/T + c*RH$, and found no significant dependence on RH at any of the sites.

Table 2.2 lists the regression fits for individual sites. We tested them for statistical distinctness following *Galarneau et al.* [2006]. Reno, Thompson Farm, and Experimental Lakes are statistically indistinct, as are Milwaukee, Pensacola, Thompson Farm, and Experimental Lakes. Reno is distinct from Pensacola and Milwaukee. Differences in aerosol composition between sites would be expected to affect the fits [*Rutter and Schauer*, 2007a,b] but no obvious relationship was found. The regression fit for the combined data set (all sites) is $\log(K^{-1}) = (10\pm1)–(2500\pm300)/T$ (r^2=0.49), and will be used in the analysis below.

The regression coefficients from this work fall in the envelope of those reported by *Rutter and Schauer* [2007b] for urban measurements using a filter-based method vs. a Tekran instrument (**Figure 2.3**). Our derived coefficients are statistically indistinguishable from their laboratory data for partitioning of $HgCl_2$ with adipic acid aerosol and differ most from their partitioning of $HgCl_2$ to dry, synthesized $(NH_4)_2SO_4$ aerosol (**Table 2.2**). *Rutter and Schauer* [2007b] hypothesized that the difference in partitioning between their filter-based method and the Tekran instrument could reflect a Tekran sampling artifact associated with internally heating the instrument to 50°C but this remains speculative. Filter-based methods are also prone to artifacts [*Lyman et al.*, 2009]. The filter-based method used by *Rutter and Schauer* [2007b] relied on KCl coated filters to collect RGM, which *Lyman et al.* [2009] show to have poor collection efficiency after a week. Both of these potential sampling artifacts would lead to higher RGM measurements by the Tekran than by the filter-based method, consistent with the differences in partitioning shown here.

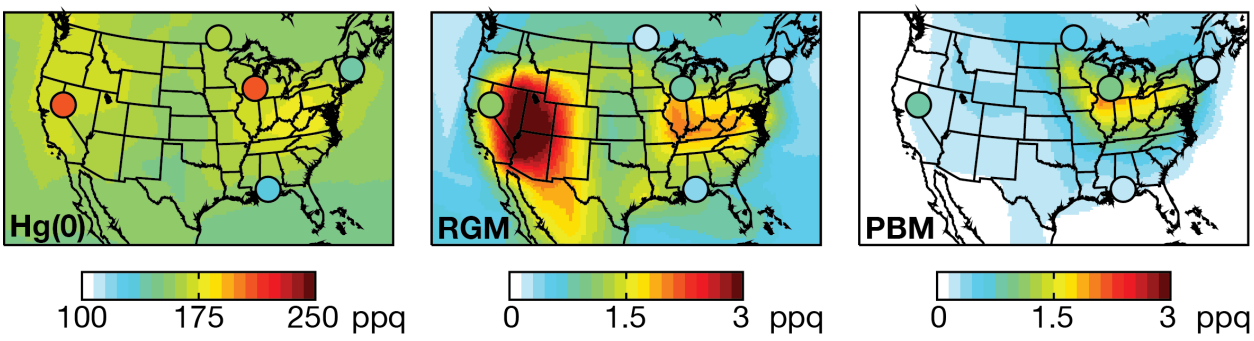

Figure 2.1: Simulated (background solid contours) and observed (circles) annual mean concentrations of speciated Hg. Measurement sites and measurement periods are listed in Table 2.1. Model results are for 2007-2009.

2.3 GEOS-Chem model simulation

We use version 9-01-01 of the GEOS-Chem Hg coupled atmosphere-ocean-land model (www.geos-chem.org), which includes an atmosphere from *Holmes et al.* [2010], a surface ocean from *Soerensen et al.* [2010], and a land surface from *Selin et al.* [2008]. The simulation is conducted for 2004-2009 with GEOS-5 assimilated meteorological and surface data from the NASA Global Modeling and Assimilation Office (GMAO). The years 2004-2006 are used for initialization and 2007-2009 for analysis. The original GEOS-5 data have $1/2^{o}$x$2/3^{o}$ horizontal resolution and 72 vertical levels. The horizontal resolution is degraded here to 4°x5° for input to GEOS-Chem for computational expediency. The GEOS-Chem simulation transports three Hg species in the atmosphere: elemental Hg (Hg(0)), semi-volatile divalent Hg (Hg(II)), and inert refractory particulate Hg (Hg(p)) [*Selin et al.*, 2008]. Atmospheric Hg(0)/Hg(II) redox chemistry follows *Holmes et al.* [2010], with oxidation of Hg(0) by Br atoms and photoreduction of Hg(II) in liquid cloud droplets.

Direct emissions of Hg(II) and Hg(p) in GEOS-Chem are entirely of anthropogenic origin, while emissions of Hg(0) are from both natural and anthropogenic sources [*Schroeder and Munthe*, 1998]. Anthropogenic emissions are from *Pacyna et al.* [2010] for the year 2005.

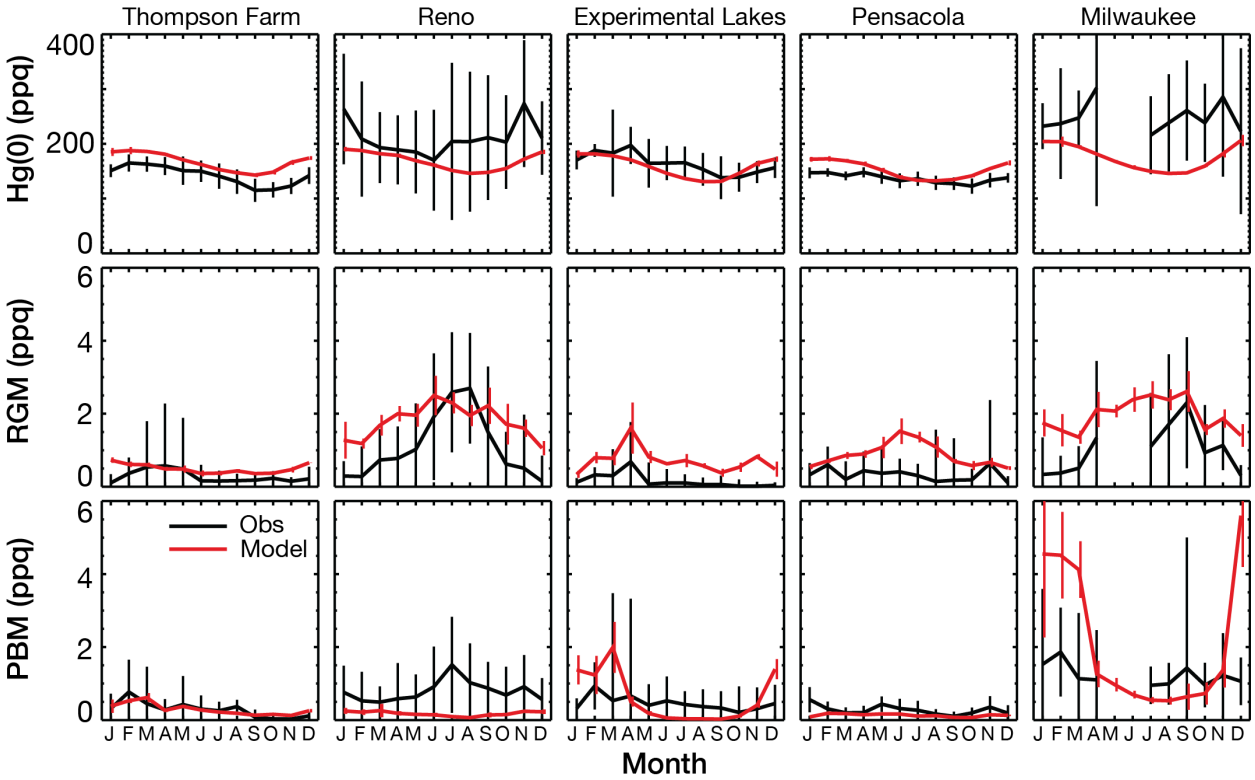

Figure 2.2: Monthly mean observed (black, ±1σ) and simulated (red, ±1σ) concentrations of speciated Hg during daytime hours (10:00-16:00 local time). Standard deviations for simulated Hg(0) are less than the width of the line. Measurement sites and measurement periods are listed in Table 2.1. Each month contain at least two weeks of daily measurements. Model results are for 2007-2009.

There is considerable ambiguity surrounding anthropogenic Hg(p) in the literature, which confounds the interpretation of how it should treated in models and compared to Tekran measurements of PBM. Hg(p) in the emission inventories is intended to represent chemically inert Hg that is incorporated into soot or fly ash particles [*J. Pacyna*, personal communication]. It is not clear that heating to 800^{o}C in the Tekran instrument would be sufficient to desorb such mercury from the collection filter. Considering it as PBM in the model would contradict the assumption that PBM is semi-volatile. For purpose of comparing with observations, we thus assume that gas-phase and particle-phase Hg(II) in the model correspond to RGM and PBM respectively, and that Hg(p) would not be measured as PBM. The sensitivity to this latter

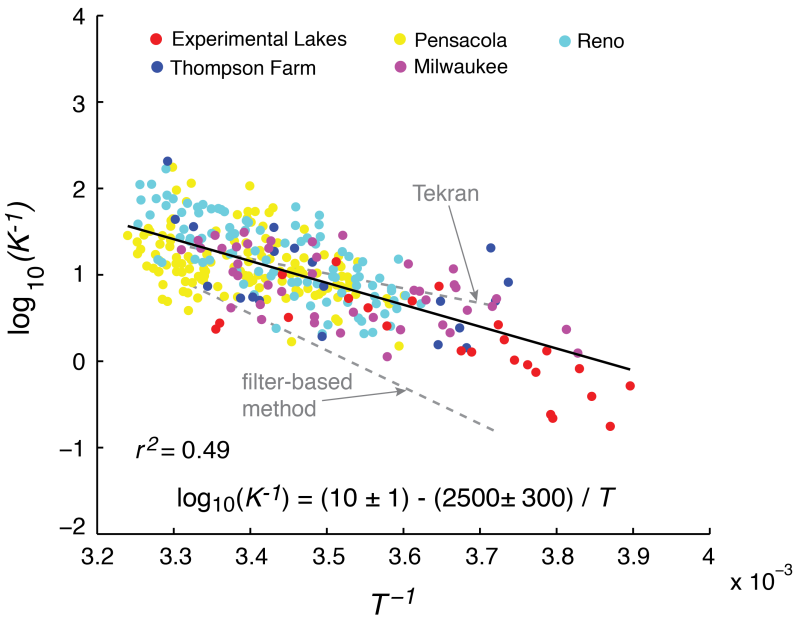

Figure 2.3: Temperature dependence of the relationship between gas-phase and particle-phase mercury as defined by Eqs. (2.1) and (2.2). Each point represents one observation day (10:00-16:00 local time) for the color-coded sites in Table 2.1. Days with RGM or PBM below 0.34 ppq, or $PM_{2.5}$ below 2 μg m^{-3} are rejected as below analytical detection limits. Temperature is in K. Also shown is the least-squares regression line (solid) and the regression parameters with 95% bootstrapped confidence intervals (legend). Shown in dashed grey are the least-squares regression lines from Rutter and Schauer (2007b) for urban data collected using a filter-based method and a Tekran instrument.

assumption is discussed in Section 2.4. We also assume that Hg(0) does not significantly partition into the aerosol on account of its high volatility [*Schroeder and Munthe*, 1998; *Seigneur et al.*, 1998] and thus does not contribute to PBM.

The Hg(0):Hg(II):Hg(p) speciation from coal combustion in the *Pacyna et al.* [2010] emission inventory is 50:40:10. Observations in power plant plumes [*Edgerton et al.*, 2006; *Weiss-Penzias et al.*, 2011; *ter Schure et al.*, 2011] indicate much lower Hg(II)/Hg(0) ratios, suggesting fast in-plume reduction of Hg(II) [*Seigneur et al.*, 2003; *Lohman et al.*, 2006]. We find in GEOS-Chem that a large decrease in the fraction of Hg emitted as Hg(II) or Hg(p) from coal combustion improves consistency with observed RGM and PBM concentrations of Figure 2.2. A 90:7:3 speciation from coal combustion is implemented to accommodate this constraint. A

Table 2.2 Regression coefficients for $\log_{10}(K^{-1}) = a + b/T$

Site[a]	*a*	*b*	r^2	Reference
Experimental Lakes	9±4	-2400±1100	0.57	this work
Milwaukee	7±2	-1900±400	0.43	this work
Pensacola	6±2	-1600±600	0.16	this work
Reno	13±2	-3300±600	0.54	this work
Thompson Farm	8±6	-2000±1600	0.33	this work
All sites (combined)	10±1	-2500±300	0.49	this work
Urban[b,c]	15±2	-4250±480	0.77	Rutter and Schauer, 2007b
Urban[d]	7±1	-1710±380	0.49	Rutter and Schauer, 2007b
Laboratory, $HgCl_2$ on $(NH_4)_2SO_4$ [e]	19±2	-5720±470	0.99	Rutter and Schauer, 2007b
Laboratory, $HgCl_2$ on adipic acid and HgCl2)[e]	9±1	-2780±240	0.96	Rutter and Schauer, 2007b

[a] Measurements of RGM and PBM were made by Tekran instruments unless otherwise indicated.
[b] Hg collected using filter-based methods (Rutter and Schauer, 2007a,b).
[c] Milwaukee (Jul 2004 – May 2005) and Riverside, California (16 Jul – 7 Aug 2005) (Rutter and Schauer, 2007b).
[d] Milwaukee (Jul 2004 – May 2005) (Rutter and Schauer, 2007b).
[e] Dry conditions (RH<1%)

90% contribution from Hg(0) is slightly larger than observed by *Edgerton et al.* [2006] (mean 84%), but is not outside the range observed by *Wang et al.* [2010] (66-94%) for coal-fired power plants. Similar corrections to the emission inventory have been implemented by *Zhang et al.* [2012] (77:20:3) in a nested GEOS-Chem Hg simulation for North America to better match MDN wet deposition measurements and by *Kos et al.* [2013] (90:8:2) in the GRAHM global model to better match surface concentrations of RGM and PBM. The implicit inclusion of Hg(II) in-plume reduction in the model comes with the important caveats that a chemical mechanism has not been identified [*Lohman et al.*, 2006], and that there are significant uncertainties associated with both the speciation of anthropogenic emission inventories [*UNEP*, 2008] and methods for measuring atmospheric Hg [*Gustin and Jaffe*, 2010].

Hg(II) in the model is partitioned between the gas and particle phases for the purpose of calculating deposition, using the parameterization from Section 2.2. Here, $PM_{2.5}$ is specified as the sum of sulfate, nitrate, ammonium, carbonaceous, and fine dust particle mass from archived

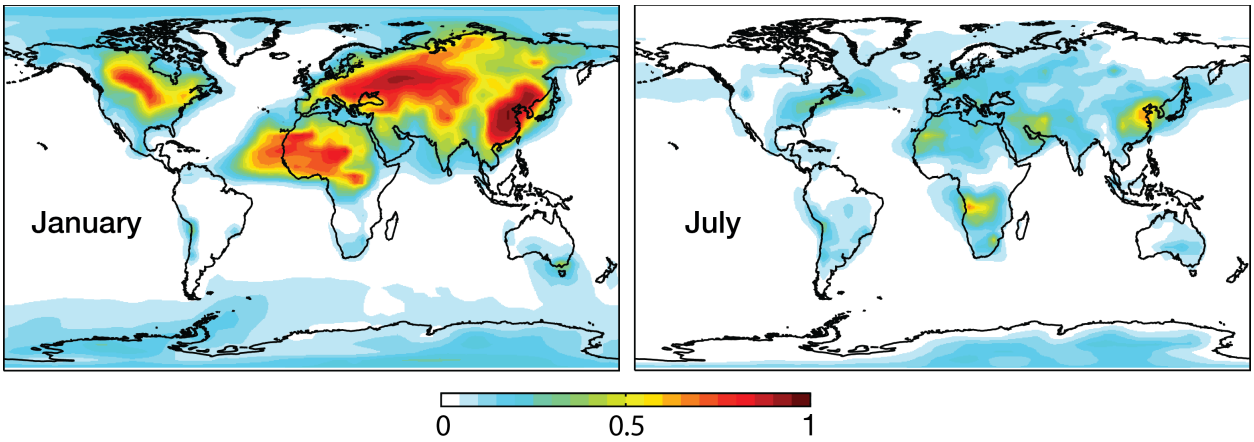

Figure 2.4: Mean fraction of Hg(II) partitioned into the particle phase in surface air in January and July. Values are 2007-2009 GEOS-Chem model results obtained using Eqs. (2.1) and (2.2), not including partitioning into sea-salt aerosol which is treated separately following Holmes et al. (2010).

GEOS-Chem monthly means of a full-aerosol simulation for the year 2007 [*L. Zhang et al.*, 2011]. The resulting Hg(II) particulate fraction in the model ranges from less than 10% in warm environments with low aerosol to more than 90% in cold environments with high aerosol (**Figure 2.4**). Gas-particle partitioning of Hg(II) with sea-salt particles in the marine boundary layer is accounted for separately in GEOS-Chem as described by *Holmes et al*. [2010]. *Holmes et al.* [2009, 2010] developed a more physical model for uptake of Hg(II) by sea-salt aerosol based on formation of Hg-Cl complexes [*Clever et al.*, 1985; *Hedgecock and Pirrone*, 2001].

Dry deposition in GEOS-Chem is computed with a standard resistance-in-series scheme and is much faster for water-soluble gases than for particles [*Wesely*, 1990]. RGM has been observed to have very high dry deposition velocities (0.4-7.6 cm s^{-1}) [*Lindberg and Stratton*, 1998; *Poissant et al.*, 2004; *Skov et al.*, 2006; *Lyman et al.*, 2007; *Lyman et al.*, 2009] and so a negligibly small surface resistance is assumed for gaseous Hg(II) [*Selin et al.*, 2007]. Dry deposition of particulate Hg(II) follows the standard surface resistance formulation of *Wesely* [1990] as implemented by *Wang et al.* [1998]. Simulated global annual mean dry deposition velocities are 0.93 cm s^{-1} for gaseous Hg(II) and 0.11 cm s^{-1} for particulate Hg(II)+Hg(p).

Wet deposition of Hg(II) and Hg(p) in GEOS-Chem includes scavenging from moist convective updrafts as well as rainout and washout by large-scale precipitation [*Liu et al.*, 2001]. Gaseous Hg(II) is scavenged as $HgCl_2$ with a Henry's law constant of 1.4×10^6 M atm^{-1} [*Lindqvist and Rodhe*, 1985]. Recent improvements from *Wang et al.* [2011] are included, which allow rainout and washout to occur in the same grid box and take into account the change in aerosol size distribution over the course of a precipitation event. Gaseous Hg(II) and particulate Hg(II)+Hg(p) are retained by supercooled water during freezing [*Holmes et al.*, 2010]. There is observational evidence that falling snow is inefficient at scavenging RGM [*Keeler et al.*, 2005; *Sigler et al.*, 2009; *Lombard et al.*, 2011; *Mao et al.*, 2012] and so below-cloud scavenging of gaseous Hg(II) by snow is suppressed. By contrast, particulate Hg is scavenged by falling snow in the same manner as its aerosol carriers. We conducted a ^{222}Rn-^{210}Pb simulation [*Liu et al.*, 2001] to test the model representation of aerosol deposition. ^{210}Pb is produced by decay of terrigenic ^{222}Rn and attaches indiscriminately to aerosols, which are then removed by wet and dry deposition. We obtained a lifetime of tropospheric ^{210}Pb against deposition of 10.4 days, consistent with a value of about 9 days in previous global 3-D model studies supported by comparisons to ^{222}Rn and ^{210}Pb observations [*Balkanski et al.*, 1993; *Koch et al.*, 1996; *Liu et al.*, 2001].

An important update in this study is to correct the washout of gases by rain in GEOS-Chem, as previous versions had an implementation error affecting the scavenging of highly soluble gases other than HNO_3 (and including gaseous Hg(II)). The GEOS-Chem washout scheme for gases had not been documented previously in the literature and we do so here (see Appendix), including the correction. After the correction we find that the global lifetime of tropospheric gaseous Hg(II) against wet deposition is reduced from 108 days to 46 days (the

lifetime is relatively long because of the large fraction of the inventory in the upper troposphere).

A standard practice in environmental modeling of Hg is to adjust parameters within their uncertainty to fit global observations of Hg(0) concentrations and wet deposition fluxes [*Selin et al.*, 2007; *Holmes et al.*, 2010]. To account for the changes made in the current version, the rate coefficient for atmospheric in-cloud reduction is reduced by 50% relative to *Holmes et al.* [2010]. We evaluated the model against the global set of land and cruise ship measurements from *Holmes et al.* [2010] and results are similar (not shown here). Our global budget of Hg is similar to that in *Holmes et al.* [2010] and *Soerensen et al.* [2010]. Global tropospheric burdens are 3600 Mg Hg(0), 500 Mg Hg(II) (310 Mg gas and 190 Mg particulate), and 2 Mg refractory Hg(p). Net Hg(0) ocean evasion is 2900 Mg a^{-1} (14 Mmol a^{-1}), which is consistent with *Soerensen et al.* [2010] and within the 90% confidence intervals of 10-21 Mmol a^{-1} simulated by *Sunderland and Mason* [2007]. On a global scale, dry deposition is 2500 Mg a^{-1} (56% Hg(0) (land only), 43% Hg(II), 1% Hg(p)), wet deposition is 3000 Mg a^{-1} (99% Hg(II), 1% Hg(p)), and deposition of Hg(II) via sea salt is 1600 Mg a^{-1}.

2.4 Comparison to surface observations

Simulated annual mean Hg(0), RGM, and PBM show reasonable consistency with observed annual means (**Figure 2.1**). RGM in the model is maximum over the western US where warm air with low aerosol subsides from the free troposphere [*Selin and Jacob,* 2008]. PBM is maximum over the Midwest and eastern US where $PM_{2.5}$ concentrations and anthropogenic Hg emissions are high.

Simulated and observed monthly mean Hg(0), RGM, and PBM are compared in **Figure 2.2**. The observed seasonality of Hg(0) at Thompson Farm, Experimental Lakes Area, and

Pensacola in **Figure 2.2** is typical of northern mid-latitudes, with maximum in early spring and minimum in late summer/early fall. Photochemical destruction is likely the major process contributing to the summer decrease [*Bergan and Rodhe*, 2001; *Selin et al.*, 2007; *Holmes et al.*, 2010]. The concentration of Hg(0) at Reno and Milwaukee is much greater and more variable than background continental concentrations and, likely reflecting local urban sources [*Rutter et al.*, 2008b; *Lyman and Gustin*, 2009] that are not resolved by the coarse horizontal resolution of the model.

There is much greater spatial variability for observed RGM and PBM than for Hg(0), reflecting the difference in atmospheric lifetimes. An implication is that variability in RGM and PBM is not significantly driven by variability in Hg(0). *Engle et al.* [2010] previously examined the seasonality of speciated Hg at nine sites across central and eastern North America, and reported large site-to-site variability that they attributed to a complex combination of processes including local point sources, exchange between the boundary layer and the free troposphere, and coastal effects. Temperature and aerosol concentrations would also play a role through the partitioning between RGM and PBM.

RGM concentrations are highest at Reno and Milwaukee in summer, both in the observations and in the model. The summer maximum at Reno is due to entrainment of RGM-rich free tropospheric air during deep diurnal mixed layer growth [*Lyman and Gustin*, 2009; *Weiss-Penzias et al.*, 2009]. This entrainment is associated with low aerosol concentrations and high temperatures, so that there is little associated enhancement of PBM. *Lyman and Gustin* [2009] suggest that the observed summer peak in PBM at Reno is due to extensive wildfire plumes during the summer of 2008 affecting the area [*Gyawali et al.*, 2009], and this is consistent with other observations of enhanced PBM during wildfires [*Friedli et al.*, 2003a,b;

Finley et al., 2009]. The model does not capture this particulate event of wildfire enhancement. The elevated summer RGM at Milwaukee is due in the model to regional anthropogenic sources in the Midwest [*Rutter et al.*, 2008b], with a corresponding enhancement of PBM in winter when low temperatures cause this anthropogenic Hg(II) to be partitioned into the aerosol. The simulated seasonality of RGM is reasonably consistent with observations, but the model over predicts both RGM and PBM during the winter.

RGM and PBM at Thompson Farm and Experimental Lakes Area peak in winter-spring, both in the observations and the model. This seasonality in the model is due to the upper troposphere and lower stratosphere (UT/LS), which is thought to contain a large reservoir of Hg(II) [*Swartzendruber et al.*, 2006; *Faïn et al.*, 2009]. Similar seasonality is found in model and observations for aerosol ^{7}Be, which is cosmogenically produced in the UT/LS and removed by deposition [*Liu et al.*, 2001; *Yoshimori*, 2005; *Muramatsu et al.*, 2008; *Alegría et al.*, 2010]. We find in the model that surface RGM and ^{7}Be have similar seasonal behavior; correlating the two in the observations would provide a test of UT/LS influence on surface Hg(II). At Pensacola, the spurious summer peak of RGM in the model appears to be due to excessively deep boundary layer mixing. That site is affected by sea breezes, which are not resolved by the model and would restrict boundary layer growth.

As discussed above, we have assumed that primary refractory Hg(p) simulated by the model is not measured as PBM, consistent with our general assumption that PBM is semi-volatile. Inclusion of Hg(p) would increase monthly mean model PBM by a factor of 1.4-3 (Experimental Lakes Area – Pensacola), degrading the agreement with observations. Even though Hg(p) is a negligible (<1%) component of the global Hg budget in the model, it is relatively important in surface air over source regions. We previously speculated that refractory

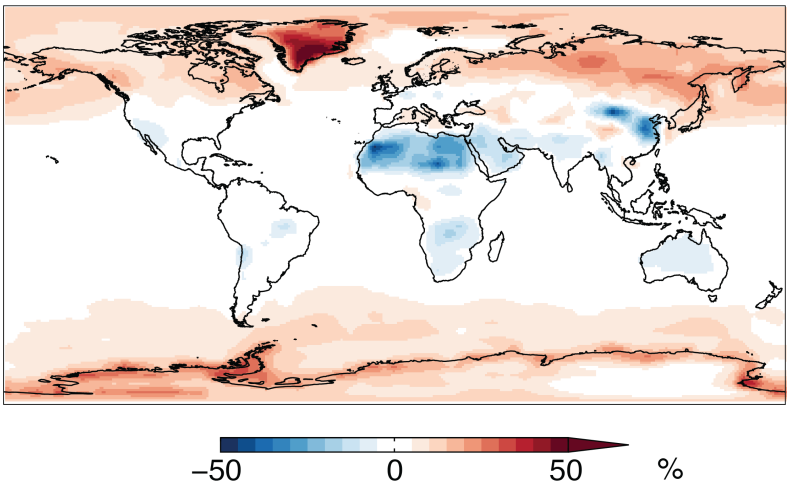

Figure 2.5: Percent difference in total annual Hg(II) deposition between our standard simulation and a simulation where all Hg(II) is assumed to deposit as gas. Positive values indicate higher deposition in the standard simulation.

Hg(p) might not be desorbed from the aerosol collection filter of the Tekran instrument. In addition, field observations show that >2.5 μm diameter particles (not sampled by the Tekran instrument) can represent up to 68% of total particulate Hg in polluted air and up to 37% in rural air [*Keeler et al.*, 1995; *Gildemeister et al.*, 2005]. Comparison of Tekran and filter-based sampling methods suggests that the Tekran instrument underestimates the total aerosol concentration [*Talbot et al.*, 2011]. Finally, the model assumption that Hg(p) is refractory could be flawed; if it were semi-volatile and behaving as Hg(II), its influence on surface concentrations would be much less because of losses from volatilization and reduction.

2.5 Implications for Hg deposition

Gas-particle partitioning impacts the global spatial distribution of Hg(II) deposition in the model. **Figure 2.5** shows the relative difference in total Hg(II) deposition between the standard simulation using equations (2.1)-(2.2) and a sensitivity simulation where all Hg(II) is deposited as a gas. The standard simulation includes all model updates described in Section 2.3. The effect

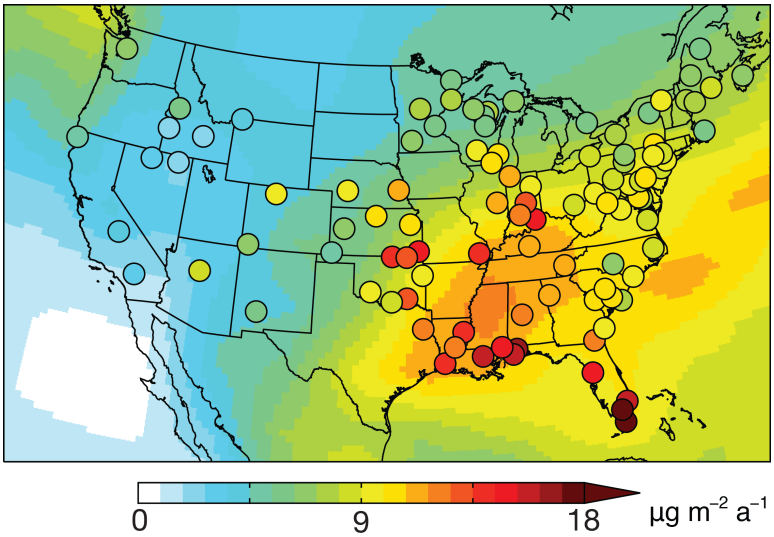

Figure 2.6: Annual Hg wet deposition fluxes for 2007-2009. Model results (solid contours) are compared to measurements (circles) from the Mercury Deposition Network (MDN). The MDN observations have been averaged as in Holmes et al. (2010).

is largest at high latitudes because particulate Hg(II) is scavenged by snow but gaseous Hg(II) is not. The competing effect of faster dry deposition of gaseous Hg(II) dominates only over dry regions of the subtropics. The effect over tropical and subtropical oceans is small because there is little non-sea-salt aerosol and so Hg(II) is either in the gas phase or in the sea-salt aerosol (which is treated the same in the two simulations).

The extensive wet deposition flux data from the Mercury Deposition Network (MDN, 2011) in the US has been used in previous GEOS-Chem studies to evaluate the model deposition [*Selin et al.*, 2007, 2008; *Selin and Jacob*, 2008; *Holmes et al.*, 2010]. Uncertainty in the MDN measurements is 10-25% [*Gustin and Jaffe*, 2010]. **Figure 2.6** compares model results to the MDN observed annual Hg wet deposition fluxes for 2007-2009. The model version presented here shows an improved ability to reproduce observed Hg wet deposition fluxes over the US, including the decreasing gradient from Southeast to Northeast and the seasonal phase and amplitude. This is an important result because the poor simulation of the MDN data in *Holmes et*

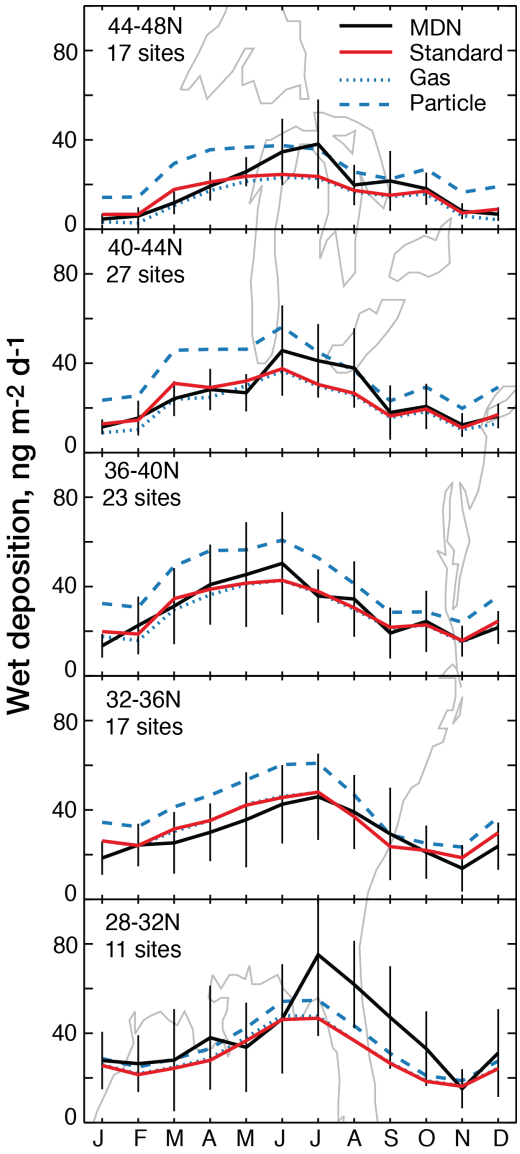

Figure 2.7: Seasonal variation of Hg wet deposition fluxes in the eastern US for different latitude bands. Values are monthly means for 2007-2009 in the observations (black) and in the model (red, blue). Observations from Fig. 2.6 are averaged over all sites in the latitude band that meet data density criteria described by Holmes et al. (2010). Model results are sampled at the same sites and are shown for the standard simulation (red) and for sensitivity simulations where all Hg(II) is assumed to deposit as a gas (blue dotted) or as a particle (blue dashed). Standard deviations are calculated from monthly means for individual MDN sites and individual years.

al. [2010] argued against Br atoms serving as the main Hg(0) oxidant (better simulation was achieved using OH and O_3 as oxidants). Our improved simulation of the MDN data (still using Br as the Hg(0) oxidant) largely reflects improvements in the washout algorithm, including

corrected washout of gas-phase Hg(II) and updated aerosol washout coefficients adopted from *Wang et al.* [2011].

Selin and Jacob [2008] pointed out that the dominant modes of variability in the MDN data over the eastern US are a latitudinal gradient and a seasonal variation that decreases in amplitude with increasing latitude. **Figure 2.7** compares observed and simulated seasonal variations of Hg wet deposition over the eastern US as a function of latitude, for the standard simulation and for sensitivity simulations with Hg(II) depositing either entirely as a gas or as a particle. The sensitivity simulations illustrate the effect of Hg(II) phase on simulated wet deposition. The standard model is able to capture the observed seasonal patterns of wet deposition and, except over the Gulf of Mexico, their latitude-dependent amplitudes. The sensitivity simulation with all Hg(II) depositing as a particle and thus scavenged by snow shows significant overestimate of wet deposition in winter. This lends support to the notion that gaseous Hg(II) (~50% of total Hg(II) over US in winter, see **Figure 2.4**) is not efficiently scavenged by snow. However, questions remain as to the MDN collection efficiency of snow [*Sanei et al.*, 2010; *Fain et al.*, 2011].

2.6 Summary

We have used long-term measurements of reactive gaseous mercury (RGM) and particle-bound mercury (PBM) at five sites in North America to derive an empirical gas-particle Hg(II) partitioning coefficient as a function of $PM_{2.5}$ and temperature. A single parameterization is used to describe the Hg(II) partitioning across sites. We implemented this parameterization in the global 3-D GEOS-Chem Hg model, compared model results with measurements of speciated Hg and wet deposition fluxes over the US, and discussed the implications for global Hg deposition.

We fit the RGM and PBM observations to a temperature-dependent gas-particle Hg(II) partitioning coefficient of the form $\log_{10}(K^{-1}) = (10 \pm 1) - (2500 \pm 300)/T$ where K = (PBM/$PM_{2.5}$)/RGM; here PBM and RGM are in common mixing ratio units, $PM_{2.5}$ is in μg m^{-3}, and T is in K .

Implementation of this Hg(II) gas-particle partitioning in GEOS-Chem yields Hg(II) fractions in the particle phase ranging from more than 90% in cold air masses with high aerosol burdens to less than 10% in warm air with low aerosol. Relative to a model simulation assuming all Hg(II) to be in the gas phase, Hg(II) deposition is increased at high latitudes because particulate Hg is more efficiently scavenged by snow, and decreased at subtropical latitudes because particulate Hg is less efficiently dry deposited.

Additional updates implemented in this version of GEOS-Chem include improvements to the washout algorithm and a change in the Hg(0):Hg(II):Hg(p) emission speciation for fossil fuel combustion from 50:40:10 to 90:7:3 to account for assumed rapid in-plume reduction. As previously noted by *Kos et al.* [2013] and *Zhang et al.* [2012], decreasing the Hg(II) emission fraction is necessary to avoid large model overestimate of PBM observations at North American sites. There is ambiguity about the nature of Hg(p) included in current anthropogenic emission inventories. If it represents refractory mercury embedded in soot or fly ash particles then it might not be operationally measured as PBM. If it semi-volatile and behaves as Hg(II), then it is inconsequential beyond the immediate source area because most Hg(II) is of secondary origin.

We compare model results to seasonal observations of Hg(0), RGM, and PBM at the five North American surface sites used to construct the *K(T)* parameterization. Observations in Reno and Milwaukee show particularly large summertime RGM that we attribute to subsidence of free tropospheric air (Reno) and regional anthropogenic sources (Milwaukee). Observations in rural

New Hampshire (Thompson Farm) and Ontario (Experimental Lakes Area) show spring maxima in RGM and PBM that we attribute to UT/LS influence. These maxima are correlated in the model with cosmogenic ^{7}Be, suggesting that ^{7}Be measurements would be of value to separate global and local contributions in RGM and PBM observations.

Compared to the previous version of GEOS-Chem [*Holmes et al.*, 2010], our model shows an improved ability to reproduce observed Hg wet deposition fluxes over the US from the Mercury Deposition Network (MDN), including the decreasing gradient from Southeast to Northeast and the seasonal phase and amplitude. This is an important result because the poor simulation of the MDN data in *Holmes et al.* [2010] argued against Br atoms serving as the main Hg(0) oxidant (better simulation was achieved using OH and O_3 as oxidants). Our improved simulation of the MDN data (still using Br as the Hg(0) oxidant) largely reflects improvements in the washout algorithm. The wintertime minima in the MDN data are attributed to inefficient snow scavenging of gaseous Hg(II).

Acknowledgments: This work was funded by the NSF Atmospheric Chemistry Program and AMS and NSF Graduate Fellowships to HMA. HMA would like to thank Lee T. Murray for helpful instruction on using the GEOS-Chem Be-Pb-Rn simulation. Funding for the collection of data at the Experimental Lakes Area was provided by NSERC, Environment Canada and Manitoba Hydro.

References:

Alegria, N., M. Herranz, R. Idoeta, F. Legarda (2010), Study of 7-Be activity concentration in the air of northern Spain, *J. Radioanal. Nucl. Chem.*, *286*, 347-351.

AMAP/UNEP (2008), Technical background report to the global atmospheric mercury assessment. *Rep.*, 159 pp, Arctic Monitoring and Assessment Program / UNEP Chemicals Branch.

Balkanski, Y. J., D. J. Jacob, G. M. Gardner (1993), Transport and residence times of tropospheric aerosols inferred from a global three-dimensional simulation of 210-Pb, *J. Geophys. Res.*, *98*(D11), 20573-20586.

Bergan, T., H. Rodhe (2001), Oxidation of elemental mercury in the atmosphere; constraints imposed by global scale modeling, *J. Atmos. Chem.*, *40*, 191-212.

Bullock, O. R., K. A. Brehme (2002), Atmospheric mercury simulation using the CMAQ model: Formulation description and analysis of wet deposition results, *Atmos. Environ.*, *36*, 2135-2146.

Chung, S. H., and J. H. Seinfeld (2002), Global distribution and climate forcing of carbonaceous aerosols, *J. Geophys. Res.-Atmos.*, *107*(D19), 33.

Clarkson, T. W., L. Magos (2006), The toxicology of mercury and its chemical compounds, *Critical Rev. in Toxic.* , *36*, 609-662.

Clever, H. L., et al. (1985), The solubility of mercury and some sparingly soluble mercury salts in water and aqueous-electrolyte solutions, *J. of Phys. and Chem. Ref. Data*, *14*(3), 631-681.

Cole, A. S., and A. Steffen (2010), Trends in long-term gaseous mercury observations in the Arctic and effects of temperature and other atmospheric conditions, *Atmospheric Chemistry and Physics*, *10*(10), 4661-4672.

Corbitt, E. S., et al. (2011), Global source-receptor relationships for mercury deposition under present-day and 2050 emissions scenarios, *Environ. Sci. Technol.*, *45*(24), 10477-10484.

Corn, M., et al. (1971), Suspended particulate matter - seasonal variation in specific surface areas and densities, *Environ. Sci. Tech.*, *5*(2).

Dastoor, A. P., and Y. Larocque (2004), Global circulation of atmospheric mercury: A modeling study, *Atmos. Environ.*, *38*(1), 147-161.

Edgerton, E. S., et al. (2006), Mercury speciation in coal-fired power plant plumes observed at three surface sites in the southeastern us, *Environ. Sci. Technol.*, *40*(15), 4563-4570.

Engle, M. A., et al. (2010), Comparison of atmospheric mercury speciation and deposition at nine sites across central and eastern North America, *J. Geophys. Res.*, *115*, 13.

Fain, X., et al. (2009), High levels of reactive gaseous mercury observed at a high elevation research laboratory in the Rocky Mountains, *Atmospheric Chemistry and Physics*, *9*(20), 8049-8060.

Fain, X., et al. (2011), Whole-watershed mercury balance at Sagehen Creek, Sierra Nevada, CA, *Geochim. Cosmochim. Acta*, *75*(9), 2379-2392.

Feichter, J., et al. (1991), 3-dimensional modeling of the concentration and deposition of Pb-210 aerosols, *J. Geophys. Res.*, *96*(D12), 22447-22460.

Friedli, H. R., et al. (2003a), Mercury emissions from the august 2001 wildfires in Washington State and an agricultural waste fire in Oregon and atmospheric mercury budget estimates, *Glob. Biogeochem. Cycle*, *17*(2), 8.

Friedli, H. R., et al. (2003b), Mercury emissions from burning of biomass from temperate North American forests: Laboratory and airborne measurements, *Atmospheric Environment*, *37*(2), 253-267.

Galarneau, E., et al. (2006), Seasonality and interspecies differences in particle/gas partitioning of PAHs observed by the Integrated Atmospheric Deposition Network (IADN), *Atmos. Environ.*, *40*(1), 182-197.

Gildemeister, A. E., et al. (2005), Source proximity reflected in spatial and temporal variability in particle and vapor phase Hg concentrations in Detroit, MI, *Atmos. Environ.*, *39*(2), 353-358.

Gustin, M., and D. Jaffe (2010), Reducing the uncertainty in measurement and understanding of mercury in the atmosphere, *Environ. Sci. Technol.*, *44*(7), 2222-2227.

Gyawali, M., et al. (2009), In situ aerosol optics in Reno, NV, USA during and after the summer 2008 California wildfires and the influence of absorbing and non-absorbing organic coatings on spectral light absorption, *Atmospheric Chemistry and Physics*, *9*(20), 8007-8015.

Hedgecock, I. M., and N. Pirrone (2001), Mercury and photochemistry in the marine boundary layer-modeling studies suggest the in situ production of reactive gas phase mercury, *Atmos. Environ.*, *35*(17), 3055-3062.

Holmes, C. D., et al. (2009), Sources and deposition of reactive gaseous mercury in the marine atmosphere, *Atmos. Environ.*, *43*(14), 2278-2285.

Holmes, C. D., et al. (2010), Global atmospheric model for mercury including oxidation by bromine atoms, *Atmos. Chem. Phys.*, *10*, 12037-12057.

Hynes, A., et al. (2009), Our current understanding of major chemical and physical processes affecting mercury dynamics in the atmosphere and at air-water/terrestrial interfaces, in: *Mercury Fate and Transport in the Global Atmosphere*, edited by: Pirrone, N. and Mason, R. P., chap. 14, Springer.

Keeler, G., et al. (1995), Particulate mercury in the atmosphere - its significance, transport, transformation and sources, *Water Air Soil Pollut.*, *80*(1-4), 159-168.

Keeler, G. J., et al. (2005), Long-term atmospheric mercury wet deposition at Underhill, Vermont, *Ecotoxicology*, *14*(1-2), 71-83.

Koch, D. M., et al. (1996), Vertical transport of tropospheric aerosols as indicated by Be-7 and Pb-210 in a chemical tracer model, *J. Geophys. Res.*, *101*(D13), 18651-18666.

Kos, G., et al. (2013), Evaluation of discrepancy between measured and modeled oxidized mercury species, *Atmospheric Chemistry and Physics*, *13*(9), 4839-4863.

Lamborg, C. H., et al. (1995), Atmospheric mercury in northern Wisconsin - sources and species, *Water Air Soil Pollut.*, *80*(1-4), 189-198.

Landis, M. S., et al. (2002), Development and characterization of an annular denuder methodology for the measurement of divalent inorganic reactive gaseous mercury in ambient air, *Environ. Sci. Technol.*, *36*(13), 3000-3009.

Levine, S. Z., and S. E. Schwartz (1982), In-cloud and below-cloud scavenging of nitric acid vapor, *Atmos. Environ.*, *16*, 1725-1734.

Lin, C. J., et al. (2006), Scientific uncertainties in atmospheric mercury models I: Model science evaluation, *Atmos. Environ.*, *40*(16), 2911-2928.

Lindberg, S., et al. (2007), A synthesis of progress and uncertainties in attributing the sources of mercury in deposition, *Ambio*, *36*(1), 19-32.

Lindberg, S. E., and W. J. Stratton (1998), Atmospheric mercury speciation: Concentrations and behavior of reactive gaseous mercury in ambient air, *Environ. Sci. Technol.*, *32*(1), 49-57.

Lindqvist, O., and H. Rodhe (1985), Atmospheric mercury - a review, *Tellus Series B-Chem. Phys. Met.*, *37*(3), 136-159.

Liu, H. Y., et al. (2001), Constraints from Pb-210 and Be-7 on wet deposition and transport in a global three-dimensional chemical tracer model driven by assimilated meteorological fields, *J. Geophys. Res.*, *106*(D11), 12109-12128.

Lohman, K., et al. (2006), Modeling mercury in power plant plumes, *Environ. Sci. Technol.*, *40*(12), 3848-3854.

Lombard, M. A. S., et al. (2011), Mercury deposition in southern New Hampshire, 2006-2009, *Atmos. Chem. Phys.*, *11*(15), 7657-7668.

Lyman, S. N., and M. S. Gustin (2009a), Determinants of atmospheric mercury concentrations in Reno, Nevada, USA, *Sci. Total Environ.*, *408*(2), 431-438.

Lyman, S. N., et al. (2010), Release of mercury halides from KCl denuders in the presence of ozone, *Atmospheric Chemistry and Physics*, *10*(17), 8197-8204.

Lyman, S. N., et al. (2007), Estimation of dry deposition of atmospheric mercury in Nevada by direct and indirect methods, *Environ. Sci. & Technol.*, *41*(6), 1970-1976.

Lyman, S. N., et al. (2009b), Testing and application of surrogate surfaces for understanding potential gaseous oxidized mercury dry deposition, *Environ. Sci. Technol.*, *43*(16), 6235-6241.

Lynam, M. M., and G. J. Keeler (2005), Artifacts associated with the measurement of particulate mercury in an urban environment: The influence of elevated ozone concentrations, *Atmospheric Environment*, *39*(17), 3081-3088.

Mahaffey, K. R., et al. (2004), Blood organic mercury and dietary mercury intake: National health and nutrition examination survey, 1999 and 2000, *Environ. Health Persp.*, *112*(5), 562-570.

Mahaffey, K. R., et al. (2009), Adult women's blood mercury concentrations vary regionally in the United States: Association with patterns of fish consumption (NHANES 1999-2004), *Environ. Health Persp.*, *117*(1), 47-53.

Malcolm, E. G., and G. J. Keeler (2007), Evidence for a sampling artifact for particulate-phase mercury in the marine atmosphere, *Atmospheric Environment*, *41*(16), 3352-3359.

Mao, H., et al. (2012), Speciated mercury at marine, coastal, and inland sites in New England - Part 2: Relationships with atmospheric physical parameters, *Atmospheric Chemistry and Physics*, *12*(9), 4181-4206.

Mao, H., et al. (2008), Seasonal and diurnal variations of Hg(0) over New England, *Atmos. Chem. Phys.*, *8*(5), 1403-1421.

Mergler, D., et al. (2007), Methylmercury exposure and health effects in humans: A worldwide concern, *Ambio*, *36*(1), 3-11.

Muramatsu, H., et al. (2008), Variation of Be-7 concentration in surface air at Nagano, Japan, *J. Radioanal. Nuc. Chem.*, *275*(2), 299-307.

National Atmospheric Deposition Program: Mercury Deposition Network (MDN): A NADP

Network, available at: http://nadp. sws.uiuc.edu/MDN/, 2011.

Odum, J. R., et al. (1996), Gas/particle partitioning and secondary organic aerosol yields, *Environ. Sci. Technol.*, *30*(8), 2580-2585.

Pacyna, E. G., et al. (2010), Global emission of mercury to the atmosphere from anthropogenic sources in 2005 and projections to 2020, *Atmos. Environ.*, *44*(20), 2487-2499.

Pacyna, J.: personal communication in, Halifax, Nova Scotia, Canada, 26 July 2011.

Pankow, J. F. (1987), Review and comparative-analysis if the theories on partitioning between the gas and aerosol particulate phases in the atmosphere, *Atmos. Environ.*, *21*(11), 2275-2283.

Pankow, J. F. (1994), An absorption-model of the gas aerosol partitioning involved in the formation of secondary organic aerosol, *Atmos. Environ.*, *28*(2), 189-193.

Pankow, J. F., et al. (1993), Effects of relative humidity on gas-particle partitioning of semivolatile organic-compounds to urban particulate matter, *Environ. Sci. Technol.*, *27*(10), 2220-2226.

Petersen, G., et al. (1998), A comprehensive Eulerian modeling framework for airborne mercury species: Development and testing of the tropospheric chemistry module (tcm), *Atmos. Environ.*, *32*(5), 829-843.

Poissant, L., et al. (2004), Atmospheric mercury speciation and deposition in the Bay St. Francois wetlands, *J. of Geophys. Res.* , *109*(D11), 11.

Rutter, A. P., and J. J. Schauer (2007a), The effect of temperature on the gas-particle partitioning of reactive mercury in atmospheric aerosols, *Atmos. Environ.*, *41*(38), 8647-8657.

Rutter, A. P., and J. J. Schauer (2007b), The impact of aerosol composition on the particle to gas partitioning of reactive mercury, *Environ. Sci. Technol.*, *41*(11), 3934-3939.

Rutter, A. P., et al. (2008a), Evaluation of an offline method for the analysis of atmospheric reactive gaseous mercury and particulate mercury, *J. Air Waste Manage. Assoc.*, *58*(3), 377-383.

Rutter, A. P., et al. (2008b), A comparison of speciated atmospheric mercury at an urban center and an upwind rural location, *J. Environ. Monit.*, *10*(1), 102-108.

Sakata, M., and K. Marumoto (2002), Formation of atmospheric particulate mercury in the Tokyo metropolitan area, *Atmospheric Environment*, *36*(2), 239-246.

Sanei, H., et al. (2010), Wet deposition mercury fluxes in the Canadian sub-arctic and southern Alberta, measured using an automated precipitation collector adapted to cold regions,

Atmospheric Environment, *44*(13), 1672-1681.

Scheulhammer, A. M., et al. (2007), Effects of environmental methylmercury on the health of wild birds, mammals, and fish, *Ambio*, *36*(1), 12-18.

Schroeder, W. H., and J. Munthe (1998), Atmospheric mercury - an overview, *Atmospheric Environment*, *32*(5), 809-822.

Seigneur, C., et al. (2001), Multiscale modeling of the atmospheric fate and transport of mercury, *J. Geophys. Res.-Atmos.*, *106*(D21), 27795-27809.

Seigneur, C., et al. (2003), On the effect of spatial resolution on atmospheric mercury modeling, *Sci. Total Environ.*, *304*(1-3), 73-81.

Seigneur, C., et al. (1998), Mercury adsorption to elemental carbon (soot) particles and atmospheric particulate matter, *Atmos. Environ.*, *32*(14-15), 2649-2657.

Seinfeld, J. H., and S. N. Pandis (2006), *Atmospheric chemistry and physics: From air pollution to climate change*, 2nd ed., 1203 pp., John Wiley & Sons, Inc.

Selin, N. E., and D. J. Jacob (2008a), Seasonal and spatial patterns of mercury wet deposition in the United States: Constraints on the contribution from North American anthropogenic sources, *Atmos. Environ.*, *42*, 5193-5204.

Selin, N. E., et al. (2008b), Global 3-D land-ocean-atmosphere model for mercury: Present-day versus preindustrial cycles and anthropogenic enrichment factors for deposition, *Global Biogeochem. Cycles*, *22*(3), GB3099.

Selin, N. E., et al. (2007), Chemical cycling and deposition of atmospheric mercury: Global constraints from observations, *J. Geophys. Res.*, *112*(D2), 14.

Sheffield, A. E., and J. F. Pankow (1994), Specific surface-area of urban atmospheric particulate matter in Portland, Oregon, *Environ. Sci. Technol.*, *28*(9), 1759-1766.

Sigler, J. M., et al. (2009), Gaseous elemental and reactive mercury in southern New Hampshire, *Atmos. Chem. Phys.*, *9*(6), 1929-1942.

Skov, H., et al. (2006), Fluxes of reactive gaseous mercury measured with a newly developed method using relaxed eddy accumulation, *Atmospheric Environment*, *40*(28), 5452-5463.

Soerensen, A. L., et al. (2010), An improved global model for air-sea exchange of mercury: High concentrations over the North Atlantic, *Environ. Sci. Technol.*, *44*(22), 8574-8580.

Sunderland, E. M., and R. P. Mason (2007), Human impacts on open ocean mercury concentrations, *Global Biogeochem. Cycles*, *21*(4), GB4022.

Swartzendruber, P. C., et al. (2006), Observations of reactive gaseous mercury in the free troposphere at the Mount Bachelor Observatory, *J. Geophys. Res.-Atmos.*, *111*(D24), 12.

Talbot, R., et al. (2011), Comparison of particulate mercury measured with manual and automated methods, *Atmosphere*, *2*, 1-20.

ter Schure, A., et al. (2011), An integrated approach to asses elevated mercury wet deposition and concentrations in the south eastern United States, paper presented at 10th International Conference on Mercury as a Global Pollutant, Halifax, Nova Scotia, Canada, 26 July 2011.

Vijayaraghavan, K., et al. (2008), Plume-in-grid modeling of atmospheric mercury, *J. Geophys. Res.*, *113*, 12.

Wang, Q., et al. (2011), Sources of carbonaceous aerosols and deposited black carbon in the arctic in winter-spring: Implications for radiative forcing, *Atmospheric Chemistry and Physics*, *11*, 12453-12473.

Wang, S. X., et al. (2010), Mercury emission and speciation of coal-fired power plants in China, *Atmospheric Chemistry and Physics*, *10*(3), 1183-1192.

Wang, Y. H., et al. (1998), Global simulation of tropospheric O_3-NO_x-hydrocarbon chemistry 1. Model formulation, *J. Geophys. Res.*, *103*(D9), 10713-10725.

Weiss-Penzias, P., et al. (2009), Observations of speciated atmospheric mercury at three sites in Nevada: Evidence for a free tropospheric source of reactive gaseous mercury, *J. Geophys. Res.*, *114*, 11.

Weiss-Penzias, P. S., et al. (2011), Sources of gaseous oxidized mercury and mercury dry deposition at two southeastern US sites, *Atmospheric Environment*, *45*(27), 4569-4579.

Wesely, M. L. (1989), Parameterization of surface resistances to gaseous dry deposition in regional-scale numerical-models, *Atmos. Environ.*, *23*(6), 1293-1304.

Xiu, G. L., et al. (2009), Speciated mercury in size-fractionated particles in Shanghai ambient air, *Atmospheric Environment*, *43*(19), 3145-3154.

Yamasaki, H., et al. (1982), Effects of ambient temperature on aspects of airborne polycyclic aromatic hydrocarbons, *Environ. Sci. Technol.*, *16*(4), 189-194.

Yoshimori, M. (2005), Beryllium 7 radionucleide as a tracer of vertical air mass transport in the troposphere, in *Atmos. Remote sensing*, edited by J. P. Burrows and K. U. Eichmann, pp. 828-832, Elsevier Science Ltd, Oxford.

Zhang, L., et al. (2011), Improved estimate of the policy-relevant background ozone in the united states using the GEOS-chem global model with 1/2 degrees x 2/3 degrees horizontal resolution over North America, *Atmospheric Environment*, *45*(37), 6769-6776.

Zhang, Y., et al. (2012), Nested-grid simulation of mercury over North America, *Atmospheric Chemistry and Physics*, *12*(14), 6095-6111.

Chapter 3. Legacy impacts of all-time anthropogenic emissions on the global mercury cycle

[Amos, H. M., Jacob, D. J., Streets, D. G., Sunderland, E. M., 2013. Legacy impacts of all-time anthropogenic emissions on the global mercury cycle. Global Biogeochemical Cycles, 27, GBC20040.

Abstract

Elevated mercury (Hg) in marine and terrestrial ecosystems is a global health concern because of the formation of toxic methylmercury. Humans have emitted Hg to the atmosphere for millennia and this Hg has deposited and accumulated into ecosystems globally. Here we present a global biogeochemical model with fully-coupled atmospheric, terrestrial and oceanic Hg reservoirs to better understand human influence on Hg cycling and timescales for responses. We drive the model with a historical inventory of anthropogenic emissions from 2000 BC to present. Results show that anthropogenic perturbations introduced to surface reservoirs (atmosphere, ocean, or terrestrial) accumulate and persist in the subsurface ocean for decades to centuries. The simulated present-day atmosphere is enriched by a factor of 2.6 relative to 1840 levels, consistent with sediment archives, and by a factor of 7.5 relative to natural levels (2000 BC). Legacy anthropogenic Hg re-emitted from surface reservoirs accounts for 60% of present-day atmospheric deposition, compared to 27% from primary anthropogenic emissions, and 13% from natural sources. We find that only 17% of the present-day Hg in the surface ocean is natural, and that half of its anthropogenic enrichment originates from pre-1950 emissions. Although Asia is presently the dominant contributor to primary anthropogenic emissions, only

17% of the surface ocean reservoir is of Asian anthropogenic origin, as compared to 30% of North American and European origin. The accumulated burden of legacy anthropogenic Hg means that future deposition will increase even if primary anthropogenic emissions are held constant. Aggressive global Hg emissions reductions will be necessary just to maintain oceanic Hg concentrations at present levels.

3.1 Introduction

Hg cycles naturally through geochemical reservoirs, but human activities such as mining and more recently fossil fuel combustion have been increasing the Hg flux from the deep mineral reservoir to the atmosphere for millennia [*Nriagu*, 1993; 1994; *Lacerda et al.*, 1997; *Camargo*, 2002]. Here we present a global biogeochemical model of Hg that dynamically couples the ocean, atmosphere, and terrestrial reservoirs. We force the model with a historical inventory of anthropogenic emissions [*Streets et al.*, 2011], quantify the resulting present-day enrichment of the various global Hg reservoirs, and discuss implications for the future.

Hg is liberated from the deep mineral reservoir naturally (e.g., volcanoes) or by human activities cycles between the atmosphere and surface reservoirs (ocean and terrestrial ecosystems) on timescales of years to decades [*Mason et al.*, 1994; *Mason and Sheu*, 2002; *Selin et al.*, 2008]. It is eventually transferred to recalcitrant soil pools [*Smith-Downey et al.*, 2010] and the deep ocean [*Gill and Fitzgerald*, 1988; *Sunderland and Mason*, 2007] over centuries, and back to the deep mineral reservoir over millennia [*Andren and Nriagu*, 1979]. Anthropogenic enrichment of the ocean is of particular interest because Hg exposure for most human populations is from methylmercury in marine fish [*Johansen et al.*, 2004; *Sunderland*, 2007; *Kim et al.,* 2010].

Sedimentary and ice core records provide evidence of a two- to five-fold enrichment in present-day atmospheric Hg deposition relative to preindustrial (ca. 1840) levels [*Fitzgerald et al.*, 1998; *Schuster et al.*, 2002; *Biester et al.*, 2007; *Lindberg et al*., 2007]. This reflects growing emissions in Europe and North America over the 19th and 20th centuries, compounded by growth in Asian emissions over the past decades [*Pacyna et al.*, 2003, 2006; *Wu et al.,* 2006; *Pacyna et al.*, 2010; *Streets et al.*, 2011]. However, pre-1850 anthropogenic emissions were also large [*Nriagu*, 1993; *Streets et al*., 2011], as shown by long-term peat and sediment records [*Roos-Barraclough et al.*, 2002, 2006; *Cooke et al.*, 2009; *Elbaz-Poulichet et al.*, 2011]. This historical anthropogenic Hg continues to cycle through biogeochemical reservoirs, representing a legacy of Hg enrichment in the environment.

Understanding how the legacy of past historical anthropogenic emissions impacts the present-day Hg cycle is necessary for projecting future changes. Global anthropogenic emissions are expected to increase in the future in the absence of directed efforts to control Hg [*Streets et al.*, 2009]. The new global Hg treaty negotiated by the United Nations Environment Program (UNEP) aims to reduce anthropogenic sources [*UNEP*, 2013]. Here we examine how the global ocean, atmosphere, and terrestrial ecosystems will respond to future changes in emissions.

3.2 Model description

We develop a fully coupled, seven-reservoir box model of the global Hg cycle by building on previous models that focused on individual components of the cycle [*Sunderland and Mason*, 2007; *Selin et al*., 2008; *Soerensen et al*., 2010; *Holmes et al*.2010; *Smith-Downey et al*., 2010]. Much of this previous work used the GEOS-Chem global 3-D model for atmospheric Hg coupled to 2-D surface reservoirs (http://geos-chem.org). Our seven-box model allows full

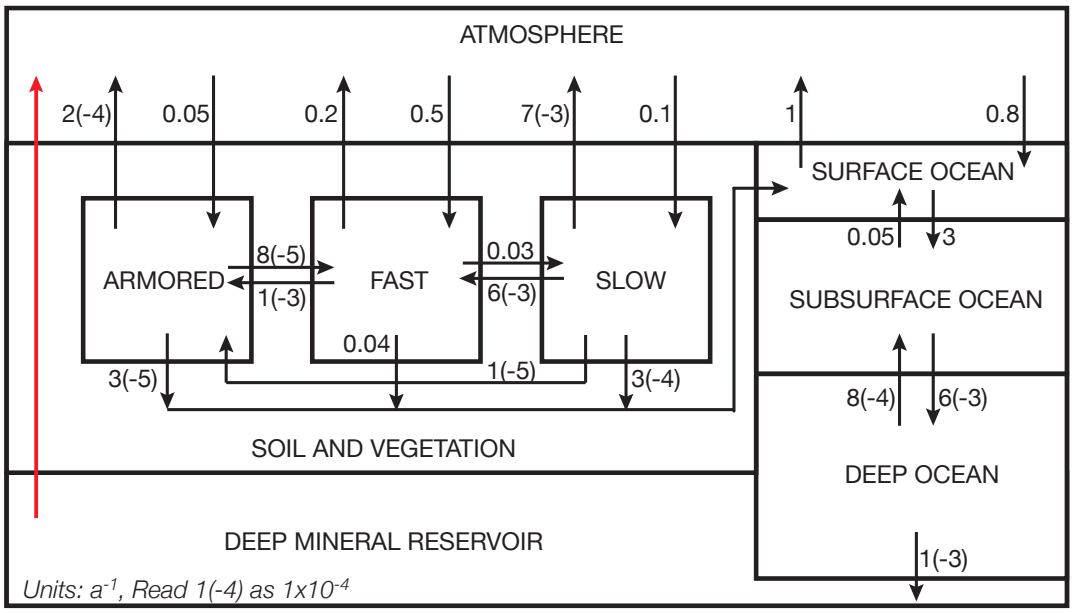

Figure 3.1: Rate coefficients k_{ij} (a^{-1}) driving our 7-reservoir global biogeochemical box model for Hg. k_{ij} defines the first-order transfer from reservoir i to reservoir j as $F_{ij}=k_{ij}m_i$, where F_{ij} (Mg a^{-1}) is the Hg flow from reservoir i to reservoir j and m_i (Mg) is the mass of Hg in reservoir i. Values of k_{ij} are derived from best estimates of present-day flows and masses from the literature (Table 3.1) and are assumed to be constant in time. The red arrow represents the external forcing by primary emissions (geogenic or anthropogenic) from the deep mineral reservoir. Geogenic emissions are constant (90 Mg a^{-1}) and anthropogenic emissions are time-dependent (Figure 3.2).

coupling of the ocean, atmosphere, and terrestrial reservoirs for millennium-scale simulations. The seven reservoirs include the atmosphere, ocean (surface, subsurface, deep), and terrestrial ecosystems (fast terrestrial, slow soil, armored soil), as described below. Hg transferred from the deep mineral reservoir to the atmosphere by geogenic or anthropogenic emissions is viewed as an external forcing since the residence time of Hg in the deep mineral reservoir is ~1 billion years [*Andren and Nriagu*, 1979]. Burial from the deep ocean returns Hg to the deep mineral reservoir.

Figure 3.1 provides a schematic of the box model. Mass transfer between model reservoirs is represented by a system of coupled first-order differential equations

Table 3.1 Present-day Hg reservoirs and flows[a]

	Flows (Mg a^{-1})
Atmosphere: 5000 Mg	
Hg(II) deposition to ocean	3900
Hg(0) deposition to ocean	40
Hg(II) deposition to land[b]	1500
Hg(0) deposition to land[c]	1500
Surface ocean[d]**:** 2900 Mg	
Hg(0) evasion	3000
Particle settling to subsurface ocean	3300
Water transfer to subsurface ocean	5100
Subsurface ocean[e]**:** 130,000 Mg	
Particle settling to deep ocean	480
Water transfer to surface ocean	7100
Water transfer to deep ocean	340
Deep ocean: 220,000 Mg	
Burial to deep sediments	210
Water transfer to subsurface ocean	180
Fast terrestrial pool: 9600 Mg	
Evasion due to respiration of organic carbon	460
Photochemical re-emission of deposited Hg	850
Biomass burning[f]	290
Transfer to slow pool	330
Transfer to armored pool	10
River runoff to surface ocean[g]	365
Slow soil pool: 35,000 Mg	
Evasion due to respiration of organic carbon	250
Biomass burning	8
Transfer to fast pool	210
River runoff to surface ocean	10
Armored soil pool: 190,000 Mg	
Evasion due to respiration of organic carbon	25
Biomass burning	4
Transfer to fast pool	15
River runoff to surface ocean	5
Deep mineral reservoir: 3×10^{11} Mg	
Geogenic emission	90
Anthropogenic emissions	2000[h]

[a] The best estimates of present-day reservoirs m_I and flows F_{ij} given in this Table are used to derive the rate coefficients $k_{ij} = F_{ij} / m_i$ in Figure 3.1. References are *Holmes et al.* [2010] for the atmosphere and biomass burning, *Soerensen et al.* [2010] for the surface ocean, *Sunderland and Mason* [2007] for the subsurface/deep ocean and river runoff, *Smith-Downey et al.* [2010] for the terrestrial/soil pools, and *Andren and Nriagu* [1979] and *Pirrone et al.* [2010] for the deep mineral reservoir.

(Continued)
[b]Partitioned 50% to the fast terrestrial pool, 32% to the slow soil pool, and 18% to the armored soil pool following *Smith-Downey et al.* [2010].
[c]All Hg(0) deposition is delivered to the fast terrestrial pool.
[d]Extending down to the base of the ocean mixed layer.
[e]Extending from the base of the ocean mixed layer down to the depth of the permanent thermocline.
[f]Total biomass burning is 300 Mg a^{-1} [*Holmes et al.*, 2010] and is apportioned as 95% from vegetation (fast terrestrial pool) and 5% from the three soil pools (fast, slow, armored) based on carbon content [*Smith-Downey et al.*, 2010].
[g]Total river runoff is 380 Mg a^{-1} [*Sunderland and Mason*, 2007] and is partitioned among the soil pools in the same manner as biomass burning.
[h]Anthropogenic emissions are time-dependent (see Figure 3.2a). 2000 Mg a^{-1} corresponds to the year 2008 from *Streets et al.* [2011].

$$\frac{d\mathbf{m}}{dt} = \mathbf{Km} + \mathbf{s} \qquad (3.1)$$

where **m** is a 7-element vector of reservoir masses (Mg of Hg), **s** is a vector describing the external forcing (Mg a^{-1}) from the deep mineral reservoir (0 for all reservoirs except for the atmosphere), and **K** is a 7x7 matrix of first-order time-invariant rate coefficients k_{ij} (a^{-1}) describing the flow from reservoir i to reservoir j . Thus $k_{ij} = F_{ij}/m_i$, where F_{ij} (Mg a^{-1}) is the flow (sink) from reservoir i to reservoir j, and m_i (Mg) is the mass of reservoir i. The flows are not thought to be limited by Hg, so the assumption of first-order behavior is reasonable. We derive values of k_{ij} from literature estimates of present-day masses and flows, as summarized in **Table 3.1** and described below. Estimates in **Table 3.1** account for Hg speciation (Hg(0), Hg(II), particulate Hg), but here we only track total Hg.

The physical and chemical processes driving the flows F_{ij} are unlikely to have changed significantly over the Holocene, supporting the use of time-invariant k_{ij}. An exception may be the rate of atmospheric oxidation of Hg(0), which determines the rate coefficient for transfer from

the atmosphere to the surface reservoirs (1.5 a^{-1} in **Figure 3.1**, corresponding to an atmospheric lifetime of 8 months). Atmospheric oxidant levels may have been affected by human activity, but the resulting atmospheric lifetime of Hg is unlikely to have changed by more than a factor of 2 from present to pre-industrial or over the Holocene [*Thompson et al.*, 1993; *Parrella et al.*, 2012] and is therefore short relative to the decadal and longer time scales of interest here. Changing the pre-industrial atmospheric lifetime of Hg by a factor of 2 in our model has an inverse effect on the simulated atmospheric reservoir amount but no effect on any other model results including the pre-industrial-to-present enrichment factor for atmospheric deposition.

3.2.1 Atmosphere

We adopt the present-day atmospheric reservoir and deposition estimates from the GEOS-Chem simulation of *Holmes et al.* [2010] (**Table 3.1**), which show no systematic biases against observations. The atmospheric reservoir is 5000 Mg and the total deposition is 6900 Mg a^{-1}, corresponding to an atmospheric lifetime of 0.7 years. Other literature estimates give a range of 4600-5600 Mg for the atmospheric reservoir, 4200-9000 Mg a^{-1} for total deposition, and 0.5-1.5 years for atmospheric lifetime [*Slemr et al.*, 1985; *Lindqvist and Rhode*, 1985; *Mason et al.,* 1994; *Shia et al.*, 1999; *Mason and Sheu*, 2002; *Lamborg et al.*, 2002b; *Seigneur et al.*, 2004; *Selin et al.,* 2008; *Amos et al.,* 2012].

3.2.2 Ocean

We partition the ocean into three reservoirs: (1) the surface ocean extending to the base of the mixed layer, (2) the subsurface ocean extending to the depth of the permanent thermocline (1500 m based on *Sunderland and Mason* [2007]), and (3) the deep ocean extending to the sea

floor. Our surface ocean budget, including air-sea exchange, is based on the GEOS-Chem simulation of *Soerensen et al.* [2010], which uses a global mean mixed layer depth of 54 m based on observations [*Montegut et al*., 2004]. Subsurface and deep ocean reservoirs are estimated from vertical Hg profile data following *Sunderland and Mason* [2007].

Hg flows/sinks from ocean reservoirs include evasion to the atmosphere, settling of particulate matter including eventual burial in deep-sea sediments, and vertical transport of seawater. Particle settling is based on carbon export fluxes (ocean rain) using the parameterization of *Antia et al.* [2001] and global ocean productivity from MODIS satellite data (see *Soerensen et al.* [2010] and *Sunderland and Mason* [2007] for details). Burial to deep ocean sediments returns Hg to the deep mineral reservoir. *Sunderland and Mason* [2007] estimate the present-day range in burial to be 180-260 Mg a^{-1}. Model results are relatively insensitive (<10%) to this range.

3.2.3 Terrestrial ecosystems

Terrestrial Hg is partitioned into three reservoirs based on the Global Terrestrial Mercury Model (GTMM) of *Smith-Downey et al.* [2010]: fast terrestrial reservoir, slow soil, and armored soil. The fast terrestrial reservoir includes vegetation, litter, labile organic carbon soil pools, and ice and snow-covered terrestrial surfaces [*Smith-Downey et al.*, 2010]. Slow and armored soil pools are defined by long turnover times for organic carbon mineralization, with armored soils being the most recalcitrant. GTMM is based on the association of Hg with organic carbon and uses soil carbon pools and turnover times from the CASA biogeochemical model for carbon [*Potter et al.*, 1993; *van der Werf et al.*, 2003]

Hg from terrestrial reservoirs is transferred to the atmosphere by respiration of organic carbon, photoreduction, and biomass burning; and to the surface ocean by river runoff. Hg emissions associated with organic carbon decomposition (740 Mg a^{-1}) are from *Smith-Downey et al.* [2010]. Global estimates of photoreduction are in the range 260-1100 Mg a^{-1} [*Selin et al*., 2008; *Smith-Downey et al.*, 2010; *Holmes et al.*, 2010]. We adopt a value of 850 Mg a^{-1} to balance emissions and deposition in our atmospheric budget. Global biomass burning emission estimates range from 300 Mg a^{-1} [*Holmes et al.*, 2010] to 675 Mg a^{-1} [*Friedli et al.*, 2009]. We use 300 Mg a^{-1} here, but a larger biomass burning source could be equivalently accommodated in our model by decreasing the photoreduction source. We assume that 95% of the biomass burning source is from the fast terrestrial reservoir (which includes vegetation) and the remaining 5% is partitioned among the fast, slow, and armored soils based on their respective soil organic carbon content, following *Smith-Downey et al.* [2010]. River runoff is 380 Mg a^{-1} from *Sunderland and Mason* [2007] and is partitioned among terrestrial pools in the same manner as biomass burning.

3.2.4 Geogenic emission

We define geogenic emission as Hg liberated from the deep mineral reservoir by volcanic activity, crustal degassing, and weathering [*Nriagu and Becker*, 2003]. *Andren and Nriagu* [1979] estimated the size of the deep mineral reservoir to be $3x10^{11}$ Mg. Estimates of geogenic range from ~1 to 1000 Mg a^{-1} [*Varrekamp and Buseck*, 1986; *Ferrara et al.*, 2000; *Nriagu and Becker*, 2003; *Pyle and Mather*, 2003; *Bagnato et al.*, 2011], but little confidence is placed in the extrema of this range [*Pyle and Mather*, 2003; *Bagnato et al.,* 2011]. We use 90 Mg a^{-1} from *Pirrone et al.* [2010], which is consistent with the estimate of *Bagnato et al.* [2011] (95 Mg a^{-1}) derived from atmospheric observations of volcanic plumes.

3.2.5 Anthropogenic emissions

We force the model from 2000 BC to 2008 AD with primary anthropogenic emissions of total Hg, as shown in **Figure 3.2a**. "Primary" refers to direct transfer from the deep mineral reservoir to the atmosphere. *Streets et al.* [2011] give a best estimate of 2000 Mg a^{-1} for 2008 emissions (referred to here as "present-day"), a total of 215 Gg for 1850-2008 emissions with decadal information on emission sectors and source regions, and a pre-1850 total of 137 Gg without temporal information. Based on the work of *Nriagu* [1993] and *Streets et al.* [2011], we estimate that 111 Gg of that total was emitted between 1570 and 1850, mainly in association with silver mining in Spanish America. The remaining 26 Gg is emitted before 1570 AD.

Sediment cores [*Cooke et al.*, 2009; *Elbaz-Poulichet et al.*, 2011] and archaeological evidence [*Goldwater*, 1972 and references therein; *Nriagu*, 1979 and references therein] suggest more than 3500 years of Hg releases from human activity. We initiate anthropogenic Hg emissions in 2000 BC based on use of Hg as pigment as far back as 2500-1600 BC by the Greeks, reports of quicksilver found in a tomb dating to ~2000 BC, and use of Hg (as quicksilver and cinnabar) by the Assyrians as early as 1900 BC [*Goldwater*, 1972]. We assume a linear increase in emissions from 2000 BC until 1570 AD, a step increase at 1570 AD due to silver production in Spanish America [*Nriagu*, 1993; 1994; *Camargo* et al., 2002] and constant emissions between 1570 and 1850 AD. Model results are insensitive to the details of this emission schedule, as discussed in Section 3.3.

Streets et al. [2009] projected future Hg emissions out to 2050 using the IPCC SRES scenarios [*Nakicenovic et al.,* 2000]. The A1B business-as-usual scenario features continued growth in emissions such that primary anthropogenic emissions in 2050 are a factor of 3.6 higher than present-day. The most optimistic SRES scenario (B1) has effectively constant emissions

relative to present-day levels [*Streets et al.,* 2009]. These scenarios assume no direct policy intervention for Hg control, but some level of intervention may be anticipated in light of the recent Hg treaty negotiated by UNEP [*UNEP,* 2013]. To illustrate the potential benefit of emission controls, we consider a "mercury controls" scenario where primary anthropogenic emissions decline by 2050 to 50% of their present-day value. Achieving this level of reduction would require implementation of Hg-specific control technologies across multiple sectors (fuel combustion, mining, waste incineration, industry). We also consider a "zero emissions" scenario where primary anthropogenic emissions are completely eliminated as of 2015. This bounds the maximum achievable global benefit from regulating emissions. Business-as-usual is assumed between 2008 and 2015, and all scenarios take effect in 2015.

3.3 Historical reconstruction and uncertainty

3.3.1 Historical reconstruction and model evaluation

We first apply the model to simulate natural steady state conditions, defined by solving (3.1) for $d\mathbf{m}/dt = \mathbf{0}$ with $\mathbf{s}$ = 90 Mg a^{-1} as the constant geogenic source. **Table 3.2** shows the resulting natural distribution of Hg between reservoirs. From this initial condition we force the model with historical anthropogenic emissions (2000 BC - present), shown in **Figure 3.2a**. **Table 3.2** shows the resulting pre-industrial (1840) and present-day reservoir masses.

Figure 3.3 depicts our simulated present-day global budget. Reservoir masses and flows are comparable to the literature values of **Table 3.1** used to construct the model, even though these literature values were used only to constrain the first-order rate coefficients in the model. This demonstrates consistency between present-day anthropogenic enrichments and our historical inventory of anthropogenic emissions. It provides an independent check because we do

Table 3.2 Hg reservoir masses and historical anthropogenic enrichments

	Reservoir mass (Mg)			Enrichment factor	
Reservoir	Natural	Preindustrial (1840)	Present-day	All-time[a]	Modern[b]
Atmosphere	700	2,000	5,300	7.5	2.6
Terrestrial					
Fast	1,900	4,800	11,000	5.8	2.3
Slow	9,800	24,000	50,000	5.1	2.1
Armored	170,000	180,000	210,000	1.2	1.1
Ocean					
Surface	530	1,300	3,100	5.9	2.3
Subsurface	26,000	67,000	140,000	5.3	2.1
Deep	95,000	130,000	200,000	2.1	1.5

[a]Ratio of present-day to natural reservoir mass
[b]Ratio of present-day to preindustrial (1840) reservoir mass

not impose a preindustrial-to-present enrichment in atmospheric deposition unlike previous reconstructions [*Mason et al.*, 1994; Mason *and Sheu*, 2002; *Seigneur et al.*, 2004; *Selin et al*., 2008; *Smith-Downey et al*., 2010]. The present-day atmospheric Hg reservoir is simulated to be 5300 Mg, within the range of 4600-5600 Mg constrained by observations (see Section 3.2.1). The mean ocean concentration above the thermocline (surface+subsurface) is 1.4 pM, consistent with the range of 0.5-2.5 pM given by *Mason et al*. [2012] from compiled observations. We find a modern (preindustrial-to-present) enrichment factor of 2.6 for atmospheric deposition, which is consistent with sediment core data indicating that atmospheric Hg deposition has increased by 2 to 5 times relative to pre-industrial levels [*Lamborg et al. 2002a*; *Biester et al.*, 2007; *Drevnick et al.*, 2012]. We conclude that our box model provides a realistic representation of the present-day budget of Hg in the different geochemical reservoirs and a plausible reconstruction of the historical anthropogenic enrichment.

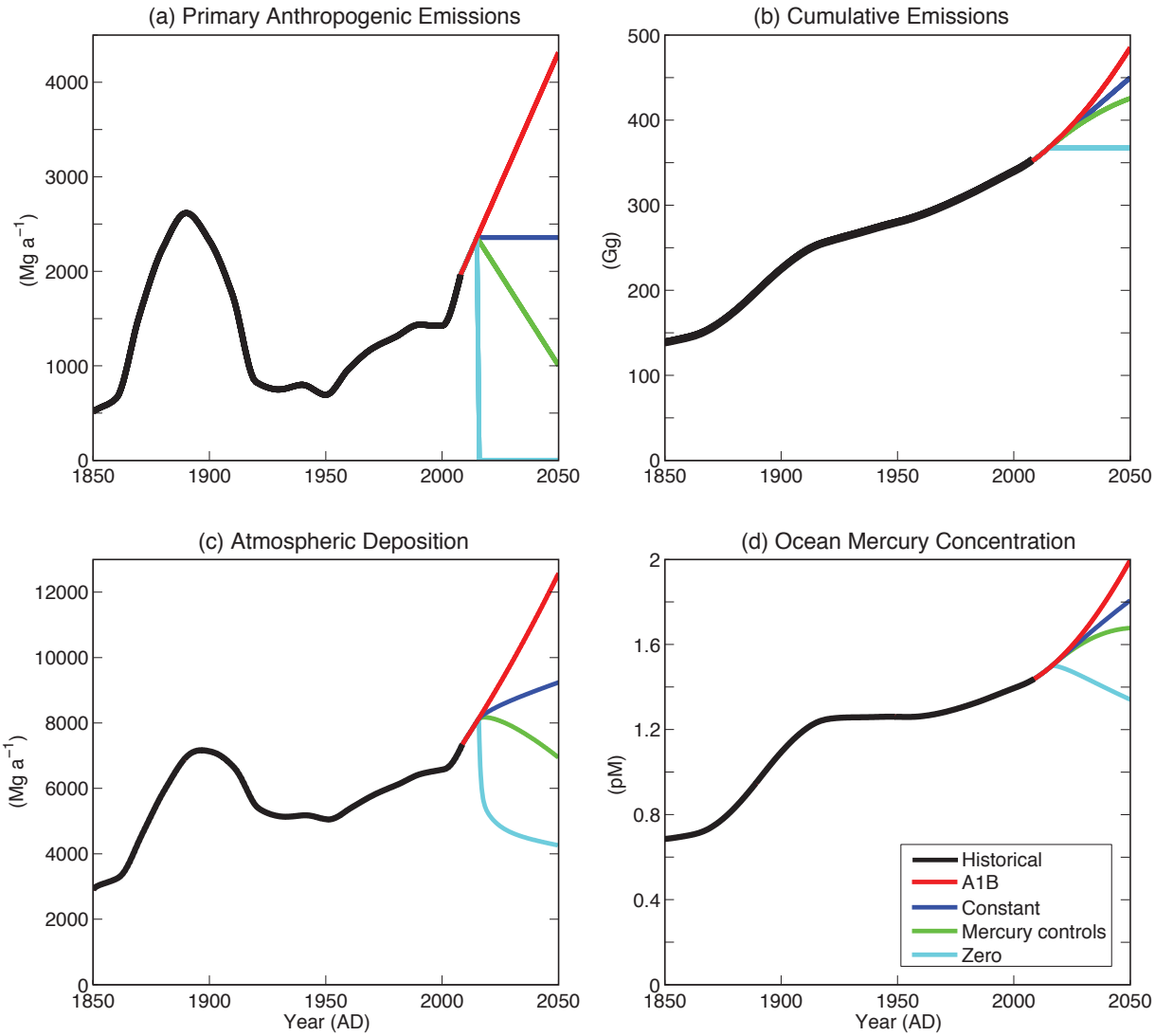

Figure 3.2: History of global anthropogenic influence on environmental Hg. (a) Primary anthropogenic emissions to the atmosphere, (b) corresponding cumulative emissions, (c) atmospheric deposition, and (d), combined surface+subsurface ocean mercury concentrations. 1850-2008 emissions are from *Streets et al*. [2011]. Pre-1850 emissions are as described in the text. Post-2008 emissions assume the business-as-usual A1B scenario of *Streets et al.* [2009] from 2008 to 2015 and different hypothetical emission trajectories afterward as described in the text.

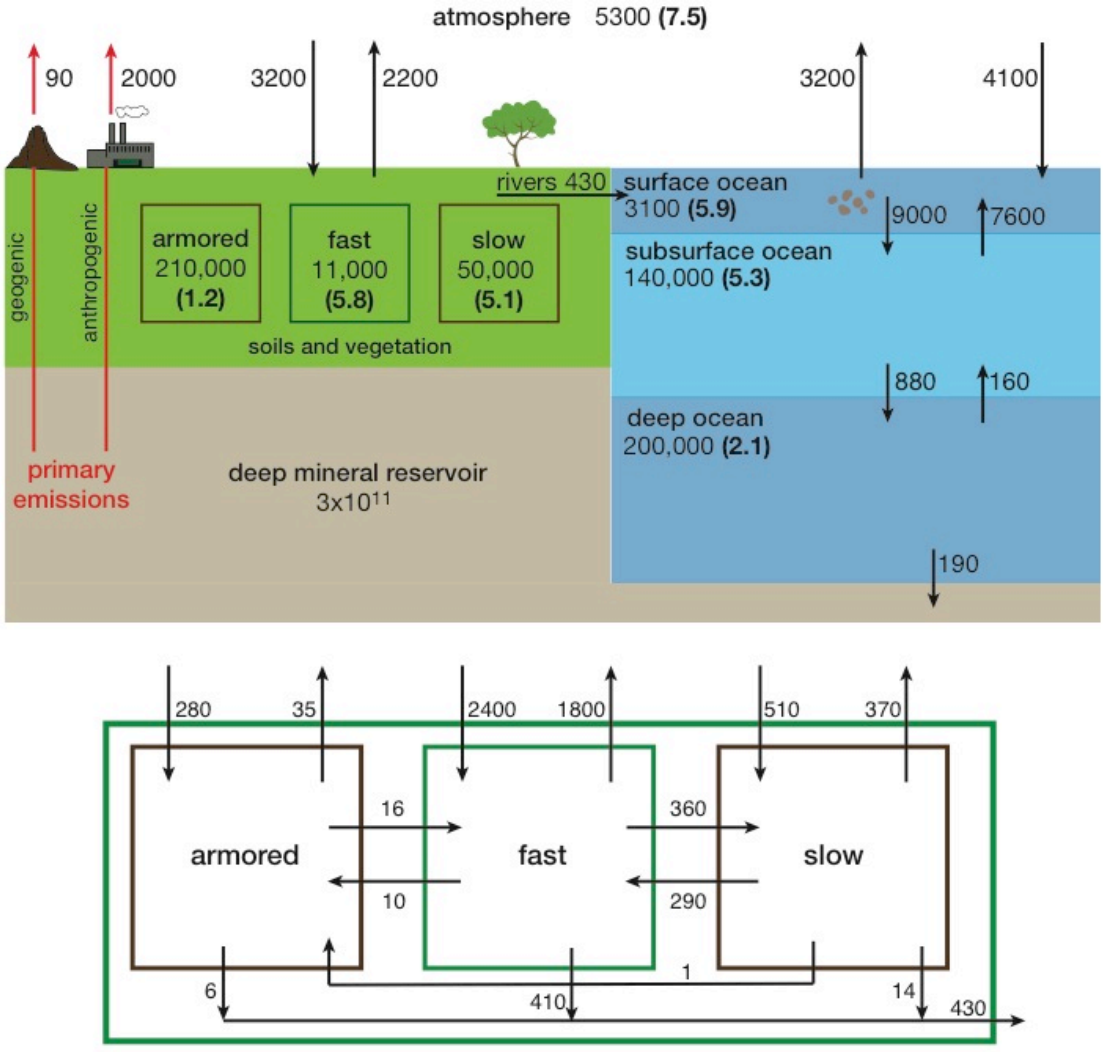

Figure 3.3: Simulated present-day global Hg budget and all-time anthropogenic enrichments factors. Terrestrial-atmosphere exchange is given in the top panel for the sum of terrestrial reservoirs. The bottom panel shows the breakdown and cycling between the different terrestrial reservoirs. All terrestrial reservoirs receive inputs from Hg(II) deposition (fast = 800, slow = 510, armored = 280 Mg a^{-1}). The fast reservoir also receives inputs from Hg(0) deposition (1600 Mg a^{-1}). All terrestrial reservoirs lose Hg through respiration (fast = 520, slow = 360, armored =30 Mg a^{-1}) and biomass burning (fast = 320, slow = 9, armored = 5 Mg a^{-1}). Photoreduction from the fast terrestrial reservoir is 950 Mg a^{-1}.

3.3.2 Uncertainty in natural processes

We applied perturbation analysis to examine how uncertainties in individual model terms affect simulated anthropogenic enrichments of the different Hg reservoirs, using the three observational constraints defined above: (1) present-day atmospheric reservoir (4600-5600 Mg), (2) present-day surface+subsurface ocean concentration (0.5-2.5 pM), and (3) pre-industrial-to-present enrichment factor in atmospheric deposition (2-5). We find that the simulated pre-industrial-to-present enrichment factor is most sensitive to uncertainties in geogenic emissions and oceanic evasion. The magnitude of geogenic emissions dictates the natural Hg loading and the resulting relative enrichment from primary anthropogenic emissions. Based on the observational constraints and reasonable estimates for primary anthropogenic emissions, geogenic emissions are unlikely to be more than four times larger than our adopted value of 90 Mg a^{-1} and could be smaller. Larger geogenic emissions decrease the relative anthropogenic enrichment and vice versa.

Oceanic evasion is the largest single input of Hg to the atmosphere and is a major removal pathway of Hg from the surface ocean (**Table 3.1** and **Figure 3.3**). *Qureshi et al.* [2011] highlighted the uncertainty in ocean evasion and its influence on the global biogeochemical cycle of Hg. Removal of Hg from the surface ocean is a competitive process between evasion and export to the subsurface ocean by particle scavenging. If evasion rates decrease, the net transfer to the subsurface ocean increases while atmospheric deposition decreases and there is an associated increase in the relative anthropogenic enrichment of atmospheric deposition. To be consistent with both the present-day atmospheric reservoir and the preindustrial-to-present enrichment in atmospheric deposition, we find that the rate coefficient of ocean evasion in our model must be within ±30% of our best estimate from **Figure 3.1**.

Perturbations to the rate coefficients for terrestrial cycling have less effect on our model results than geogenic emissions or oceanic evasion, in terms of the three observational constraints above. This is because, as discussed below, Hg perturbations to surface reservoirs propagate principally to the ocean. We see from **Figure 3.3** that the terrestrial reservoirs are only weakly coupled to one another and instead exchange principally with the atmosphere. However, such a result is contingent on the mechanistic basis for our terrestrial Hg model that presumes a strong association of Hg with organic matter [*Smith-Downey et al.*, 2010]. Better understanding of terrestrial cycling of Hg is needed.

3.3.3 Uncertainty in anthropogenic emissions

Streets et al. [2011] give uncertainties in the range of -30% to +60% for 1920-2008 anthropogenic emissions, with somewhat larger uncertainties before 1920. We estimate an uncertainty range of -50% and +300% for pre-1850 emissions, with additional uncertainty in the timing of these emissions. We conducted sensitivity simulations to investigate the effect of these uncertainties using the same three observational constraints as above to guide the analysis. We find that the timing and initiation (between 2000 and 500 BC) of pre-1570 anthropogenic emissions has no significant effect on model results because these emissions are small (best estimate of 26 Gg) and the associated Hg has been transferred by now to the deep ocean, armored soil, and deep mineral reservoir. Simulated all-time enrichment and the present-day budget (**Figure 3.3**) are also insensitive (<5%). We find also little sensitivity to the timing of 1570-1850 AD anthropogenic emissions. The simulated pre-industrial-to-present enrichment in atmospheric deposition decreases from a factor of 2.6 to 2.4 if the timing is shifted (based on *Nriagu* [1993]) to release 70% of these emissions during 1700-1850 AD rather than 50%.

The magnitude of all-time anthropogenic emissions has more impact on model results. We conducted sensitivity simulations following the lower or upper envelope of the historical range of emission uncertainties (see above). The resulting ranges for the lower-upper envelope of emissions are 4100-9000 Mg for the present-day atmospheric reservoir, 1.1-2.6 pM for the present-day surface+subsurface ocean concentration, and 2.9-2.0 for the pre-industrial-to-present enrichment factor in atmospheric deposition. The upper envelope is unrealistic, as reflected by its large overestimate of the present-day atmospheric reservoir. The lower envelope is within the uncertainty of observational constraints and will be used below to provide a lower limit on anthropogenic influence (Section 3.5). The all-time anthropogenic emissions for the lower envelope amount to 232 Gg, as compared to 352 Gg for our best estimate.

3.4 Timescales for Hg cycling and response to perturbations

3.4.1 Eigenanalysis of characteristic timescales

Understanding the timescales involved in Hg biogeochemical cycling is critical to interpreting the effects of anthropogenic perturbations. Residence times ($\tau_i = 1/\Sigma k_{ij}$) for individual reservoirs in our 7-box model provide a first estimate of these timescales but do not account for the coupling between reservoirs. Eigenanalysis of the 7x7 mass transfer matrix $\mathbf{K} = (k_{ij})$ in equation (1) identifies the true timescales of the coupled system [*Prather*, 1996]. Each eigenvector $\mathbf{x}_p$ ($p \in [1,7]$) with eigenvalue λ_p represents a normal mode of the model, and any perturbation to that mode decays exponentially with a characteristic timescale $-1/\lambda_p$.

Figure 3.4 shows the normal modes of our model and the corresponding characteristic timescales. Any initial-time perturbation $\mathbf{\Delta m}(0)$ to the model can be projected on the basis of

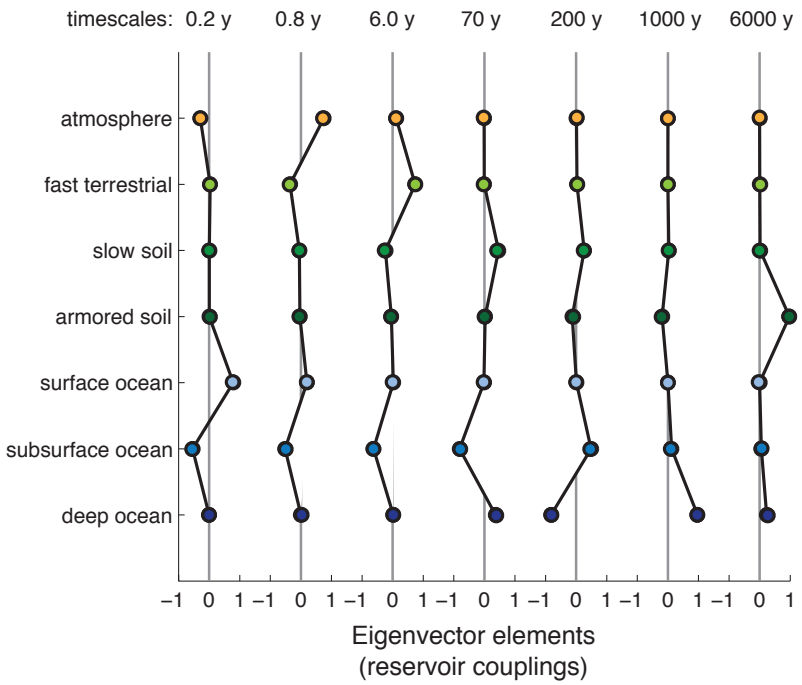

Figure 3.4: Normal modes of the Hg biogeochemical model. Each column describes an eigenvector of the mass transfer matrix **K** and represents a normal mode of the system. Perturbation to a normal mode decays exponentially with a timescale equal to the inverse of the corresponding eigenvalue. These timescales are displayed above the modes. The elements of the eigenvectors indicate the coupling between reservoirs associated with each timescale. For example, mode 1 (0.2 years) describes a strong coupling between the surface and subsurface ocean reservoirs, and a weak coupling with the atmosphere. Mode 2 (0.8 years) describes a strong coupling between the atmosphere and subsurface ocean. Figure 3.5 gives a schematic summary of the information in this figure highlighting the dominant couplings associated with each mode.

these normal modes as

$$\Delta\mathbf{m}(0) = \sum_{p=1}^{7} \alpha_p \mathbf{x}_p \tag{3.2}$$

where α_p are coefficients. Thus the perturbation decays as a sum of exponentials following

$$\Delta\mathbf{m}(t) = \sum_{p=1}^{7} \alpha_p \mathbf{x}_p \exp[\lambda_p t] \tag{3.3}$$

where the eigenvalues λ_p must be real and negative for the system to show stable behavior.

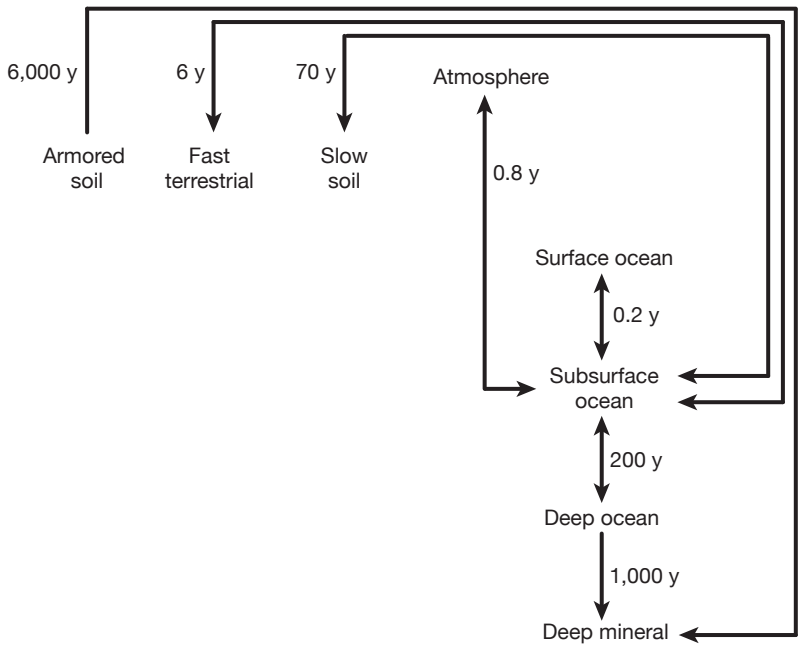

Figure 3.5: Characteristic timescales (years) for Hg biogeochemical cycling derived from eigenanalysis of our seven-compartment box model (see Section 3.4.1). The arrows indicate the principal reservoirs coupled over each timescale. These couplings often involve a combination or succession of transfers through intermediate reservoirs. More detail is presented in Figure 3.4.

Different perturbations will excite different combinations of modes (and hence reservoir couplings). The eigenlifetimes $-1/\lambda_p$ are the true timescales describing the dynamics of the model.

Each mode in **Figure 3.4** is defined by its eigenvector elements, describing the nature of the coupling between reservoirs for the corresponding timescale. Although all reservoirs are coupled on any of the timescales, there is always a dominant pair as is highlighted in the simplified schematic of **Figure 3.5**, which summarizes the information contained in **Figure 3.4**. The shortest Mode 1 ($-1/\lambda_1 = 0.2$ years) principally describes the fast exchange between the surface and subsurface ocean. Mode 2 (0.8 years) describes the coupling between the atmosphere and subsurface ocean via the surface ocean. Modes 3 (6 years) and 4 (70 years) couple

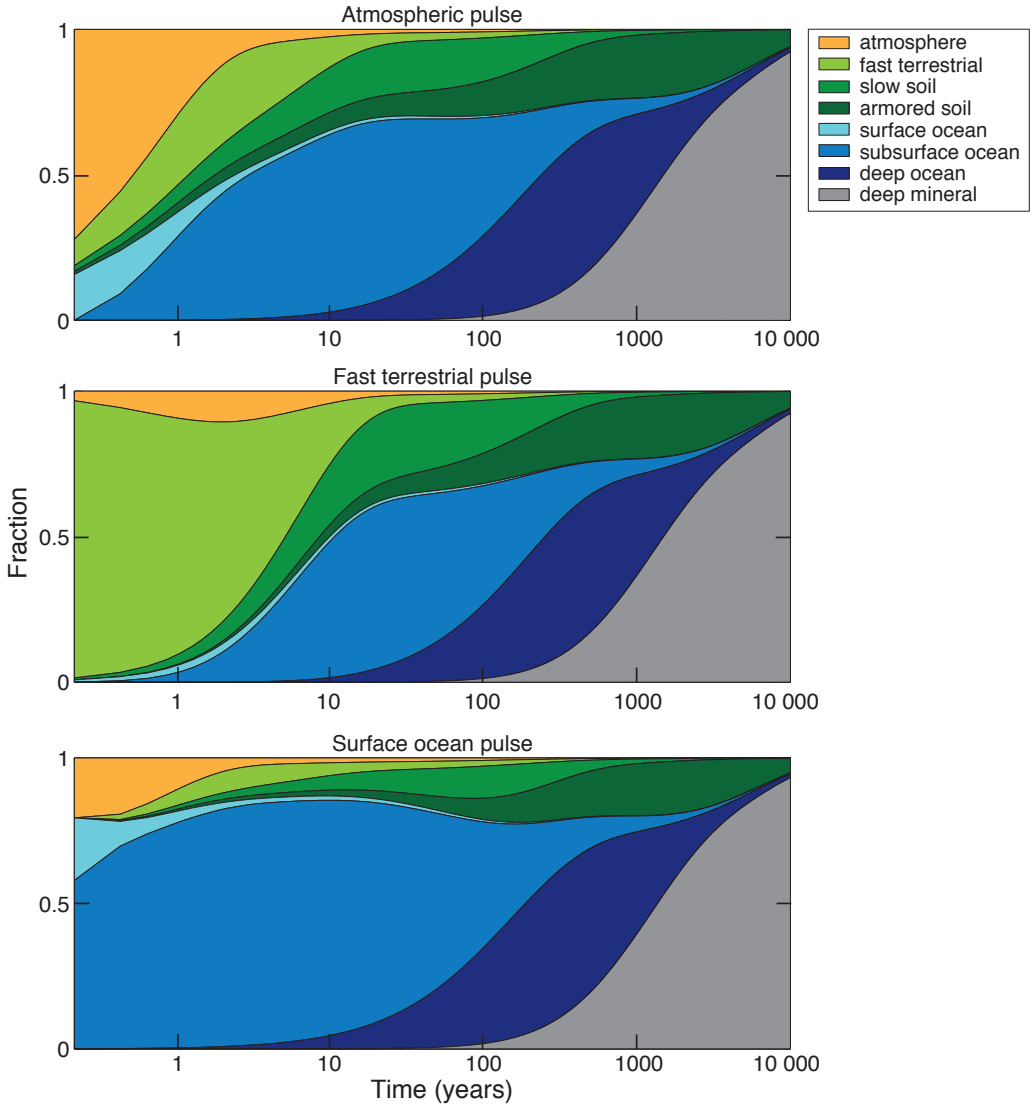

Figure 3.6: Time-dependent fate of a pulse of Hg released to the atmosphere (top panel), fast terrestrial pool (center), or surface ocean (bottom). A unit pulse of Hg is injected into the corresponding reservoir at time $t = 0$ years and the resulting mass fraction from that pulse in individual reservoirs is plotted as a function of time. Note the log scale for time.

respectively the fast and slow terrestrial pools to the subsurface ocean via the atmosphere and surface ocean. Mode 5 (200 years) couples the subsurface and deep ocean by vertical seawater mixing. Mode 6 (1000 years) describes the return of Hg to the deep mineral reservoir by burial from the deep ocean. Mode 7 (6,000 years) describes the ultimate decay of the perturbation by transfer from the armored soil reservoir to the deep mineral reservoir via ocean burial.

The subsurface ocean is known to be central in driving the biogeochemical Hg cycle [*Mason et al*., 1994; *Mason and Sheu*, 2002; *Sunderland and Mason*, 2007; *Mason et al.*, 2012; *Soerensen et al.*, 2012], and this is apparent in **Figure 3.5**. We see from **Figure 3.5** that the subsurface ocean is coupled to the atmosphere via deposition and air-sea exchange (0.8 years), to the fast and slow terrestrial reservoirs via river runoff and atmospheric cycling (6-70 years), and to the deep ocean (200 years) from which Hg is eventually buried in deep-sea sediments. We also see from **Figures 3.4** and **3.5** that the different terrestrial reservoirs are only weakly coupled between themselves and instead exchange Hg principally through the atmosphere-ocean system, emphasizing again the role of the subsurface ocean.

3.4.2 Fate of Hg released in surface reservoirs

Figure 3.6 illustrates the fate of a pulse of Hg released in different surface reservoirs as computed from our box model. Here a unit pulse of Hg is released at time $t = 0$ in the atmosphere (top panel), the fast terrestrial reservoir (center panel), or the surface ocean (bottom panel), with no further releases for $t > 0$. We find that the pulse is transferred away from the reservoir of origin on a time scale of months (surface ocean, atmosphere) to a decade (fast terrestrial). In all three cases, the transfer of Hg is principally to the subsurface ocean due to the fast timescales coupling the subsurface ocean to all three surface reservoirs (**Figure 3.5**).

Even when the initial release is to the fast terrestrial reservoir, we find that most of the Hg ends up in the subsurface ocean on a time scale of a decade. In our model, terrestrial Hg can be transferred to the surface ocean either by re-emission to the atmosphere (photoreduction, respiration of organic matter, biomass burning) and subsequent deposition, or by river runoff.

Cycling through the atmosphere is the dominant pathway (**Figure 3.3**). Transfer of Hg from the fast terrestrial reservoir to more recalcitrant soil pools is slow in comparison.

Even though the armored soil is the dominant Hg reservoir under natural (i.e. steady-state) conditions (**Table 3.2**), we find that a Hg perturbation to the surface reservoirs propagates principally to the ocean. Regardless of the location of the pulse of origin, after 1000 years we find that 40% is in the ocean, 20% is in the soil, and 40% has been returned to the deep mineral reservoir (**Figure 3.6**). The preferential long-lived reservoir for the perturbed system is the deep ocean, imposing a continued legacy on the subsurface/surface ocean reservoirs through vertical exchange of seawater. The implication of our work is that in the decades following release to the atmosphere, surface ocean, or terrestrial ecosystem a large fraction of anthropogenic Hg will end up in the subsurface ocean.

3.5 Anthropogenic enrichment and the importance of legacy Hg

Table 3.2 shows that the present-day anthropogenic enrichment of the surface and subsurface ocean is similar to that in the atmosphere, reflecting the short timescales for coupling of these reservoirs. Even the deep ocean shows a factor of two enrichment. We find that the present-day atmospheric Hg reservoir (and deposition) is enriched 7.5 times relative to natural levels (**Table 3.2**, **Figure 3.3**). Modeled enrichment is still 5.8 for the lower bound of anthropogenic emissions (Section 3.3.3). This enrichment is larger than the observed 3-fold anthropogenic enrichment from sediment cores that extend back to the mid-19th century [*Biester et al.*, 2007; *Lindberg et al.*, 2007] and reflects anthropogenic Hg emissions prior to 1850 (Section 3.2.5). Several long-term archives corroborate the importance of anthropogenic Hg emissions prior to 1850 [*Roos-Barraclough et al.*, 2002; *Givelet et al.*, 2003; *Roos-Baraclough et*

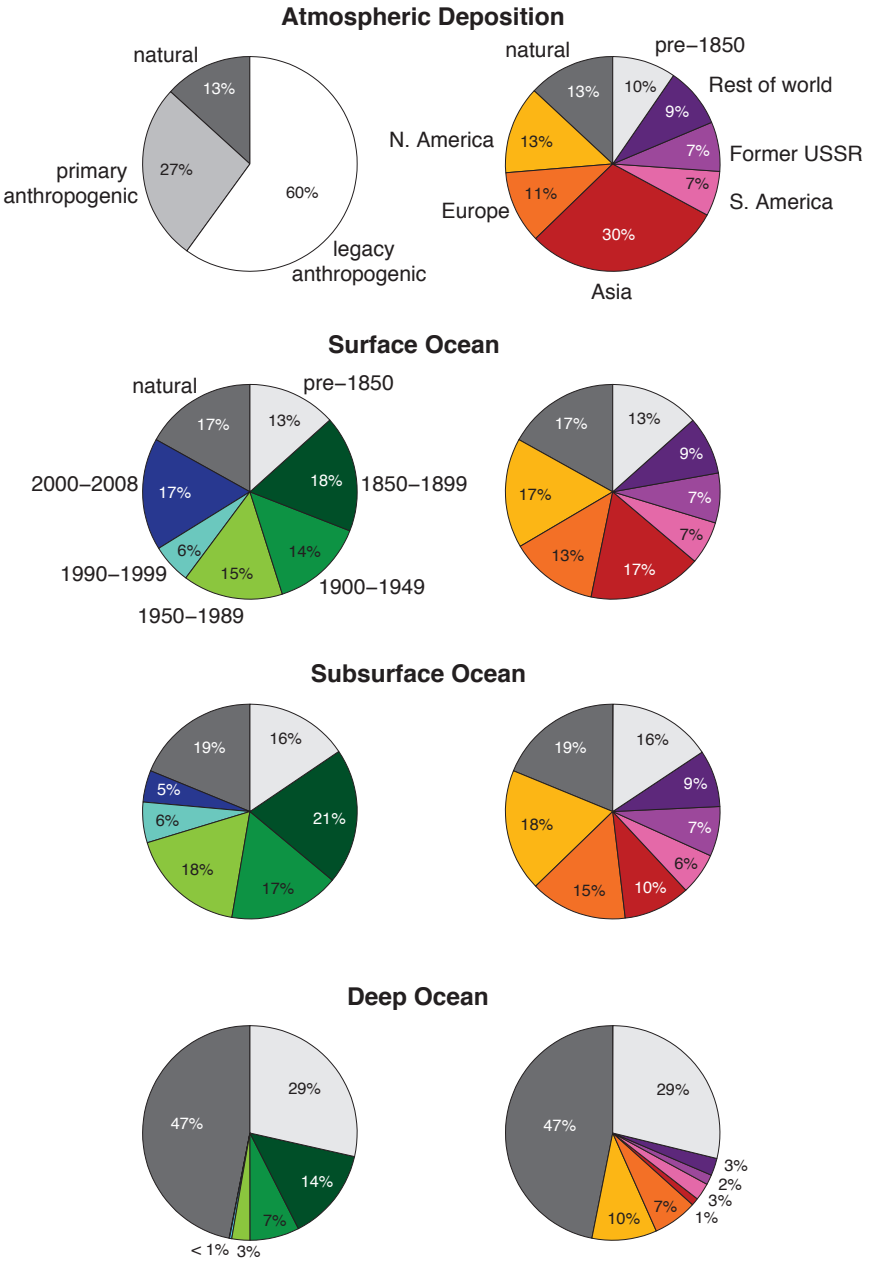

Figure 3.7: Natural and anthropogenic contributions to present-day atmospheric deposition and ocean reservoirs. The contribution from natural Hg is defined by steady state in our biogeochemical model without anthropogenic emissions. The primary anthropogenic contribution to deposition is from direct emissions (Figure 3.2a), while the legacy contribution is from anthropogenic Hg previously deposited and then re-emitted by surface reservoirs. The contribution from legacy Hg is calculated as total deposition minus primary anthropogenic emissions and natural emissions. For the ocean reservoirs, we partition the anthropogenic contribution by time period (left column) and region (right column). "Rest of world" includes Africa, the Middle East, and Oceania.

al., 2006; *Cooke et al.*, 2009, 2011; *Thevenon et al.*, 2011; *Conaway et al.*, 2012].

Figure 3.7 gives the source contributions to present-day atmospheric deposition and oceanic reservoirs as computed from our model. 27% of atmospheric deposition is from primary anthropogenic emissions, which is consistent with previous estimates [*Mason and Sheu*, 2002; *Selin et al.*, 2008; *Pirrone et al.*, 1996; 2010; *Corbitt et al*., 2011]. We find that natural emissions contribute only 13% of present-day deposition when accounting for pre-1850 anthropogenic emissions. 60% of present-day deposition is legacy anthropogenic Hg previously deposited and subsequently re-emitted. For the lower bound of anthropogenic emissions (Section 3.3), 26% of atmospheric deposition is from primary anthropogenic emissions, 57% is legacy, and 17% is natural. Past model studies had concluded that 1/3 of present-day deposition is natural and 1/3 is legacy anthropogenic, but this was built on the assumption of negligible anthropogenic emissions prior to 1850 and an imposed factor of 3 increase in deposition relative to 1850 based on sediment core data [*Mason et al.*, 1994; *Mason and Sheu*, 2002; *Seigneur et al.*, 2004; *Selin et al.*, 2008]. Our results suggest that the contribution from natural emissions to present-day deposition is much smaller than is generally recognized, and that the contribution from legacy anthropogenic emissions is correspondingly much larger. This result is sensitive to the magnitude of geogenic emissions (assumed here to be 90 Mg a^{-1}) emphasizing the importance of improved estimates of these emissions.

Figure 3.7 also shows the sensitivity of the present-day ocean reservoirs to anthropogenic emissions released in different historical periods. We find that 81% of the anthropogenic Hg in the deep ocean originates from pre-1900 emissions. This legacy Hg exerts a sustained effect on the surface and subsurface ocean, which is demonstrated by the result that

pre-1950 anthropogenic emissions account for more than half of the present-day enrichment in the surface and subsurface reservoirs.

Lastly, **Figure 3.7** shows the contributions of post-1850 anthropogenic emissions from different source continents (from *Streets et al.* [2011]) to the present-day anthropogenic enrichments of the different reservoirs. Although Asia presently accounts for 65% of global primary anthropogenic emissions [*Streets et al.*, 2011], we find that Hg of Asian anthropogenic origin accounts for only 17% and 10% of the surface and subsurface ocean reservoirs, respectively. The legacy of past North American and European anthropogenic emissions together accounts for 24% of present-day deposition and 30% of surface ocean Hg.

3.6 Implications for the future

We project future changes in the Hg cycle under four illustrative emission trajectories (Section 3.2.5, **Figure 3.2a**): (1) the business-as-usual A1B scenario of *Streets et al.* [2009] with continued increases in global emissions, (2) constant future emissions, (3) 50% decrease of emissions by 2050 ("mercury controls"), and (4) zero future anthropogenic emissions as a bounding case. These scenarios are assumed to take effect in 2015.

Figure 3.2c shows the atmospheric deposition for each of the four future emission scenarios. Primary anthropogenic emissions increase by 2000 Mg a^{-1} between 2015 and 2050 under A1B, but atmospheric deposition increases by 4600 Mg a^{-1}. Even if primary anthropogenic emissions stay constant between 2015 and 2050, atmospheric deposition increases by 30%. Under these scenarios, new anthropogenic Hg is being added to the pool of legacy Hg faster than it can be sequestered into longer-lived reservoirs and the legacy contribution to deposition grows as a result. *Corbitt et al.* [2011] projected that atmospheric deposition would remain at present-

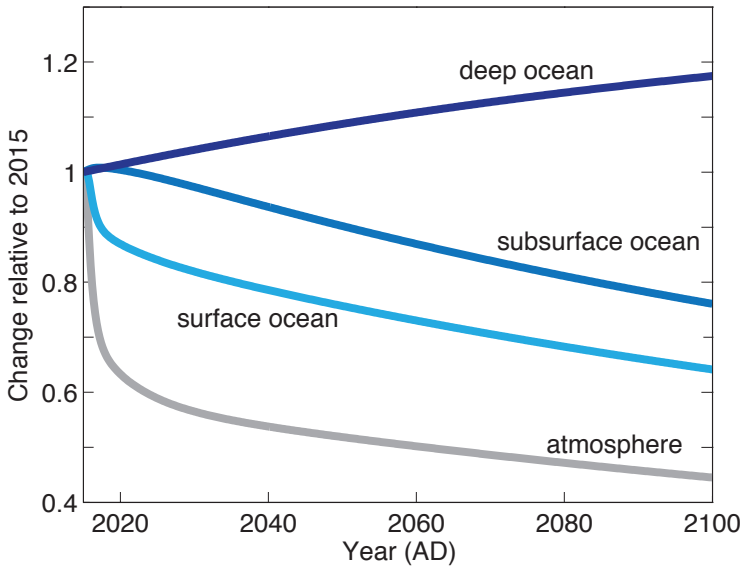

Figure 3.8: Change in reservoir masses relative to 2015 under a scenario of zero primary anthropogenic emissions after 2015.

day levels under the B1 scenario of *Streets et al*. [2009] (effectively constant emissions), but they assumed the legacy Hg pool to remain constant. Our work highlights the importance of accounting for changing legacy Hg when modeling the future atmosphere.

We find that a decrease in Hg emission is needed just to maintain Hg deposition at its present-day level. Under our hypothetical "mercury controls" scenario with 50% decrease in primary anthropogenic emissions by 2050, deposition begins to decrease by 2020 as the legacy contribution stabilizes (reflecting a balance between new anthropogenic Hg inputs and transfer to the longer-lived reservoirs). In this scenario, primary emissions decrease by 1400 Mg a^{-1} from 2015 to 2050 while deposition decreases by 1200 Mg a^{-1}. In the bounding case of zero future anthropogenic emissions, there is an immediate 30% decrease in deposition (associated with primary anthropogenic emissions) and slower subsequent decrease limited by the time scale for transfer from the subsurface to the deep ocean (**Figure 3.6**).

To illustrate the timescales required for dissipation of anthropogenic influence, **Figure 3.8** shows the time-dependent responses of the atmosphere and ocean Hg reservoirs to complete

elimination of anthropogenic Hg emissions from 2016 on. We previously pointed out the immediate 30% decrease in the atmosphere. There is also an immediate 10% decline in the surface ocean that is dampened relative to the atmosphere by the persistent legacy influence from the subsurface ocean. Subsequent decline in the surface ocean is more gradual, with 65% of the initial loading remaining in 2100. The subsurface ocean begins to slowly decrease after a decade, mostly by transfer to the deep ocean, but the anthropogenic signal persists for centuries. The deep ocean reservoir continues to increase throughout the 21st century even in the absence of primary anthropogenic emissions.

Future Hg concentrations in the surface+subsurface ocean are of particular concern because they are critical for determining the reservoir available for oceanic methylmercury production [*Mason et al.,* 2012] and associated concentrations in pelagic marine fish. Under the business-as-usual emissions trajectory, Hg concentrations in the combined surface+subsurface ocean will increase by 40% (relative to present day) by 2050. Under the "mercury controls" scenario, the Hg concentration in the surface/subsurface will still increase by 20%. Our results suggest that stabilization of ocean concentrations at present-day levels will require more aggressive reductions in primary anthropogenic emissions than is usually recognized.

3.7 Summary

We have developed a seven-compartment biogeochemical box model to describe the global cycling of mercury (Hg) between the atmosphere, ocean, and terrestrial reservoirs. The model is based on our best current understanding from observations and process models, and is described by first-order rate constants (coupled ODEs) for the transfer of Hg between compartments. We forced the model with time-dependent historical emissions (2000 BC –

present), initializing from natural steady state, and showed consistency with observational constraints for the present-day budget and anthropogenic enrichments. We used the model to analyze the timescales involved in Hg cycling and to quantify the impact of legacy anthropogenic Hg in the present-day global budget and under various future emission scenarios.

We find that characteristic timescales for Hg global biogeochemical cycling range from less than a year for coupling between the subsurface/surface ocean and the atmosphere to thousands of years for transfer from the armored soil to the deep mineral pool via the deep ocean. The subsurface ocean, extending from the base of the ocean mixed layer down to the permanent thermocline, plays a central role in the global biogeochemical cycling of Hg. A perturbation to the surface reservoirs (atmosphere, ocean, fast terrestrial) propagates to the subsurface ocean on a time scale of years to decades, and persists there for decades to centuries. Under natural conditions, terrestrial reservoirs contain a larger Hg inventory than the ocean. However, perturbations to surface reservoirs first propagate to the deep ocean because transfer of Hg to the armored soil reservoir is extremely slow, and persist in the deep ocean for centuries to millennia with upwelling causing a sustained effect on the surface+subsurface ocean. The persistence of Hg in the ocean is of particular environmental consequence because of the importance of marine fish as source of methylmercury exposure for humans and wildlife.

Atmospheric deposition in the model increases by a factor of 2.6 from 1840 to present, consistent with sediment archives. This factor of three has been regarded in previous studies as the anthropogenic enrichment relative to natural conditions, but in fact the anthropogenic perturbation to the Hg cycle extends back for millennia. We find that all-time anthropogenic Hg emissions have enriched the present-day atmosphere, surface ocean, and deep ocean by factors of

7.5, 5.9, and 2.1, respectively, relative to natural conditions. This is a much larger relative anthropogenic perturbation than is usually recognized.

Model results show that most (60%) of present-day Hg atmospheric deposition is legacy anthropogenic Hg re-emitted from surface reservoirs. Natural emissions and primary anthropogenic emissions contribute 13% and 27% to present-day deposition, respectively. Over half of the anthropogenic enrichment of the surface ocean is from pre-1950 emissions, and most of the anthropogenic enrichment of the deep ocean is from pre-1900 emissions. Although Asia accounts for 65% of present-day primary anthropogenic emissions [*Streets et al.*, 2011], Hg of Asian anthropogenic origin only accounts for 30% of present-day atmospheric deposition and 17% of the surface ocean reservoir. By contrast, North America and Europe together account for 30% of the surface ocean reservoir.

Understanding how the legacy of past anthropogenic emissions contributes to present-day Hg enrichment is essential for anticipating the effectiveness of future Hg emission reduction strategies. If anthropogenic emissions continue to rise, the resulting growth in atmospheric deposition will be greater than the increase in primary emissions due to sustained growth of the legacy component. Even if emissions stay constant, atmospheric deposition will continue to increase because new anthropogenic Hg will add to the surface+subsurface ocean reservoir faster than Hg can be transferred from that reservoir to the deep ocean. Our work shows that projecting future atmospheric deposition under changing emissions requires a full accounting of the coupling between the biogeochemical reservoirs. Aggressive reduction in primary anthropogenic emissions will be needed just to maintain oceanic Hg concentrations at present-day levels.

We investigated the response of the global Hg cycle to zeroing primary anthropogenic emissions after 2015 as a bound on the maximum global benefits to be expected from regulating

emissions. We find a nearly instantaneous 30% decrease in atmospheric deposition and 10% decrease in the surface ocean reservoir. Subsequent declines are slower, limited by the time scale for transfer to the deep ocean. By 2100 there is a 55% decrease in atmospheric deposition and 35% decrease in surface ocean loading. The subsurface ocean responds more slowly to the elimination of primary anthropogenic emissions and by 2100 has decreased by 25%.

Our analysis has focused on the global background. However, Hg concentrations in the surface ocean and terrestrial reservoirs vary depending on local environmental conditions, and many historic Hg problems have occurred as site-specific contamination issues from point sources. Ecosystem-scale studies indicate large variability in biotic Hg response to total Hg loading, depending on conditions facilitating methylmercury production [*Harris et al.*, 2007; *Knightes et al.*, 2009]. The global information provided here needs to be combined with site-specific understanding of the factors driving biological exposures.

Our analysis points to the need for improved, empirically constrained estimates of ocean evasion, geogenic emissions, and primary anthropogenic emissions. Whether or not organic carbon serves as the best analogue for modeling terrestrial Hg cycling also deserves further investigation. Ocean evasion and terrestrial cycling influence the fate and accumulation of Hg. Geogenic emissions determine the natural environmental burden of Hg and hence the impact of all-time anthropogenic Hg emissions, which may also be inferred from multi-millennia sedimentary records. Improved estimates of these quantities will allows us to better estimate the impact of present-day and future anthropogenic Hg emissions and more confidently establish the effectiveness of implemented regulation.

Acknowledgements: We thank Jeroen Sonke and an anonymous reviewer for their thoughtful comments. We acknowledge financial support from NSF Atmospheric Chemistry (ATM0961357), NSF Chemical Oceanography (OCE1130549), and the Electric Power Research Institute (EPRI). H.M.A. acknowledges support from NSF GRFP. We thank Anne Soerensen and Mauricio Santillana for thoughtful discussions.

References:

Amos, H. M., et al. (2012), Gas-particle partitioning of atmospheric Hg(II) and its effect on global mercury deposition, *Atmos. Chem. Phys.*, *12*(1), 591-603.

Andren, M. O. and J. O. Nriagu (1979), The global cycle of mercury, in *Biogeochemistry of mercury in the environment*, edited by J. O. Nriagu, Elsevier, Amsterdam.

Antia, A. N., et al. (2001), Basin-wide particulate carbon flow in the Atlantic Ocean: Regional export patterns and potential for atmospheric CO_2 sequestration, *Glob. Biogeochem. Cycle*, *15*(4), 845-862.

Bagnato, E., et al. (2011), New clues on the contribution of Earth's volcanism to the global mercury cycle, *Bull. Volcanol.*, *73*(5), 497-510.

Biester, H., et al. (2007), Modeling the past atmospheric deposition of mercury using natural archives, *Environ. Sci. Technol.*, *41*(14), 4851-4860.

Camargo, J. A. (2002), Contribution of Spanish-American silver mines (1570-1820) to the present high mercury concentrations in the global environment: a review, *Chemosphere*, *48*(1), 51-57.

Conaway, C. H., et al. (2012), Recent paleorecords document rising mercury contamination in Lake Tanganyika, *Appl. Geochem.*, *27*(1), 352-359.

Cooke, C. A., et al. (2009), Over three millennia of mercury pollution in the Peruvian Andes, *Proc. Natl. Acad. Sci. U. S. A.*, *106*(22), 8830-8834.

Cooke, C. A., et al. (2011), Pre-Colombian Mercury Pollution Associated with the Smelting of Argentiferous Ores in the Bolivian Andes, *Ambio*, *40*(1), 18-25.

Corbitt, E. S., et al. (2011), Global source-receptor relationships for mercury deposition under present-day and 2050 emissions scenarios, *Environ. Sci. Technol.*, *45*(24), 10477-10484.

Drevnick, P. E., et al. (2012), Spatial and temporal patterns of mercury accumulation in lacustrine sediments across the Laurentian Great Lakes region, *Environ. Pollut.*, *161*, 252-260.

Elbaz-Poulichet, F., et al. (2011), A 3500-Year Record of Hg and Pb Contamination in a Mediterranean Sedimentary Archive (The Pierre Blanche Lagoon, France), *Environ. Sci. Technol.*, *45*(20), 8642-8647.

Ferrara, R., et al. (2000), Volcanoes as emission sources of atmospheric mercury in the Mediterranean basin, *Sci. Total Environ.*, *259*(1-3), 115-121.

Fitzgerald, W. F., et al. (1998), The case for atmospheric mercury contamination in remote areas, *Environ. Sci. Technol.*, *32*(1), 1-7.

Friedli, H. R., et al. (2009), Initial estimates of mercury emissions to the atmosphere from global biomass burning, *Environ. Sci. Technol.*, *43*(10), 3507-3513.

Gill, G. A., and W. F. Fitzgerald (1988), Vertical mercury distributions in the ocean, *Geochim. Cosmochim. Acta*, *52*(6), 1719-1728.

Givelet, N., et al. (2003), Predominant anthropogenic sources and rates of atmospheric mercury accumulation in southern Ontario recorded by peat cores from three bogs: comparison with natural "background" values (past 8000 years), *J. Environ. Monit.*, *5*(6), 935-949.

Goldwater, L. (1972), *Mercury: A history of quicksilver*, York Press, Baltimore, MD.

Harris, R. C., et al. (2007), Whole-ecosystem study shows rapid fish-mercury response to changes in mercury deposition, *Proc. Natl. Acad. Sci. U. S. A.*, *104*(42), 16586-16591.

Holmes, C. D., et al. (2010), Global atmospheric model for mercury including oxidation by bromine atoms, *Atmos. Chem. Phys.*, *10*, 12037-12057.

Johansen, P., et al. (2004), Human exposure to contaminants in the traditional Greenland diet, *Sci. Total Environ.*, *331*(1-3), 189-206.

Kim, N. S., and B. K. Lee (2010), Blood total mercury and fish consumption in the Korean general population in KNHANES III, 2005, *Sci. Total Environ.*, *408*(20), 4841-4847.

Knightes, C. D., et al. (2009), Application of ecosystems-scale fate and bioaccumulation models to predict fish mercury response times to changes in atmospheric deposition, *Environ. Toxicol. Chem.*, *28*(4), 881-893.

Lacerda, L. D. (1997), Global mercury emissions from gold and silver mining, *Water Air Soil Pollut.*, *97*(3-4), 209-221.

Lamborg, C. H., et al. (2002a), Modern and historic atmospheric mercury flows in both hemispheres: Global and regional mercury cycling implications, *Glob. Biogeochem. Cycle*, *16*(4), 1104.

Lamborg, C. H., et al. (2002b), A non-steady-state compartmental model of global-scale mercury biogeochemistry with interhemispheric atmospheric gradients, *Geochim. Cosmochim. Acta*, *66*(7), 1105-1118.

Lindberg, S., et al. (2007), A synthesis of progress and uncertainties in attributing the sources of mercury in deposition, *Ambio*, *36*(1), 19-32.

Lindqvist, O., and H. Rodhe (1985), Atmospheric mercury - a review, *Tellus Series B-Chem. Phys. Met.*, *37*(3), 136-159.

Mason, R. P., et al. (1994), The biogeocheical cycling of elemental mercury – anthropogenic influences, *Geochim. Cosmochim. Acta*, *58*(15), 3191-3198.

Mason, R. P., and G. R. Sheu (2002), Role of the ocean in the global mercury cycle, *Glob. Biogeochem. Cycle*, *16*(4), 1093.

Mason, R. P., et al. (2012), Mercury biogeochemical cycling in the ocean and policy implications, *Environ. Res.*, *119*, 101-117.

Montegut, C. D., et al. (2004), Mixed layer depth over the global ocean: An examination of profile data and a profile-based climatology, *J. Geophys. Res.-Oceans*, *109*(C12), C12003.

Nakicenovic, N. (2000), Greenhouse gas emissions scenarios, *Technol. Forecast. Soc. Chang.*, *65*(2), 149-166.

Nriagu, J. O. (1979), Production and uses of mercury, in *Biogeochemistry of mercury in the environment*, edited by M. O. Andren and J. O. Nriagu, Elsevier, Amsterdam.

Nriagu, J. O. (1993), Legacy of mercury pollution, *Nature*, *363*(6430), 589-589.

Nriagu, J. O. (1994), Mercury pollution from the past mining of gold and silver in the Americas, *Sci. Total Environ.*, *149*(3), 167-181.

Nriagu, J., and C. Becker (2003), Volcanic emissions of mercury to the atmosphere: global and regional inventories, *Sci. Total Environ.*, *304*(1-3), 3-12.

Pacyna, J. M., et al. (2003), Mapping 1995 global anthropogenic emissions of mercury, *Atmos. Environ.*, *37*, S109-S117.

Pacyna, E. G., et al. (2006), Global anthropogenic mercury emission inventory for 2000, *Atmos. Environ.*, *40*(22), 4048-4063.

Pacyna, E. G., et al. (2010), Global emission of mercury to the atmosphere from anthropogenic sources in 2005 and projections to 2020, *Atmos. Environ.*, *44*(20), 2487-2499.

Parrella, J. P., et al. (2012), Tropospheric bromine chemistry: implications for present and pre-industrial ozone and mercury, *Atmos. Chem. Phys.*, *12*(15), 6723-6740.

Pirrone, N., et al. (1996), Regional differences in worldwide emissions of mercury to the atmosphere, *Atmos. Environ.*, *30*(17), 2981-2987.

Pirrone, N., et al. (2010), Global mercury emissions to the atmosphere from anthropogenic and natural sources, *Atmos. Chem. Phys.*, *10*(13), 5951-5964.

Potter, C. S., et al. (1993), Terrestrial ecosystem production – a process model-based on global satellite and surface data, *Glob. Biogeochem. Cycle*, *7*(4), 811-841.

Prather, M. J. (1996), Timescales in atmospheric chemistry: Theory, GWPs for CH4 and CO, and runaway growth, *Geophys. Res. Lett.*, *23*(19), 2597-2600.

Pyle, D. M., and T. A. Mather (2003), The importance of volcanic emissions for the global atmospheric mercury cycle, *Atmos. Environ.*, *37*(36), 5115-5124.

Qureshi, A., et al. (2011), Quantifying uncertainties in the global mass balance of mercury, *Glob. Biogeochem. Cycle*, *25*, GB4012.

Roos-Barraclough, F., et al. (2002), A 14 500 year record of the accumulation of atmospheric mercury in peat: volcanic signals, anthropogenic influences and a correlation to bromine accumulation, *Earth Planet. Sci. Lett.*, *202*(2), 435-451.

Roos-Barraclough, F., et al. (2006), Use of Br and Se in peat to reconstruct the natural and anthropogenic fluxes of atmospheric Hg: A 10000-year record from Caribou Bog, Maine, *Environ. Sci. Technol.*, *40*(10), 3188-3194.

Schuster, P. F., et al. (2002), Atmospheric mercury deposition during the last 270 years: A glacial ice core record of natural and anthropogenic sources, *Environ. Sci. Technol.*, *36*(11), 2303-2310.

Seigneur, C., et al. (2004), Global source attribution for mercury deposition in the United States, *Environ. Sci. Technol.*, *38*(2), 555-569.

Selin, N. E., et al. (2008), Global 3-D land-ocean-atmosphere model for mercury: Present-day versus preindustrial cycles and anthropogenic enrichment factors for deposition *Global Biogeochem. Cycles*, *22*(3), GB3099.

Shia, R. L., et al. (1999), Global simulation of atmospheric mercury concentrations and deposition fluxes, *J. Geophys. Res.-Atmos.*, *104*(D19), 23747-23760.

Slemr, F., et al. (1985), Distribution, speciation, and budget of atmospheric mercury, *J. Atmos. Chem.*, *3*(4), 407-434.

Smith-Downey, N. V., et al. (2010), Anthropogenic impacts on global storage and emissions of mercury from terrestrial soils: Insights from a new global model, *J. Geophys. Res.-Biogeosci.*, *115*, G03008.

Soerensen, A. L., et al. (2010), An improved global model for air-sea exchange of mercury: High concentrations over the North Atlantic, *Environ. Sci. Technol.*, *44*(22), 8574-8580.

Soerensen, A. L., et al. (2012), Multi-decadal decline of mercury in the North Atlantic atmosphere explained by changing subsurface seawater concentrations, *Geophys. Res. Lett.*, *39*, L21810.

Streets, D. G., et al. (2009), Projections of Global Mercury Emissions in 2050, *Environ. Sci. Technol.*, *43*(8), 2983-2988

Streets, D. G., et al. (2011), All-Time Releases of Mercury to the Atmosphere from Human Activities, *Environ. Sci. Technol.*, *45*(24), 10485-10491.

Sunderland, E. M. (2007), Mercury exposure from domestic and imported estuarine and marine fish in the US seafood market, *Environ. Health Perspect.*, *115*(2), 235-242.

Sunderland, E. M., and R. P. Mason (2007), Human impacts on open ocean mercury concentrations, *Global Biogeochem. Cycles*, *21*(4), GB4022.

Thevenon, F., et al. (2011), (Pre-) historic changes in natural and anthropogenic heavy metals deposition inferred from two contrasting Swiss Alpine lakes, *Quat. Sci. Rev.*, *30*(1-2), 224-233.

Thompson, A. M., et al. (1993), The atmospheric CH_4 increase since the Last Glacial Maximum. 2. Interactions with oxidants, *Tellus Ser. B-Chem. Phys. Meteorol.*, *45*(3), 242-257.

United Nations Environment Program (UNEP) (2013), http://www.iisd.ca/mercury/inc5/, 08 February 2013.

van der Werf, G. R., et al. (2003), Carbon emissions from fires in tropical and subtropical ecosystems, *Glob. Change Biol.*, *9*(4), 547-562.

Varekamp, J. C., and P. R. Buseck (1986), Global mercury flow from volcanic and geothermal sources, *Appl. Geochem.*, *1*(1), 65-73.

Wu, Y., et al. (2006), Trends in anthropogenic mercury emissions in China from 1995 to 2003, *Environ. Sci. Technol.*, *40*(17), 5312-5318.

Chapter 4. Global biogeochemical implications of mercury discharges from rivers and sediment burial

[Amos, H. M., Jacob, D. J., Sunderland, E. M., et al., submitted to co-authors, in preparation for Environmental Science & Technology]

Abstract

Mercury (Hg) is a neurotoxin that cycles globally in the environment and bioaccumulates in marine food webs. Rivers link anthropogenic Hg releases on land to marine ecosystems. We estimate global present-day Hg discharges from rivers to ocean margins of 5400 ± 2700 Mg a^{-1}, of which 28% reaches the open ocean and the rest is deposited to ocean margin sediments. This is larger than previously estimated due to our accounting for elevated concentrations in Asian rivers and variability in offshore transport across different types of estuaries. Inputs from rivers to the North Atlantic have decreased several-fold since the 1970s but increased to the North Pacific. Our analysis shows these trends have large effects at ocean margins but are small offshore and thus do not explain observed declines in vertical seawater profiles in the North Atlantic or increases in the North Pacific. Burial in nearshore marine sediments represents a major sink in the global Hg biogeochemical cycle that has not previously been considered. Its inclusion in a fully coupled global biogeochemical box model helps to accommodate new findings of a large historical anthropogenic Hg source from commercial use. It implies that natural environmental Hg levels are lower than previously estimated, suggesting a relatively larger impact from human activity and a potentially faster timescale (centuries instead of millennia) for resequestration of anthropogenic Hg from active cycling.

4.1 Introduction

Human exposure to methylmercury, a potent neurotoxin, is primarily through consumption of marine fish [*Mahaffey et al.*, 2011]. Anthropogenic mercury (Hg) is transported globally by the atmosphere [*Corbitt et al.*, 2011; *Strode et al.*, 2008; *Swartzendruber et al.*, 2006] and the oceans [*Sunderland et al.*, 2009], resulting in worldwide contamination. Most regulatory assessments for Hg have focused on atmospheric emissions and their subsequent fate in the global environment through deposition [*AMAP/UNEP*, 2008; 2013]. Anthropogenic releases of Hg to aquatic systems and the impact of rivers as a source of Hg to the marine environment have been poorly characterized. Previous studies estimated that 3000 Mg a^{-1} of Hg is presently discharged from rivers to ocean margins [*Sunderland and Mason*, 2007], an amount comparable to atmospheric Hg deposition to the oceans (3600 Mg a^{-1} [*Holmes et al.*, 2010]), and that 90% of this Hg is buried in sediments at ocean margins (estuaries and the continental shelf). Rivers have recently been hypothesized as important contributors to the Hg budgets of the North Atlantic [*Soerensen et al.*, 2012] and Arctic Ocean [*Dastoor and Durnford*, 2013; *Fisher et al.*, 2012; *Kirk et al.*, 2012]. Here we construct a global, spatially resolved inventory of Hg discharges from major rivers for present-day, including updated information on the fraction reaching the open ocean, and estimate trends between the 1970s and present. We use global Hg models to examine the impacts of rivers on the marine environment and biogeochemical cycling.

Sunderland and Mason [2007] constructed a first global inventory of present-day Hg discharges from rivers to major ocean basins using available data from a few major rivers. *AMAP/UNEP* [2013] produced a gridded version of this inventory using data on suspended sediment discharges from rivers [*Hall et al.*, 2006; *Ludwig et al.*, 2011]. More than 80% of Hg in rivers is bound to particles (e.g., [*Schuster et al.*, 2011]), which can be sequestered during burial

of benthic sediments in estuaries and on the continental shelf before reaching the open ocean [*Chester*, 2003]. Benthic sediments at ocean margins thus serve as a large sink for Hg [*Mason et al.*, 2004; *Sunderland et al.*, 2004]. However, the fraction of the suspended particle load in rivers that is buried is highly variable depending on freshwater discharge rates and the physical characteristics of different estuaries [*McKee et al.*, 2004]. Here we use a classification scheme for export of particles from major estuarine types [*Walsh and Nittrouer*, 2009] to better estimate the fraction of particle-bound Hg reaching the open ocean and the global biogeochemical implications of Hg sequestration in ocean margin sediments.

Vertical seawater profiles from the upper ocean (1000 m) near Bermuda indicate a large (>5 pM) decrease in Hg concentrations between 1983 and 2008 [*Gill and Fitzgerald*, 1988; *Mason et al.*, 2001; *Mason et al.*, 2012], which *Soerensen et al.* [2012] postulated could be explained by a declining source of Hg from rivers. Sediment core data from Europe and North America support a decline in Hg discharges from many rivers since the 1970s due to decreases in commercial Hg use, environmental regulations, and wastewater treatment [*Bopp et al.*, 1993; *Harland et al.*, 2000; *Leermakers et al.*, 2001; *Mansson et al.*, 2009; *Steinberg et al.*, 2004; *Varekamp et al.*, 2003]. Conversely, sediment cores and inventories in China and India suggest that Hg discharges from rivers are increasing [*An et al.*, 2010; *Chakraborty et al.*, 2013; *Ram et al.*, 2003]. Conversely, seawater Hg concentrations in the North Pacific Ocean appear to have increased between the late 1980s and 2006 [*Sunderland et al.*, 2009]. Here we combine improved estimates of Hg discharges from rivers and their temporal trends with a general circulation model to better estimate the role of rivers in driving Hg concentrations in different ocean basins between the 1970s and present.

4.2 Methods

4.2.1 Riverine discharge of Hg to the oceans

We construct a global, spatially distributed estimate of present-day riverine inputs to coastal margins using published measurements collected at or near river mouths (**Table A1**). We restrict observations to 2000-2013, with the exception of the Russian Arctic (Ob, Lena, and Yenisey rivers) and Mediterranean (Po, Rhone, and Nile rivers) where data are only available from the early 1990s. Since measurements of Hg in rivers are limited, we aggregate data by continent and ocean basin to calculate flow-weighted mean dissolved concentrations [Hg(D)] for rivers draining into each ocean basin (**Table 4.1**). Fewer measurements of suspended particle Hg concentrations are available, so mean concentrations [Hg(P)] are estimated from a partition coefficient K_D = [Hg(P]/[Hg(D)], where [Hg(P)] is in units of pmol per kg of suspended particulate matter and [Hg(D)] is in units of pmol per L of river water. From the compilation of data in Table S1 we calculate $\log_{10} K_D = 4.7 \pm 0.3$. [Hg(P)] values estimated using this method fall within observed ranges (**Table A2**).

We multiply the resulting mean riverine Hg(D) and Hg(P) concentrations by gridded freshwater discharge and suspended sediment data to estimate annual Hg loads entering coastal marine systems (**Table 4.2**). Data on total suspended solids (TSS) loads have a 2^ox2.5^o horizontal resolution [*Hall et al.*, 2006; *Ludwig et al.*, 1996; *Ludwig et al.*, 2011] and freshwater discharge data (Q) have a 1^ox1^o horizontal resolution [*Dai et al.*, 2009].

The fraction of Hg(P) transported beyond the continental shelf to open marine waters varies among ocean basins and is estimated from a classification system for sediment dispersal developed by *Walsh and Nittrouer* [2009] and adapted by *Zhang et al.* [2014]. *Walsh and Nittrouer* [2009] categorized estuaries into five types of dispersal systems based on river, wave,

Table 4.1 Mean present-day riverine Hg concentrations

Ocean Basin[b]	[Hg(D)] (pM)	[Hg(P)] (nmol g^{-1})[c]	*n*[d]
Arctic			
Canada and USA	7.3 ± 2.1	0.39 ± 0.35	7
Russia	3.1 ± 1.1	0.17 ± 0.15	3
North Atlantic			
Europe	9.1 ± 2.1	0.49 ± 0.42	3
Canada and USA	8.7 ± 5.7	0.47 ± 0.32	4
South Atlantic			
South America[e]	28 ± 18	1.50 ± 1.24	2
Africa[f]	2.0 ± 1.3	0.11 ± 0.10	1
North Pacific			
Canada and USA	6.4 ± 3.2	0.34 ± 0.33	3
China	110 ± 55	5.9 ± 5.8	3
South Pacific			
Southeast Asia[g]	3.6 ± 2.3	0.19 ± 0.19	1
South America[h]	28 ± 18	1.5 ± 1.2	-
China[i]	110 ± 55	5.9 ± 5.8	-
Indian			
India[j]	50 ± 33	2.7 ± 2.9	1
Southeast Asia[k]	3.6 ± 2.3	0.19 ± 0.19	-
Africa[f]	2.0 ± 1.3	0.11 ± 0.10	1
Mediterranean[l]	1.8 ± 0.8	0.10 ± 0.09	4

[a] Flow-weighted mean dissolved concentrations [Hg(D)] are based on a survey of published measurements collected in rivers flowing into estuaries. The complete compilation of observations is in Table S1. The standard error on the weighted mean (SE) [*Gatz & Smith*, 1995] is calculated when n is ≥ 3 and ranges from 30% to 65%. When $n < 3$ we assume SE = 65%. See text for estimation of [Hg(P)]. The SE of [Hg(P)] is calculated by propagating the relative SEs of [Hg(D)] and of the partition coefficient K_D in quadrature.

[b] Observations are aggregated by continental regions flowing into each ocean basin (indented). Ocean basin boundaries are given in **Figure A1**.

[c] Per gram dry weight suspended sediment.

[d] Number (n) of estuarine regions used to calculate the flow-weighted mean.

[e] South American mean Hg concentrations are also applied to Central America.

[f] Based on data for the Nile River [*Cossa & Coquery*, 2005]

[g] The original publication [*Noh et al.*, 2013] only provides a range. We use the mid-range value as estimate of the mean.

[h] Based on observations for South American rivers entering the South Atlantic.

[i] Based on observations for Chinese rivers entering the North Pacific.

(Continued)
[j] Limited observations available suggest that rivers are highly contaminated ([Hg(D)] = 50 - 400 pM [*Ram et al.,* 2003], and [THg] = [Hg(D)] + [Hg(P)] > 6000 pM [*Sankar et al.*, 2010]). We use [Hg(D)] = 50 pM as a conservative estimate.
[k] Based on observations for Southeast Asian rivers entering the South Pacific.
[l] Based on rivers draining from the European continent and the Nile River (**Table A1**).

tide, and margin characteristics. *Zhang et al.* [2014] used data on suspended sediment export for representative rivers in each type to estimate the fraction of particle-bound Hg which reaches the open ocean.

We also considered point sources located on coastlines and discharging Hg directly to coastal waters. We used the *AMAP/UNEP* [2013] global 2010 inventory of anthropogenic releases to water (0.5° x 0.5° horizontal resolution) and isolated coastal grid cells not associated with rivers. We find that coastal point sources discharges are negligible (<1 Mg a^{-1}) relative to rivers and do not discuss them further.

Temporal changes in Hg inputs from rivers to estuaries between 1970 and present are estimated using dated sediment core data from estuarine river mouths. Time series of Hg concentrations in estuarine river mouths are used as available. In India, sediment core and time series data are unavailable, so we estimate the change in recent decades based on country-specific inventory data [*Chakraborty et al.*, 2013]. All available observations and associated temporal patterns are provided in the Appendix. **Table 4.3** summarizes regional enrichment factors (EFs) and their upper and lower bounds used to scale present-day discharges. We assume Hg discharges have been constant at present-day levels since the 1970s in regions with no temporal information.

Table 4.2 Present-day discharges to ocean margins

Ocean[a]	Freshwater discharge, Q[b] ($km^3\ a^{-1}$)	Total suspended sediment flux, TSS[c] ($Tg\ a^{-1}$)	Riverine Hg(D) input[d] ($Mmol\ a^{-1}$)	Riverine Hg(P) input[e] ($Mmol\ a^{-1}$)	Fraction of Hg(P) reaching open ocean[f]
Arctic	2900	260	$1.4x10^{-2} \pm 2.5x10^{-3}$	$7.5x10^{-2} \pm 7.0x10^{-2}$	0.17
North Atlantic	4500	330	$4.0x10^{-2} \pm 2.2x10^{-2}$	0.16 ± 0.13	0.11
South Atlantic	9900	4000	$8.5x10^{-2} \pm 6.0x10^{-2}$	5.0 ± 4.0	0.31
North Pacific	5100	2400	0.40 ± 0.20	10 ± 9.5	0.28
South Pacific	5700	4700	0.10 ± 0.06	8.5 ± 8.0	0.19
Indian	2600	3500	0.02 ± 0.01	2.5 ± 2.5	0.29
Mediterranean[g]	410	680	$7.5x10^{-4} \pm 2.0x10^{-4}$	0.07 ± 0.05	0.16
Southern Ocean[h]	290	180	$8.0x10^{-3} \pm 5.5x10^{-3}$	0.26 ± 0.20	0.48
Global	31,000	16,000	0.65 ± 0.23[i]	26 ± 13[i]	0.28[j]

[a] Geographical boundaries from **Figure A1**.
[b] *Dai et al.* [2009]
[c] ISSLCP II (http://daac.ornl.gov/ISLSCP_II/islscpii.shtml) [*Ludwig et al.*, 2011]
[d] Product of [Hg(D)] and Q, where [Hg(D)] is from **Table 4.1** and has units of pM. The error on individual basins reflects ± 1 standard error (SE) on [Hg(D)]. Errors for individual ocean basins are added in quadrature to estimate the error on global total Hg(D) inputs.
[e] Product of [Hg(P)] and TSS, where [Hg(P)] is from **Table 4.1** and has units of $nmol\ g^{-1}$.
[f] Based on the *Walsh and Nittrouer* [2009] classification scheme for dispersal of suspended sediment and observations from rivers belonging to each major class (see Methods).
[g] Includes the Black Sea, assuming the same Hg(D) and Hg(P) concentrations as for the Mediterranean (**Table 4.1**).
[h] Hg inputs based on riverine concentrations in South America, which contribute most of total Q and TSS inputs.
[i] Errors for individual ocean basins are added in quadrature to estimate the error on global total Hg inputs.
[j] Global total is weighted by Hg(P) inputs and associated export fraction in each basin.

4.2.2 Model descriptions

We use the MIT global three-dimensional ocean general circulation model (MITgcm) [*Marshall et al.*, 1997] to examine the impact of 1970s-present changes in riverine discharges on seawater Hg concentrations. The Hg simulation in the MITgcm was developed by *Zhang et al.* [2014]. It includes air-sea exchange, redox reactions, and sorption to particles following *Soerensen et al.* [2010] in the surface mixed layer and *Zhang et al.* [2014a] in subsurface and deep waters. Particle dynamics driving settling of organic carbon (and Hg) are from the ecosystem model embedded within the MITgcm [*Dutkiewicz et al.*, 2012]. The horizontal resolution is 1° x 1° with 23 vertical levels between the ocean surface and the seafloor. To isolate the impact of rivers, we initialize seawater Hg concentrations at zero and shut off atmospheric deposition. We then perform two separate 10-year simulations, one forced by present-day Hg discharges from rivers and the other by 1970s inputs. Ten years provides sufficient time for the coastal signal from rivers to be transported to the interior of an ocean basin by surface currents.

We examine the impact of rivers on the global Hg biogeochemical cycle using an updated version of the 7-box model developed by *Amos et al.* [2013]. Mercury is cycled between reservoirs representing the ocean (surface, subsurface, deep), atmosphere, and terrestrial environment (fast, slow, armored pools), and is ultimately removed by burial of marine sediments. Sediments are compacted and subducted to the lithosphere, eventually returning Hg to surface reservoirs by erosion and volcanism on geologic time scales. Exchange of mass between reservoirs is described by first-order rate coefficients. The model is initialized from a natural steady-state simulation without anthropogenic Hg releases, then forced with all-time (2000 BC to 2008 AD) anthropogenic atmospheric emissions from *Streets et al.* [2011] and additional 1850-2008 atmospheric emissions from commercial Hg use [*Horowitz et al.*, 2014]. We decrease the

Table 4.3 Enrichment factors relative to 2008 for riverine Hg inputs to oceans[a]

Ocean	1970	1980	1990	2000	2008
North Atlantic					
Europe	10 (5 -14)	5 (2 - 7)	2 (2 -3)	1 (1 - 2)	1
North America	8 (4 - 30)	3 (1 - 4)	2 (1 - 3)	1 (1 - 2)	1
North Pacific					
North America	4 (2 - 6)	2 (1 - 3)	1 (1 - 2)	1 (1 - 2)	1
China	0.7 (0.3 - 1)	0.6 (0.3 - 0.9)	0.8 (0.4 - 1)	0.9 (0.5 - 1)	1
Indian Ocean					
India	0.2 (0 - 0.6)	0.3 (0.1 - 1)	0.4 (0.1 - 2)	0.7 (0.2 - 3)	1
Mediterranean	5 (2 - 7)	2 (2 - 3)	1 (1 - 2)	1 (1 - 2)	1

[a] Best estimates and observational ranges from estuarine sediment cores collected at the mouths of major freshwater tributaries and riverine Hg concentration time series. See Appendix for details.

terrestrial rate coefficients for loss to the atmosphere (photoreduction, respiration) by a factor of 10, based on recent field data indicating greater Hg retention by soils [*Hararuk et al.*, 2013; *Obrist*, 2012; *Obrist et al.*, 2014].

Amos et al. [2013] treated riverine discharges as a first-order process transferring Hg from the terrestrial reservoirs to the surface ocean. The rate coefficient was based on the estimated mass of Hg from rivers that reaches the open ocean (380 Mg a^{-1}) from *Sunderland and Mason* [2007]. A term representing sequestration in ocean margin sediments was not included, so this Hg was stored in biogeochemically active reservoirs. We account for burial in ocean margin sediments here, which represents an important sink for anthropogenic Hg.

We also further characterize river discharges of Hg to ocean margins by distinguishing between Hg directly released to a river or its watershed by human activity ("primary

anthropogenic Hg") versus terrestrial runoff of naturally occurring or atmospherically deposited Hg ("background"). A present-day background is estimated based on Hg concentrations measured in pristine Arctic rivers (**Table A1**; [*Emmerton et al.*, 2013; *Leitch et al.*, 2007; *Schuster et al.*, 2011]). Extrapolated globally this amounts to 740 Mg a^{-1}, which is consistent with *Kocman et al.* [2014] (range, 320-940 Mg a^{-1}). From this we infer a first-order rate coefficient for loss of Hg from terrestrial ecosystems to ocean margins by rivers. Between the 1970s and present total Hg discharges to ocean margins from rivers are constrained by observations (**Tables 4.2-4.3**). Prior to 1970, we scale total Hg discharges from rivers using the historical inventory of global releases to water from commercial Hg use [*Horowitz et al.*, 2014]. The primary anthropogenic contribution is calculated by difference between total and background discharges and treated as an external forcing. Of the total Hg discharged to ocean margins by rivers, 28% is transferred to the surface ocean and 72% removed to ocean margin sediments based on **Table 4.2**. All rate coefficients for the updated box model are provided in **Table A3**.

4.3 Results & Discussion

4.3.1 Global river inputs and trends

Global present-day Hg inputs from rivers to coastal margins are estimated to be 5400 ± 2700 Mg a^{-1} (**Table 4.2**). This is larger than the previous estimate of 3000 Mg a^{-1} from *Sunderland and Mason* [2007] and is driven by recently published data suggesting greater contamination in Asian rivers [*An et al.*, 2010; *Bi et al.*, 2012; *Jiang et al.*, 2003; *Liu et al.*, 2012; *Ram et al.*, 2003; *Sankar et al.*, 2010; *Tong et al.*, 2013]. Riverine Hg inputs to the margins of the Pacific and Indian Oceans account for 80% of our global total (**Table 4.2**). Our estimates of

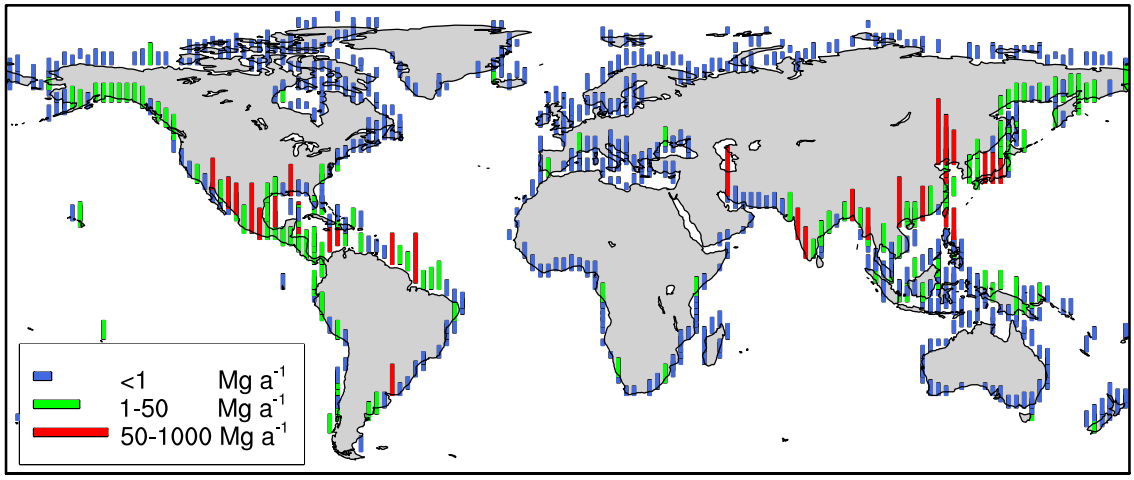

Figure 4.1: Present-day annual discharges of total (dissolved + particulate) mercury to ocean margins from rivers.

discharges to ocean margins of the Atlantic, Arctic, and Mediterranean are within the ranges of previously published values [*Cossa and Coquery*, 2005; *Dastoor and Durnford*, 2013; *Fisher et al.*, 2012; *Outridge et al.*, 2008; *Rajar et al.*, 2007; *Sunderland and Mason*, 2007].

Figure 4.1 illustrates the spatial distribution of our present-day riverine inputs of total Hg to ocean margins, which is driven by both variability in Hg(P) concentrations (**Table 4.1**) and suspended sediment discharges [*Ludwig et al.*, 2011]. Major rivers and highly contaminated systems are prominent (e.g., Yangtze, Amazon, Ganges). Large Hg discharges from Mexican rivers to the Pacific Ocean reflect high TSS values. **Figure 4.1** shows low Hg discharges from African rivers, based solely on data for the Nile [*Cossa and Coquery*, 2005] and might be an underestimate. For example, the Congo River is known to be polluted by unregulated discharges from chemical industries, leaching from solid waste dumps, and artisanal gold mining [*AMAP/UNEP*, 2013; *UNEP*, 2004].

We estimate that 28% of particle-bound Hg in rivers is exported to the open ocean globally (**Table 4.2**), as compared to 10% in *Sunderland and Mason* [2007]. The export fraction

is higher for the North Pacific (29%) than for the North Atlantic (11%) due to a greater prevalence of large rivers that efficiently transport suspended particles containing Hg offshore [*Milliman and Farnsworth*, 2011; *Wright et al.*, 1988]. We find that 1500 ± 750 Mg a^{-1} of Hg discharged by rivers is delivered to the open ocean. The uncertainty is estimated by adding the uncertainties in discharge at coastal margins for individual ocean basins in quadrature, scaled by the corresponding export fractions (**Table 4.2**). Our best estimate (1500 Mg a^{-1}) amounts to ~40% of present-day atmospheric Hg(II) deposition to the oceans (3600 Mg) [*Holmes et al.*, 2010].

Discharges of Hg are decreasing in North American and European rivers but increasing in India and China. Mercury discharges from rivers to the margins of the North Atlantic Ocean peaked around the 1970s, likely due to the large quantities of Hg used and released from commercial products and industrial manufacturing at that time [*Horowitz et al.*, 2014; *Hylander and Meili*, 2005; *Maxson*, 2004; *Wilburn*, 2013]. Sediment core data suggest that Hg discharges from rivers bordering the North Atlantic in the 1970s were a factor of 9 (range, 4 to 20) larger than at present (**Table 4.3**). In India and China, riverine Hg discharges to marine ecosystems have increased by 40 to 400% since the 1970s based on sediment core data and country-level inventories of Hg releases to water [*An et al.*, 2010; *Chakraborty et al.*, 2013; *Shi et al.*, 2010]. The increase is likely driven by dense development and urbanization along major rivers [*An et al.*, 2010; *Liu and Yang*, 2012; *Yi et al.*, 2011], greater use of Hg in industrial processes (e.g., in vinyl chloride monomer production) [*Maxson*, 2006; *Pacyna et al.*, 2010], and increasing agricultural application of Hg-containing phosphate fertilizers [*Zhang and Shan*, 2008].

Figure 4.2 shows the changes in riverine contributions to total dissolved Hg in the surface ocean (0 to 55 m) as simulated by the MITgcm between the 1970s and present.

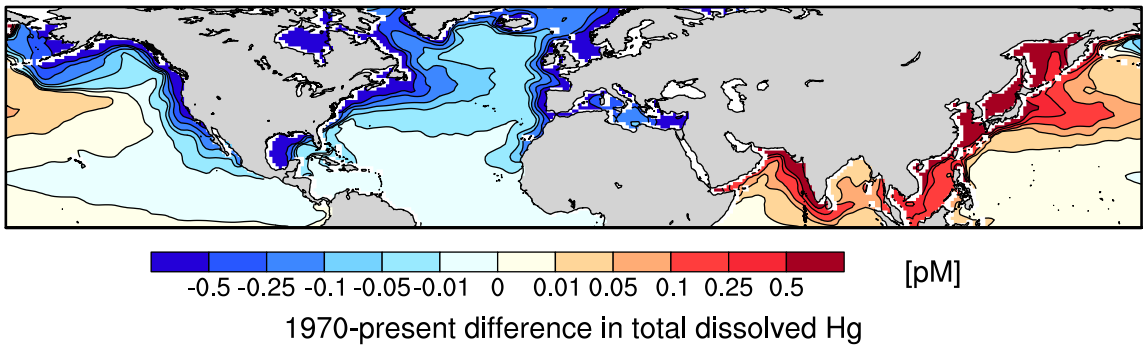

Figure 4.2: Difference between 1970 and present in riverine contributions to annual mean total dissolved Hg concentrations in the surface ocean (0-55 m). Results are from MITgcm simulations as described in the text. Red indicates an increase in oceanic Hg since 1970 and blue indicates a decrease.

Concentrations of Hg in seawater have decreased throughout the North Atlantic but increased over much of the North Pacific. The trends driven by rivers are large in coastal areas (>1 pM) but fall to less than 0.1 pM in the open oceans. *Soerensen et al.* [2012] suggested that decreasing inputs of Hg to the North Atlantic Ocean from rivers might explain the observed 5 pM decline in seawater Hg concentrations over a 1000 m vertical profile near Bermuda between 1979 and 2008 [*Mason et al.*, 2012]. In the North Pacific Ocean, *Sunderland et al.* [2009] reported an increase of up to 0.5 pM in vertical profiles from the North Pacific measured between 1987 and 2006. Our simulation shows that rivers alone are insufficient to explain the magnitude of seawater trends in the North Atlantic or North Pacific. The trend in the North Pacific is likely attributable to atmospheric deposition [*Sunderland et al.*, 2009], but the observed 5 pM decline near Bermuda is challenging to explain.

4.3.2 Broader biogeochemical implications

In our updated global biogeochemical model, cumulative anthropogenic Hg forcings since 1850 include 330 Gg of Hg emitted to the atmosphere (220 Gg from [*Streets et al.*, 2011], and an additional 110 Gg from [*Horowitz et al.*, 2014]), plus 380 Gg of anthropogenic Hg in river discharge. Sequestration of Hg in ocean margin sediments in the model provides a sink of 260 Gg for anthropogenic Hg since 1850. Thus we estimate that ocean margin sediments have sequestered up to one third of post-1850 anthropogenic Hg releases. Removal of Hg to ocean margin sediments and decreased soil re-emissions helps balance the increase in anthropogenic sources. Our simulated present-day atmosphere is 5500 Mg (compared to 4600-5600 Mg supported by observations [*Amos et al.*, 2013]), the upper ocean (0-1500 m) Hg concentration is 1.7 pM (compared to the range in mean total Hg across ocean basins 0.6-2.9 pM [*Mason et al.*, 2012]), and storage in organic soils is 250,000 Mg (compared to >300,000 Mg from *Hararuk et al.* [2013]). Our analysis suggests that increasing Hg retention on land and lowering Hg accumulation in the ocean requires improving the representation of Hg dynamics between terrestrial reservoirs.

Figure 4.3 shows the time-dependent fate of a pulse of Hg emitted to the atmosphere in our updated model and then cycled through the different model reservoirs. We find a characteristic time scale of centuries for removal to ocean margin sediments, versus thousands of years for removal to deep ocean sediments, so that ocean margin sediments are the dominant long-term sink of Hg. The atmospheric pulse cycles between surface reservoirs for decades through the legacy of storage in the subsurface ocean. Unlike in Chapter 3 (**Figure 3.6**), the deep ocean does not become a dominant reservoir over centurial time scales because of the competing sink from ocean margin sediments.

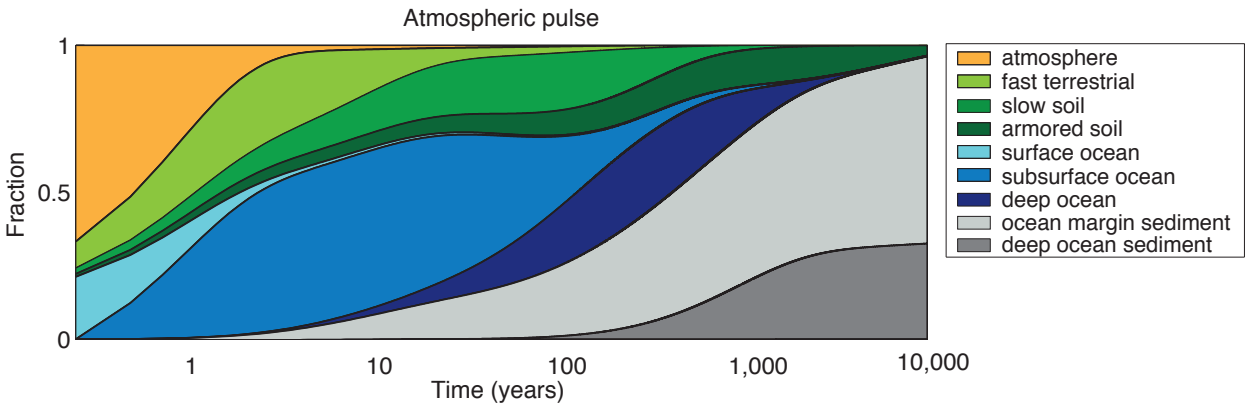

Figure 4.3: Time-dependent fate of a unit pulse of Hg emitted to the atmosphere at time $t = 0$ and then tracked by the model as it cycles between the ocean, atmosphere, and terrestrial reservoirs before eventually being removed to ocean margin sediments. This figure updates the top panel of **Figure 3.6**.

Figure 4.4 shows the future recovery of the atmosphere and ocean under a hypothetical scenario of zero releases of primary anthropogenic after 2015. The effect of sequestration in ocean margin sediments is illustrated by comparing model results with and without this sink, where the latter is more similar to the original model version in *Amos et al.* [2013]. Sequestration in ocean margin sediments in our updated model hastens recovery in the atmosphere, surface, and subsurface ocean over the 21st century. The subsurface ocean decreases by 50% by 2100, as compared to 35% when we do not account the sediment sink (**Figure 4.4**), and 25% in *Amos et al.* [2013]. **Figure 4.4** also shows that the difference between simulations widens over time due to legacy Hg being more efficiently removed from active cycling.

Accounting for the loss of Hg to ocean margin sediments lowers the simulated steady-state natural budget of Hg in all reservoirs. This increases the relative perturbation from human activity and suggests an all-time enrichment in surface reservoirs possibly twice as large as previously estimated. Simulated natural deposition is 0.8 μg m^{-2} a^{-1}, which falls within the range (0.6 – 1.7 0.8 μg m^{-2} a^{-1}) of background deposition estimated from multi-millennia peat archives

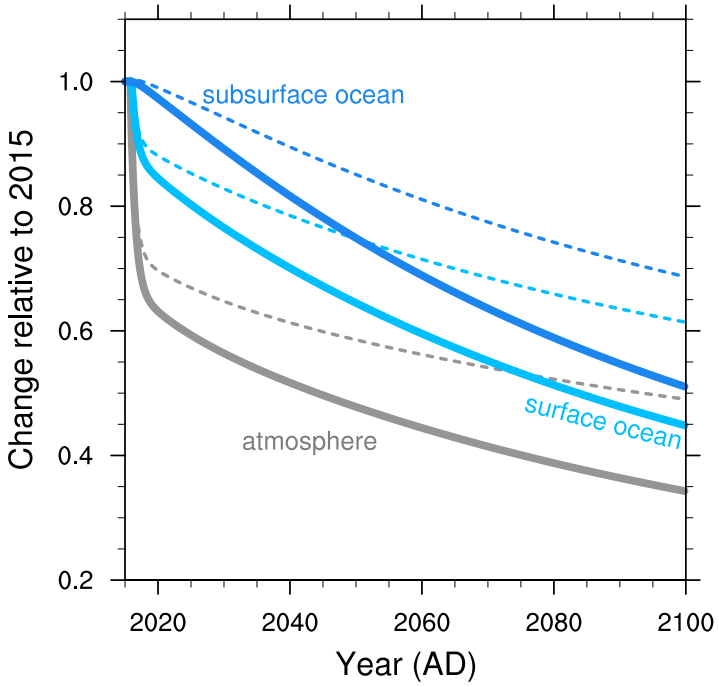

Figure 4.4: Change in global reservoir masses of Hg relative to 2015 under a hypothetical scenario of zero releases of primary anthropogenic Hg after 2015. Results are shown for the updated biogeochemical box model with sequestration in ocean margin sediments (solid) and without (dashed).

[*Biester et al.*, 2007]. However, all-time enrichment is sensitive to changes in the efficiency of long-term storage in terrestrial soils and sequestration in ocean margin sediments. Benthic sediments at ocean margins have been perturbed substantially by activities such as coastal development, dredging, and trawling [*Mayer et al.*, 1991]. Such disturbance would prolong the biogeochemical lifetime of anthropogenic Hg. Better information is needed on the long-term fate of Hg in benthic ocean margin sediments.

Acknowledgements: The US National Science Foundation Divisions of Atmospheric Chemistry (ATM0961357) and Chemical Oceanography (OCE1130549) supported this work. HMA acknowledges support from NSF GFRP. We thank Anne Soerensen, David Krabbenhoft, Mark Brigham, and Rob Mason for their thoughtful discussion. We thank Simon Wilson for data on point source releases of anthropogenic Hg to water. We acknowledge use of NCL software version 6.1.2 (http://www.ncl.ucar.edu/) to create Figures 4.1, 4.3, and 4.4.

References:

AMAP/UNEP (2008), Technical background report to the global atmospheric mercury assessment, *Rep.*, 159 pp, Arctic Monitoring and Assessment Program / UNEP Chemicals Branch.

AMAP/UNEP (2013), Technical background report for the global mercury assessment 2013.*Rep.*, vi + 263 pp pp, Arctic Monitoring and Assessment Program, Oslo, Norway / UNEP Chemicals Branch, Geneva, Switzerland.

Amos, H. M., et al. (2013), Legacy impacts of all-time anthropogenic emissions on the global mercury cycle, *Glob. Biogeochem. Cycle*, *27*(2), 410-421.

An, Q., et al. (2010), Assessment of dissolved heavy metal in the Yangtze River Estuary and its adjacent sea, China, *Environ. Monit. Assess.*, *164*(1-4), 173-187.

Bi, C. J., et al. (2012), Variations of mercury distribution in the water column during the course of a tidal cycle in the Yangtze estuarine intertidal zone, China, *Sci. China-Chem.*, *55*(10), 2224-2232.

Biester, H., et al. (2007), Modeling the past atmospheric deposition of mercury using natural archives, *Environ. Sci. Technol.*, *41*(14), 4851-4860.

Bopp, R. F., et al. (1993), Sediment-derived chronologies of persistent contaminants in Jamaica Bay, New York, *Estuaries*, *16*(3B), 608-616.

Chakraborty, L. B., et al. (2013), Anthropogenic mercury flows in india and impacts of emission controls, *Environ. Sci. Technol.*, *47*(15), 8105-8113.

Chester, R. (2003), The transport of material to the oceans: Relative flux magnitudes, in *Marine geochemistry*, edited by R. Chester, pp. 98-134, Blackwell Science, Oxford, UK.

Corbitt, E. S., et al. (2011), Global source-receptor relationships for mercury deposition under present-day and 2050 emissions scenarios, *Environ. Sci. Technol.*, *45*(24), 10477-10484.

Cossa, D., and M. Coquery (2005), The Mediterranean mercury anomaly, a geochemical or a biologocal issue, *Mediterranean Sea*, *5*, 177-208.

Dai, A., et al. (2009), Changes in continental freshwater discharge from 1948 to 2004, *Journal of Climate*, *22*(10), 2773-2792.

Dastoor, A. P., and D. A. Durnford (2013), Arctic ocean: Is it a sink or a source of atmospheric mercury?, *Environ. Sci. Technol.*, *48*(3), 1707-1717.

Dutkiewicz, S., et al. (2012), Interconnection of nitrogen fixers and iron in the Pacific Ocean: Theory and numerical simulations, *Glob. Biogeochem. Cycle*, *26*, 16.

Emmerton, C. A., et al. (2013), Mercury export to the arctic ocean from the mackenzie river, canada, *Environ. Sci. Technol.*, *47*(14), 7644-7654.

Fisher, J. A., et al. (2012), Riverine source of arctic ocean mercury inferred from atmospheric observations, *Nat. Geosci.*, *5*(7), 499-504.

Gatz, D. F., and L. Smith (1995), The standard error of a weighted mean concentration .1. Bootstrapping vs other methods, *Atmospheric Environment*, *29*(11), 1185-1193.

Gill, G. A., and W. F. Fitzgerald (1988), Vertical mercury distributions in the oceans, *Geochim. Cosmochim. Acta*, *52*(6), 1719-1728.

Hall, F. G., et al. (2006), ISLSCP initiative II global data sets: Surface boundary conditions and atmospheric forcings for land-atmosphere studies, *J. Geophys. Res.-Atmos.*, *111*(D22).

Hararuk, O., et al. (2013), Modelling the sensitivity of soil mercury storage to climate-induced changes in soil carbon pools, *Biogeosciences*, *10*(4), 2393-2407.

Harland, B. J., et al. (2000), The distribution of mercury and other trace metals in the sediments of the Mersey Estuary over 25 years 1974-1998, *Sci. Total Environ.*, *253*(1-3), 45-62.

Holmes, C. D., et al. (2010), Global atmospheric model for mercury including oxidation by bromine atoms, *Atmos. Chem. Phys.*, *10*, 12037-12057.

Horowitz, H. M., et al. (2014), Historical mercury releases from commercial products: Global environmental implications, *Environ. Sci. Technol.*, *in review*.

Hylander, L. D., and M. Meili (2005), The rise and fall of mercury: Converting a resource to refuse after 500 years of mining and pollution, *Critical Reviews in Environmental Science and Technology*, *35*(1), 1-36.

Jiang, H., et al. (2003), The distribution and speciation of mercury in Wujiang River, *J. Phys. IV*, *107*, 679-682.

Kirk, J. L., et al. (2012), Mercury in Arctic marine ecosystems: Sources, pathways and exposure, *Environ. Res.*, *119*, 64-87.

Kocman, D., et al. (2014), A global inventory of mercury releases to aquatic environments: Towards assessment of global mercury releases to aquatic environments, *in preparation*.

Leermakers, M., et al. (2001), Mercury in the southern North Sea and Scheldt Estuary, *Mar. Chem.*, *75*(3), 229-248.

Leitch, D. R., et al. (2007), The delivery of mercury to the Beaufort Sea of the Arctic Ocean by the Mackenzie River, *Sci. Total Environ.*, *373*(1), 178-195.

Liu, J. G., and W. Yang (2012), Water sustainability for China and beyond, *Science*, *337*(6095), 649-650.

Liu, J. L., et al. (2012), Spatial distribution and speciation of mercury and methyl mercury in the surface water of East River (Dongjiang) Tributary of Pearl River Delta, South China, *Environ. Sci. Pollut. Res.*, *19*(1), 105-112.

Ludwig, W., et al. (1996), Predicting the oceanic input of organic carbon by continental erosion, *Glob. Biogeochem. Cycle*, *10*(1), 23-41.

Ludwig, W., et al. (2011), ISLSCP II global river fluxes of carbon and sediments to the oceans, edited, Oak Ridge Natinal Laboratory Distributed Active Archive Center, Oak Ridge, Tennessee, USA.

Mahaffey, K. R., et al. (2011), Balancing the benefits of n-3 polyunsaturated fatty acids and the risks of methylmercury exposure from fish consumption, *Nutr. Rev.*, *69*(9), 493-508.

Mansson, N., et al. (2009), Phasing out cadmium, lead, and mercury, *J. Ind. Ecol.*, *13*(1), 94-111.

Marshall, J., et al. (1997), Hydrostatic, quasi-hydrostatic, and nonhydrostatic ocean modeling, *J. Geophys. Res.-Oceans*, *102*(C3), 5733-5752.

Mason, R. P., et al. (2001), Mercury in the Atlantic Ocean: Factors controlling air-sea exchange of mercury and its distribution in the upper waters, *Deep-Sea Res. Part II-Top. Stud. Oceanogr.*, *48*(13), 2829-2853.

Mason, R. P., et al. (2004), Metal accumulation in Baltimore Harbor: Current and past inputs, *Appl. Geochem.*, *19*(11), 1801-1825.

Mason, R. P., et al. (2012), Mercury biogeochemical cycling in the ocean and policy implications, *Environ. Res.*, *119*, 101-117.

Maxson, P. (2004), Mercury flows in Europe and the world: Impact of decommissioned chlor-alkali plants, *Rep.*, 104 pp, European Commission, Directorate General for Environment, Brussels, Belgium.

Maxson, P. (2006), Mercury flows and safe storage of surplus mercury, *Rep.*, 71 pp, European Commission Directorate General for Environment, Brussels.

Mayer, L. M., et al. (1991), Effects of commercial dragging on sedimentary organic matter, *Marine Environmental Research*, *31*(4), 249-261.

McKee, B. A., et al. (2004), Transport and transformation of dissolved and particulate materials on continental margins influenced by major rivers: Benthic boundary layer and seabed processes, *Cont. Shelf Res.*, *24*(7-8), 899-926.

Milliman, J. D., and K. L. Farnsworth (2011), Runoff, erosion, and delivery to the coastal ocean, in *River discharge to the coastal ocean: A global synthesis*, edited, pp. 13-61, Cambridge University Press, New York.

Noh, S., et al. (2013), Influence of salinity intrusion on the speciation and partitioning of mercury in the Mekong River Delta, *Geochim. Cosmochim. Acta*, *106*, 379-390.

Obrist, D. (2012), Mercury distribution across 14 U.S. Forests. Part II: Patterns of methyl mercury concentrations and areal mass of total and methyl mercury, *Environ. Sci. Technol.*, *46*(11), 5921-5930.

Obrist, D., et al. (2014), Vertical profile measurements of soil air suggest immobilization of gaseous elemental mercury in mineral soil, *Environ. Sci. Technol.*, *48*(4), 2242-2252.

Outridge, P. M., et al. (2008), A mass balance inventory of mercury in the Arctic Ocean, *Environ. Chem.*, *5*(2), 89-111.

Pacyna, E. G., et al. (2010), Global emission of mercury to the atmosphere from anthropogenic sources in 2005 and projections to 2020, *Atmos. Environ.*, *44*(20), 2487-2499.

Rajar, R., et al. (2007), Mass balance of mercury in the Mediterranean Sea, *Mar. Chem.*, *107*(1), 89-102.

Ram, A., et al. (2003), Mercury in sediments of Ulhas Estuary, *Mar. Pollut. Bull.*, *46*(7), 846-857.

Sankar, R., et al. (2010), Seasonal variations in physico-chemical parameters and heavy metals in water and sediments of Uppanar Estuary, Nagapattinam, India, *J.Environ.Biol.*, *31*(5), 681-686.

Schuster, P. F., et al. (2011), Mercury export from the Yukon River basin and potential response to a changing climate, *Environ. Sci. Technol.*, *45*(21), 9262-9267.

Shi, J. B., et al. (2010), Mercury profiles in sediments of the Pearl River Estuary and the surrounding coastal area of South China, *Environ. Pollut.*, *158*(5), 1974-1979.

Soerensen, A. L., et al. (2012), Multi-decadal decline of mercury in the north atlantic atmosphere explained by changing subsurface seawater concentrations, *Geophys. Res. Lett.*, *39*, L21810.

Soerensen, A. L., et al. (2010), An improved global model for air-sea exchange of mercury: High concentrations over the North Atlantic, *Environ. Sci. Technol.*, *44*(22), 8574-8580.

Steinberg, N., et al. (2004), Health of the harbor: The first comprehensive look at the state of the NY/NJ harbor estuary, *Rep.*, 22 pp, Hudson River Foundation, New York, NY.

Streets, D. G., et al. (2011), All-time releases of mercury to the atmosphere from human activities, *Environ. Sci. Technol.*, *45*(24), 10485-10491.

Strode, S. A., et al. (2008), Trans-pacific transport of mercury, *J. Geophys. Res.-Atmos.*, *113*(D15), 12.

Sunderland, E. M., and R. P. Mason (2007), Human impacts on open ocean mercury concentrations, *Global Biogeochem. Cycles*, *21*(4), GB4022.

Sunderland, E. M., et al. (2009), Mercury sources, distribution, and bioavailability in the North Pacific Ocean: Insights from data and models, *Glob. Biogeochem. Cycle*, *23*, 14.

Sunderland, E. M., et al. (2004), Speciation and bioavailability of mercury in well-mixed estuarine sediments, *Mar. Chem.*, *90*(1-4), 91-105.

Swartzendruber, P. C., et al. (2006), Observations of reactive gaseous mercury in the free troposphere at the Mount Bachelor Observatory, *J. Geophys. Res.-Atmos.*, *111*(D24), 12.

Tong, Y. D., et al. (2013), Behavior of mercury in an urban river and its accumulation in aquatic plants, *Environ. Earth Sci.*, *68*(4), 1089-1097.

UNEP (2004), Guinea current, GIWA regional assessment 42, *Rep.*, University of Kalamar, Kalamar, Sweden.

Varekamp, J. C., et al. (2003), Mercury contamination chronologies from Connecticut wetlands and Long Island Sound sediments, *Environ. Geol.*, *43*(3), 268-282.

Walsh, J. P., and C. A. Nittrouer (2009), Understanding fine-grained river-sediment dispersal on continental margins, *Mar. Geol.*, *263*(1-4), 34-45.

Wilburn, D. R. (2013), Changing ptterns in the use, recycling, and material substitution of mercury in the United States, *Rep.*, 32 pp, U. S. Geological Survey.

Wright, L. D., et al. (1988), Marine dispersal and deposition of Yellow River silts by gravity-driven underflows, *Nature*, *332*(6165), 629-632.

Yi, Y. J., et al. (2011), Ecological risk assessment of heavy metals in sediment and human health risk assessment of heavy metals in fishes in the middle and lower reaches of the Yangtze River basin, *Environ. Pollut.*, *159*(10), 2575-2585.

Zhang, H., and B. Shan (2008), Historical records of heavy metal accumulation in sediments and the relationship with agricultural intensification in the Yangtze–Huaihe region, China, *Sci. Total Environ.*, *399*(1–3), 113-120.

Zhang, Y., et al. (2014), Transport and fate of riverine discharged mercury in the ocean: Insights from a 3D transport model, *in prep*.

Appendix

A.1 GEOS-Chem algorithm for washout of soluble gases by rain

Below-cloud scavenging (washout) of gases by rain in GEOS-Chem is determined by Henry's law equilibrium but can be also limited by mass transfer for highly soluble gases [*Levine and Schwartz*, 1982]. The fraction F of gas scavenged from a grid box by washout over a time step Δt as determined by Henry's law equilibrium is

$$F = f\frac{K^* L_p RT}{1 + K^* L_p RT} \tag{A1}$$

Here f is the areal fraction of the grid box experiencing precipitation, K^* is the effective Henry's law constant (M atm^{-1}) including any dissociation and complexation equilibria in the aqueous phase, R is the universal gas constant, T is temperature, and L_p is the time-integrated rainwater content in the precipitating fraction of the grid box

$$L_p = \frac{P\Delta t}{f\Delta Z} \tag{A2}$$

where P (cm^3 water cm^{-2} surface s^{-1}) is the grid-averaged precipitation flux through the bottom of the grid box and ΔZ (cm) is the grid box thickness. For highly soluble gases, F may be limited by molecular diffusion to the raindrops. On the basis of the detailed mass transfer calculations by *Levine and Schwartz* [1982] for diffusion-limited uptake of HNO_3, a maximum value F_{max} for F is derived as

$$F_{\max} = f[1 - \exp(-k' \frac{P}{f} \Delta t)] \quad \text{(A3)}$$

where k' (cm^{-1}) is a washout rate constant ($k' = 1$ cm^{-1}; Table 2 of *Levine and Schwartz* [1982]).

GEOS-Chem computes F and F_{max} locally for every precipitating grid box and time step. If $F \leq F_{max}$, it is assumed that washout is limited by Henry's law and the change in mass Δm of the soluble gas due to washout over Δt is then computed as

$$\Delta m = -Fm + m_T(1 - \frac{F}{f}) \quad \text{(A4)}$$

where m is the mass of the gas in the grid box and m_T is the cumulative mass of gas scavenged via precipitation from above and entering the top of the grid box over Δt and over the fraction f. Equation (A4) allows for partial re-evaporation of the mass scavenged from above. If $F > F_{max}$, it is assumed that washout is limited by mass transfer as given by Eq. (A3) and Δm is then computed as

$$\Delta m = -F_{\max} m + \beta \alpha m_T \quad \text{(A5)}$$

where α is the fraction of precipitation falling through the top of the gridbox that evaporates within the gridbox, and β is the fraction of this re-evaporation that involves total evaporation of raindrops (which releases the gas to the gridbox) rather than partial shrinkage (which does not). It is assumed that $\beta = 0.5$ for $\alpha < 1$ and $\beta = 1$ for $\alpha = 1$ [*Liu et al.*, 2001].

Because of a coding error in GEOS-Chem, the algorithm described above was incorrectly executed in previous model versions so that washout of highly soluble gases ($F > F_{max}$) was underestimated except for HNO_3 (which was correct). This affected the scavenging of gaseous

Hg(II), for which a Henry's law constant of 1.4×10^6 M atm^{-1} is assumed based on laboratory data for $HgCl_2$ [*Lindqvist and Rodhe*, 1985]. Correcting the error, as done here in the standard simulation, increases the lifetime of gaseous Hg(II) in the troposphere from 108 days to 46 days.

A.2 Historical discharges of Hg from rivers

We construct a best estimate of the decadal change (1970 to present) in riverine inputs to coastal marine systems and the associated uncertainty range based on observations compiled from a survey of published literature. We estimate the confidence in a given scaling factor to be ±50% when data scarcity limits the estimation of an uncertainty range. We only attempt to estimate historical changes for regions where data is available. Detail on historical changes in various ocean basins is provided below.

A.2.1 North Atlantic Ocean: North America

Observations unanimously support a decline in Hg inputs from North American rivers to the North Atlantic Ocean in recent decades [*Bopp et al.*, 1993; *Bopp et al.*, 2006; *Cain et al.*, 2007; *Cardona-Marek et al.*, 2007; *Steinberg et al.*, 2004; *Turner and Lindberg*, 1978; *Varekamp et al.*, 2003; *Zelewski et al.*, 2001]. Estuarine sediment cores suggest Hg inputs peaked between the 1960s and 1970s [*Bopp et al.*, 2006; *Steinberg et al.*, 2004; *Varekamp et al.*, 2003; *Zelewski et al.*, 2001]. From the 1960s-1970s to the 1990s, Hg concentrations have decreased by a factor of ~4 (range, 1.2 - 16) [*Bopp et al.*, 2006; *Steinberg et al.*, 2004; *Varekamp et al.*, 2003; *Zelewski et al.*, 2001]. In the absence of direct measurements, we extrapolate data from *Zelewski et al.* [2001] to estimate the change between 2000 and present. Large declines (e.g., order of magnitude declines) are supported by additional inland measurements on rivers impacted by

industrial Hg inputs [*Breteler et al.*, 1984; *Turner and Lindberg*, 1978]. Sediment measurements in the St. Lawrence river also confirm high inputs of Hg to the St. Lawrence river in the 1970s [*Gagnon et al.*, 1997; *Loring and Bewers*, 1978]. The steep decline in Hg inputs through the 1970s and 1980s and leveling off beginning in the 1990s supported by estuarine sediment cores is consistent with the inventory of anthropogenic Hg releases to water from *Horowitz et al.* [2014].

A.2.2 North Atlantic Ocean: Europe

The change in Europe is consistent with North America, experiencing a rapid decline in Hg contamination in the last 50 years [*Hamzeh et al.*, 2013; *Harland et al.*, 2000; *Leermakers et al.*, 2001; *Mansson et al.*, 2009]. Hg inputs also peaked in the 1960s to 1970s [*Harland et al.*, 2000; *Leermakers et al.*, 2001; *Mansson et al.*, 2009]. From the 1970s to the 1990s, sediment cores from the Mersey (England) and Scheldt (Belgium, France, Netherlands) Estuaries and sludge samples from a wastewater treatment facility in Stockholm (Sweden) suggest, on average, there has been a 7.2-fold decrease (range, 3.4 to 10.5) [*Harland et al.*, 2000; *Leermakers et al.*, 2001; *Mansson et al.*, 2009]. From the 1990s to 2000s, the average decline has been a factor of 1.8 (range, 1.5 to 2.2) [*Harland et al.*, 2000; *Leermakers et al.*, 2001; *Mansson et al.*, 2009]. . The scaling factor for the 1980s is estimated from interpolating enrichment factors from 1970, 1990, and 2000 and assigned an uncertainty of ±50%. Due to data scarcity, we assume Europe experienced the same degree of change from present to 2008 as North America. Based on *Mansson et al.* [2009], Hg inputs double from present to 2000, which we adopt as the upper limit.

A.2.3 Pacific Ocean: China

Observational studies suggest Hg inputs from major Chinese rivers have been increasing in stride with industrial development [*An et al.*, 2010; *Liu et al.*, 2012; *Shi et al.*, 2010; *Shi et al.*, 2007; *Yi et al.*, 2011]. Declining Hg inputs have been reported in only two locations in China and appear to reflect isolated incidences including closure of an acetaldehyde plant on the Songhua River in response to local fisherman exhibiting symptoms of Minamata disease [*Zhang et al.*, 2010; *Zhu et al.*, 2012] and declines in Victoria Harbor, Hong Kong when industry was moved to inland China during the 1980s [*Shi et al.*, 2010; *Shi et al.*, 2007]. We estimate scaling factors based on sediment cores from the Pearl River Delta (1900s to 1990s) [*Shi et al.*, 2010] and dissolved Hg concentrations sampled in the Yangtze River (1984 – 2006) [*An et al.*, 2010]. *An et al.* [2010] report roughly a doubling in dissolved Hg concentrations in the north and south branches of the Yangtze River Estuary between 1984 and 2006 (1985-1990: Hg(D) = 21 ng/L, 2001-2006: Hg(D) = 45 ng/L) and a linear best-fit line of the data suggest a 0.7 ng L^{-1} per year increase. A weighted mean of Hg inputs (ng cm^{-3} decade) from sediment cores at the Pearl and West rivers indicates an exponential increase from the 1990s to present.

A.2.4 North Pacific: North America

The timing and shape of decline in cores from the San Francisco Estuary [*Hornberger et al.*, 1999] are consistent with the pattern observed in the eastern US [*Bopp et al.*, 2006; *Steinberg et al.*, 2004; *Varekamp et al.*, 2003; *Zelewski et al.*, 2001]. From the limited data available, the magnitude of change in the San Francisco Estuary is roughly half as large as in the eastern US (i.e., factor of 1.7 to 2.3 decline from the 1970s to 1990s) [*Hornberger et al.*, 1999]. *Conaway et al.* [2008] reported 17-32% decreases in sediment Hg concentrations between 1993 and 2001 in

the San Francisco Estuary. The lower limit is estimated to be unity (i.e., no change from present), otherwise the uncertainty is estimated to be ±50%. In the absence of compelling evidence for a trend, we assume inputs have been constant in the last decade.

A.2.5 Indian Ocean: India

Several studies identify rivers in India to be highly contaminated with Hg due to dumping and untreated municipal wastewater [*Chakraborty et al.*, 2013; *Ram et al.*, 2003; *Srivastava*, 2003]. From the 1970s to 1990s, sediment profiles from the Ulhas Estuary suggest a factor of ~2 increase from the 1970s to 1990s [*Ram et al.*, 2003]. A more recent study notes increased Hg concentrations in surface sediment compared to deeper layers, which is attributed to increased Hg discharges in recent years, but caution against quantitative conclusions due to suspected diagenesis [*Chatterjee et al.*, 2009]. Due to limited sediment data, we rely on a recent inventory of annual primary anthropogenic Hg releases to the environment (air, soil, water) between 2001 and 2020 to estimate the changes in Hg inputs from Indian rivers [*Chakraborty et al.*, 2013]. Hg consumption is growing exponentially in India and the authors estimate Hg releases to water will increase from 15 tonnes a^{-1} in 2001 to 41 tonnes a^{-1} in 2020 [*Chakraborty et al.*, 2013]. We interpolate to estimate Hg releases between 2001 and 2020 and extrapolate to 1970 to estimate past changes. The estimated change between 1970s and 1990s is consistent with sediment data from *Ram et al.* [2003]. *Chakraborty et al.* [2013] estimates Hg releases are uncertain by a factor of 2.

A.2.6 Mediterranean Sea

Cores from France, Italy, and Israel suggest inputs peaked in the 1970s [*Baldi and*

Damato, 1986; *Elbaz-Poulichet et al.*, 2011; *Krom et al.*, 1994]. From the 1970s to present, we estimate an average decline of a factor of 4.5 based on the factor of 2 decline in Hg concentrations observed by *Elbaz-Poulichet et al.* [2011] and a projected 7-fold decline from Krom et al. [1994]. From the 1970s to 1980s, there is a factor of 2.5 to 3 decrease [*Baldi and Damato*, 1986; *Krom et al.*, 1994]. *Krom et al.* [1994] observed a factor of 4 decreases from the 1970s to 1990s and projected concentrations would decrease by 5-fold by the 2000s. We adopt this as our upper estimate for the change between the 1970s and 1990s – 2000s. The lower limit is taken as 1 (i.e., no change between 1990s – 2000s and present) in the absence of evidence that Hg inputs to the Mediterranean have increased in recent decades. The weight of evidence suggests inputs have decreased in recent decades from continued closure of chlor-alkali facilities through the 1980s and 1990s in the eastern Mediterranean [*Bravo et al.*, 2009; *Kwokal et al.*, 2002] and the closure of Idrija mine (Slovenia) in the 1990s [*Covelli et al.*, 2001; *Horvat et al.*, 2003].

Table A1. Contemporary Hg concentrations measured near river mouths

River	Year(s)	HgP (nmol g^{-1})	HgD (pM)	Unfiltered THg (pM)	Q (km^3 a^{-1})	Reference
North Atlantic						
North America						
Quinnipiac	2007	n/a	5	n/a	0.19	*Clark and Benoit* [2009]
Major tributaries flowing into Gulf of Maine	1998-2002	3.1 (1.3 – 5.0)	11 (3.3 - 12)	22 (5.3 - 73)	88	*Sunderland et al.* [2012]
New York/New Jersey Harbor Estuary	2002 - 2003	4.5 (0.4 - 8.9)	3.1 (1.8 - 5.0)	83 (3.4 - 330)	14	*Balcom et al.* [2008]
Hudson River	1999-2000	4.5 ± 2. 8	3.1 ± 1.0	67 ± 20	14	*Balcom et al.* [2008]
Lower East	1999-2000	n/a	n/a	57 ± 14	14	*Balcom et al.* [2008]
Berry Creek Estuary[a]	2002-2003	3.9 - 270	23 - 380	1400 (210-6800)	n/a	*Cardona-Marek et al.* [2007]
Hackensack	2002-2003	0.7 - 2.1	4.3 - 17	11 - 150	$4.8x10^{-4}$	*Cardona-Marek et al.* [2007]
Europe						
Garonne River La Réole	1998, 1999, 2002 - 2003	1.3 (0.4 - 3.9)	4.6 (1.5 - 12.9)	n/a	16	*Schafer et al.* [2006]
Sado Estuary	2006	1.5 (0.4-3.5)	62 (20 - 390)	n/a	1.3	*Lillebo et al.* [2011]
Douro River	1997, 1999	1.5 - 35	0.1 - 2.0	n/a	21	*Ramalhosa et al.* [2005]
Scheldt Estuary	1995 - 1997	3.6 ± 1.0	7 (4 – 12)	n/a	2.1	*Leermakers et al.* [2001]
Mediterranean						
Po	1994-2001	0.3	2	n/a	49	*Cossa and Coquery* [2005]
Rhône	1994-1995	2.4 ± 2.0	5.5 ± 3.0	30	53	*Cossa and Coquery* [2005]; *Rajar et al.* [2007]

(Continued)						
Nile	1994-1995	0.3	1.8	11	109	*Cossa and Coquery* [2005]; *Rajar et al.* [2007]
Corno	2004	7.5	120	200	0.2	*Covelli et al.* [2009]
Ausso	2004	10 - 25	20 - 100	120 - 320	0.4	*Covelli et al.* [2009]
Danube	2001	0.6 ± 0.3	n/a	n/a	204	*Woitke et al.* [2003]
Arctic						
North America						
Mackenzie	2004	n/a	n/a	51 ± 15	330	*Graydon et al.* [2009]
Mackenzie	2003-2005	.05 ± .04	14 ± 11	35 ± 21	330	*Leitch et al.* [2007]
Mackenzie	2003-2005	n/a	n/a	34 ± 0.7	330	*Wang et al.* [2012]
Mackenzie	2007-2010	0.1 - 0.6	8.0 ± 3.0	73 ± 31	330	*Emmerton et al.* [2013]
Peel River	2007-2010	0.01 - 0.06	10 ± 4.0	110 ± 59	19	*Emmerton et al.* [2013]
Yukon	2001-2005	0.2	9.5	75	203	*Schuster et al.* [2011]
Horton	2003-2005	n/a	n/a	68 ± 18	n/a	*Wang et al.* [2012]
Churchill	2005	n/a	n/a	1.3	21	*Kirk et al.* [2008]
Churchill	2005	0.07	17	17	21	*Hare et al.* [2008]
Churchill	2003-2007	0.14	8.5	10	21	*Schuster et al.* [2011]
Churchill	2003-2007	n/a	8.5 ± 3.7	9.8 ± 4.0	21	*Kirk and St Louis* [2009]
Nelson	2005	n/a	n/a	8.1	110	*Kirk et al.* [2008]
Nelson	2003-2007	0.30	2.5	4.5	110	*Schuster et al.* [2011]
Nelson	2005	0.20	9.5	11	110	*Hare et al.* [2008]
Nelson	2003-2007	n/a	2.5 ± 0.8	4.4 ± 1.6	110	*Kirk et al.* [2008]
Grande Baeline	2005-2007	0.58	11	14	20	*Hare et al.* [2008]
St. Lawrence	1995-1996	0.63	3	14	380	*Schuster et al.* [2011]

(Continued)

Russia						
Lena	1993	0.03	5	13	530	*Coquery et al.* [1995]; *Schuster et al.* [2011]
Ob	1991	0.13	3	8.5	400	*Coquery et al.* [1995]; *Schuster et al.* [2011]
Yenisei	1993	0.3	1.5	4	630	*Coquery et al.* [1995]; *Schuster et al.* [2011]
North Pacific						
North America						
Sacramento	2000-2001	0.5 - 7.7	2.6 - 7.8	n/a	22	*Choe et al.* [2003]
San Francisco Estuary	2005-2006	n/a	7.0 ± 1.5	33 ± 13	n/a	*Bergamaschi et al.* [2012]
San Francisco Estuary	2000s	n/a	2.0 - 10	10 - 50	n/a	*Conaway et al.* [2008]
China						
Songhua	2006	n/a	n/a	50 - 500	78	*Zhang et al.* [2010]
Songhua	2005-2007	n/a	n/a	(94 - 120)	78	*Zhu et al.* [2012]
Haihe	2010	n/a	n/a	63 (18 - 160)	n/a	*Tong et al.* [2013]
Yangtze	2006	n/a	230 ± 60 (170 - 360)	n/a	950	*An et al.* [2010]
Yangtze	2006-2008	1.8 - 25	180 - 3000	n/a	950	*Bi et al.* [2012]
Wujiang (tributary of Yangtze)	2000	>50% of THg	35 (5 - 240)	220 (54 - 1600)	35	*Jiang et al.* [2003]
Pacific						
Mekong	2010-2011	0.3 - 0.5	3.2 – 4.0	22 - 61	470	*Noh et al.* [2013]
Pearl	2007-2009	~50% of THg	55 ± 23	95 ± 29	300	*Liu et al.* [2012]
Indian						
Uppanar Estuary	2007	n/a	n/a	6100 - $1.2x10^5$	n/a	*Sankar et al.* [2010]

(Continued)						
Ulhas	2000	15 – 17	56 - 370	n/a	0.2 - 0.03	*Ram et al.* [2003]
South Atlantic						
North America						
Mississippi	2001-2004	0.31	5.5	29	580	*Schuster et al.* [2011]
South America						
Sinnamary estuary	2003-2005	0.6 ± 0.2 (0.2-2.5)	6 ± 2 (3.3-11)	11 ± 3 (5.9-17)	7.9	*Muresan et al.* [2008]
Major tributaries flowing into Sepetiba Bay	n/a	n/a	0.5 - 330	1.6 - 1200	n/a	*Paraquetti et al.* [2004]
Amazon and major tributaries	1997	1.0 ± 0.2	28 ± 3.5	n/a	5400	*Maurice-Bourgoin et al.* [2003]

[a] We exclude observations from Berry Creek Estuary Superfund site in Hackensack, New Jersey, USA because they more than an order of magnitude larger (THg > 1000 pM) than mean North American riverine concentrations [*Cardona-Marek et al.*, 2007].

Table A2. Comparison of present-day riverine Hg(P) (nmol g^{-1}) concentrations

Ocean Basin	Estimated[a]	Observed[b]
Arctic		
North America	0.39 ± 0.32	0.3 (0.01 - 0.6)
Russia	0.17 ± 0.13	0.1 (0.03 - 0.3)
North Atlantic		
Europe	0.49 ± 0.40	3.4 (0.4 - 35)
North America	0.47 ± 0.38	1.6 (0.1 - 8.9)
South Atlantic		
South America	1.50 ± 1.24	1 (0.2 - 2.5)
North Pacific		
North America	0.34 ± 0.29	4.1 (0.5 - 7.7)
China	5.91 ± 4.84	4 (0.6 - 25)
South Pacific		
Southeast Asia	0.19 ± 0.16	0.4 (0.3 - 0.5)
Indian		
India	2.69 ± 2.20	(15 - 17)
Mediterranean	0.10 ± 0.08	0.7 (0.3 - 25)

[a] From Table 4.1.
[b] Flow-weighted mean and reported range based on published observations in Table A1.

Table A3. Present-day reservoirs and fluxes used to calculate first-order rate coefficients in 7-box model of Hg global biogeochemical cycling

	Flux (Mg a^{-1})
Atmosphere: 5000[a]	
Hg(II) deposition to land[b]	1500[a]
Hg(0) deposition to land[c]	1500[a]
Hg(II) deposition to ocean	3600[a]
Hg(0) air-sea exchange, gross loss to the ocean	1700[a]
Surface ocean: 2900[d]	
Hg(0) air-sea exchange, gross evasion to the atmosphere[e]	4700
Particle settling to the subsurface ocean	3300[d]
Water transfer to subsurface ocean	5100[d]
Subsurface ocean: 130,000[f]	
Particle settling to the deep ocean	480[f]
Water transfer to surface ocean	7100[d]
Water transfer to deep ocean	340[f]
Deep ocean: 220,000[f]	
Burial to deep sediments	210[f]
Water transfer to subsurface ocean	180[f]
Fast terrestrial reservoir: 9600[g]	
Evasion due to respiration of organic carbon[h]	45
Photochemical re-emission of deposited Hg[h]	85
Biomass burning[i]	290
Transfer to the slow pool	330[g]
Transfer to the armored pool	10[g]
Riverine discharge to ocean margins[j]	710
Slow soil reservoir: 35,000[g]	
Evasion due to respiration of organic carbon	25
Biomass burning	8
Transfer to fast pool	210[g]
Riverine discharge to ocean margins	20
Armored soil reservoir: 190,000[g]	
Evasion due to respiration of organic carbon	3
Biomass burning	4
Transfer to fast pool	15[g]
Riverine discharge to ocean margins	10
External inputs	
Geogenic emissions	90[k]
Anthropogenic emissions[l]	$f(t)$
Anthropogenic discharges to rivers[m]	$f(t)$

(Continue)
First-order rate coefficients *k* are calculated as $k_{ij} = F_{ij}/m_i$, where F_{ij} and m_i are the fluxes (Mg a^{-1}) and reservoir sizes (Mg) provided in the table above.
[a] *Holmes et al.* [2010]
[b] Partitioned 50% to the fast terrestrial pool, 32% to the slow soil pool, and 18% to the armored soil pool following *Smith-Downey et al.* [2010].
[c] To the fast terrestrial reservoir only *Smith-Downey et al.* [2010].
[d] *Soerensen et al.* [2010]
[e] Sum of gross Hg(0) uptake (1700 Mg a^{-1}) from *Holmes et al.* [2010] and net Hg(0) evasion (3000 Mg a^{-1}) from *Soerensen et al.* [2010].
[f] *Sunderland and Mason* [2007]
[g] *Smith-Downey et al.* [2010]
[h] Decreased by a factor of 10 from *Smith-Downey et al.* [2010] based on observations and empirically-based model suggesting retention of deposited Hg is higher than previously estimated [*Hararuk et al.*, 2013; *Obrist*, 2012; *Obrist et al.*, 2014].
[i] Total biomass burning is 300 Mg a^{-1} *Holmes et al.* [2010], of which 95% is estimated to come from vegetation and 5% from the three soil pools based on their carbon constant [*Amos et al.*, 2013].
[j] See Section 4.2.
[k] *Bagnato et al.* [2011]
[l] Inputs are a function of time. Global historical inventories from *Streets et al.* [2011] and *Horowitz et al.* [2014].
[m] Inputs are a function of time. See Section 4.2.

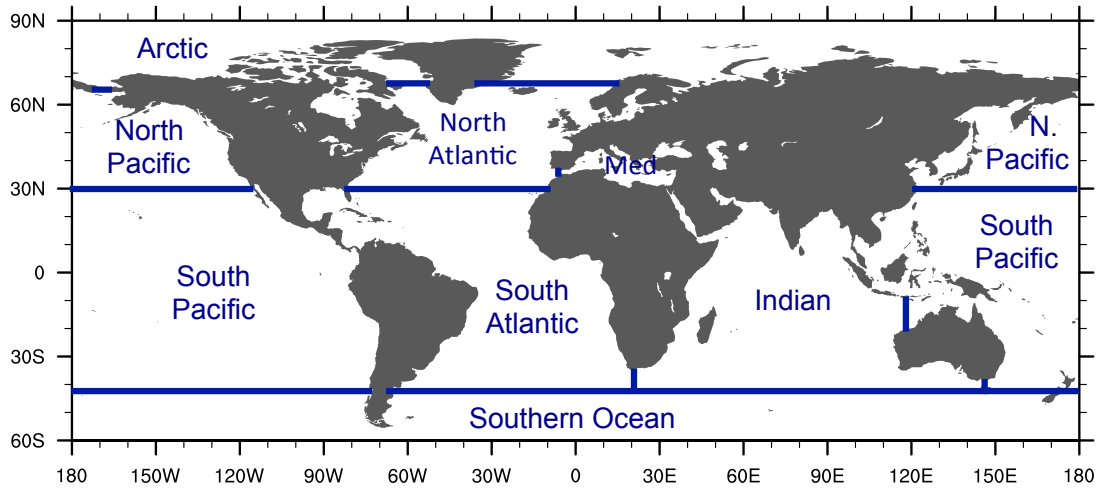

Figure A1: Ocean basins as defined in Chapter 4.

References:

Amos, H. M., et al. (2013), Legacy impacts of all-time anthropogenic emissions on the global mercury cycle, *Glob. Biogeochem. Cycle*, *27*(2), 410-421.

An, Q., et al. (2010), Assessment of dissolved heavy metal in the Yangtze River Estuary and its adjacent sea, China, *Environ. Monit. Assess.*, *164*(1-4), 173-187.

Bagnato, E., et al. (2011), New clues on the contribution of earth's volcanism to the global mercury cycle, *Bull. Volcanol.*, *73*(5), 497-510.

Balcom, P. H., et al. (2008), Seasonal distributions and cycling of mercury and methylmercury in the waters of New York/New Jersey Harbor Estuary, *Mar. Chem.*, *109*(1-2), 1-17.

Baldi, F., and M. L. Damato (1986), Mercury pollution in marine sediment cores near cinnabar deposits and a chloralkali plant, *Sci. Total Environ.*, *57*, 111-120.

Bergamaschi, B. A., et al. (2012), Mercury dynamics in a San Francisco estuary tidal wetland: Assessing dynamics using in situ measurements, *Estuaries Coasts*, *35*(4), 1036-1048.

Bi, C. J., et al. (2012), Variations of mercury distribution in the water column during the course of a tidal cycle in the Yangtze estuarine intertidal zone, China, *Sci. China-Chem.*, *55*(10), 2224-2232.

Bopp, R. F., et al. (1993), Sediment-derived chronologies of persistent contaminants in Jamaica Bay, New York, *Estuaries*, *16*(3B), 608-616.

Bopp, R. F., et al. (2006), Contaminant chronologies from Hudson River sedimentary records, in *The Hudson River Estuary*, edited by J. S. Levinton and J. R. Waldman, pp. 383-397, Cambridge University Press, New York.

Bravo, A. G., et al. (2009), Historical record of mercury contamination in sediments from the Babeni Reservoir in the Olt river, Romania, *Environ. Sci. Pollut. Res.*, *16*, 66-75.

Breteler, R. J., et al. (1984), Sedimentological reconstruction of the recent pattern of mercury pollution in the Niagara River, *Environ. Sci. Technol.*, *18*(6), 404-409.

Cain, A., et al. (2007), Substance flow analysis of mercury intentionally used in products in the United States, *J. Ind. Ecol.*, *11*(3), 61-75.

Cardona-Marek, T., et al. (2007), Mercury speciation, reactivity, and bioavailability in a highly contaminated estuary, Berry's Creek, New Jersey meadowlands, *Environ. Sci. Technol.*, *41*(24), 8268-8274.

Chakraborty, L. B., et al. (2013), Anthropogenic mercury flows in India and impacts of emission controls, *Environ. Sci. Technol.*, *47*(15), 8105-8113.

Chatterjee, M., et al. (2009), Mercury enrichments in core sediments in Hugli-Matla-Bidyadhari estuarine complex, north-eastern part of the Bay of Bengal and their ecotoxicological significance, *Environ. Geol.*, *57*(5), 1125-1134.

Choe, K. Y., et al. (2003), Distribution of particulate, colloidal, and dissolved mercury in San Francisco Bay Estuary. 1. Total mercury, *Limnol. Oceanogr.*, *48*(4), 1535-1546.

Clark, H. F., and G. Benoit (2009), Current and historic mercury deposition to New Haven Harbor (CT, USA): Implications for industrial coastal environments, *Sci. Total Environ.*, *407*(15), 4472-4479.

Conaway, C. H., et al. (2008), Mercury in the san francisco estuary, in *Reviews of environmental contamination and toxicology, vol 194*, edited by D. M. Whitacre, pp. 29-54, Springer, New York.

Coquery, M., et al. (1995), The distribution of dissolved and particulate mercury in 3 Siberian estuaries and adjacent Arctic coastal waters, *Water Air Soil Pollut.*, *80*(1-4), 653-664.

Cossa, D., and M. Coquery (2005), The Mediterranean mercury anomaly, a geochemical or a biologocal issue, *Mediterranean Sea*, *5*, 177-208.

Covelli, S., et al. (2001), Mercury contamination of coastal sediments as the result of long-term cinnabar mining activity (Gulf of Trieste, Northern Adriatic Sea), *Appl. Geochem.*, *16*(5), 541-558.

Covelli, S., et al. (2009), Recent contamination of mercury in an estuarine environment (Marano Lagoon, Northern Adriatic, Italy), *Estuar. Coast. Shelf Sci.*, *82*(2), 273-284.

Elbaz-Poulichet, F., et al. (2011), A 3500-year record of Hg and Pb contamination in a Mediterranean sedimentary archive (the Pierre Blanche Lagoon, France), *Environ. Sci. Technol.*, *45*(20), 8642-8647.

Emmerton, C. A., et al. (2013), Mercury export to the Arctic Ocean from the Mackenzie River, Canada, *Environ. Sci. Technol.*, *47*(14), 7644-7654.

Gagnon, C., et al. (1997), Behaviour of anthropogenic mercury in coastal marine sediments, *Mar. Chem.*, *59*(1-2), 159-176.

Graydon, J. A., et al. (2009), Mercury in the Mackenzie River delta and estuary: Concentrations and fluxes during open-water conditions, *Sci. Total Environ.*, *407*(8), 2980-2988.

Hamzeh, M., et al. (2013), Profile of trace metals accumulation in core sediment from Seine River Estuary (Docks Basin), *Environmental Technology*, *34*(9), 1107-1116.

Hararuk, O., et al. (2013), Modelling the sensitivity of soil mercury storage to climate-induced changes in soil carbon pools, *Biogeosciences*, *10*(4), 2393-2407.

Hare, A., et al. (2008), Contemporary and preindustrial mass budgets of mercury in the Hudson Bay marine system: The role of sediment recycling, *Sci. Total Environ.*, *406*(1-2), 190-204.

Harland, B. J., et al. (2000), The distribution of mercury and other trace metals in the sediments of the Mersey Estuary over 25 years 1974-1998, *Sci. Total Environ.*, *253*(1-3), 45-62.

Holmes, C. D., et al. (2010), Global atmospheric model for mercury including oxidation by bromine atoms, *Atmos. Chem. Phys.*, *10*, 12037-12057.

Hornberger, M. I., et al. (1999), Historical trends of metals in the sediments of San Francisco Bay, California, *Mar. Chem.*, *64*(1-2), 39-55.

Horowitz, H. M., et al. (2014), Historical mercury releases from commercial products: Global environmental implications, *Environ. Sci. Technol.*, *in review*.

Horvat, M., et al. (2003), Mercury speciation in an estuary influenced by past mercury mining activities, *Geochim. Cosmochim. Acta*, *67*(18), A158-A158.

Jiang, H., et al. (2003), The distribution and speciation of mercury in Wujiang River, *J. Phys. IV*, *107*, 679-682.

Kirk, J. L., and V. L. St Louis (2009), Multiyear total and methyl mercury exports from two major sub-arctic rivers draining into Hudson Bay, Canada, *Environ. Sci. Technol.*, *43*(7), 2254-2261.

Kirk, J. L., et al. (2008), Methylated mercury species in marine waters of the Canadian high and sub Arctic, *Environ. Sci. Technol.*, *42*(22), 8367-8373.

Krom, M. D., et al. (1994), Industrial mercury in combination with natural Pb-210 as time-dependent tracers of sedimentation and mercury removal from Haifa Bay, Israel, *Estuar. Coast. Shelf Sci.*, *38*(6), 625-642.

Kwokal, Z., et al. (2002), A comparison of anthropogenic mercury pollution in Kastela Bay (Croatia) with pristine estuaries in Ore (Sweden) and Krka (Croatia), *Mar. Pollut. Bull.*, *44*(10), 1152-1157.

Leermakers, M., et al. (2001), Mercury in the southern North Sea and Scheldt Estuary, *Mar. Chem.*, *75*(3), 229-248.

Leitch, D. R., et al. (2007), The delivery of mercury to the Beaufort Sea of the Arctic Ocean by the Mackenzie River, *Sci. Total Environ.*, *373*(1), 178-195.

Levine, S. Z., and S. E. Schwartz (1982), In-cloud and below-cloud scavenging of nitric acid vapor, *Atmos. Environ.*, 16, 1725-1734.

Lillebo, A. I., et al. (2011), Assessment of mercury in water, sediments and biota of a southern European Estuary (Sado Estuary, Portugal), *Water, Air, and Soil Pollution*, *214*(1/4), 667-680.

Lindqvist, O., and H. Rodhe (1985), Atmospheric mercury - a review, *Tellus Series B-Chem. Phys. Met.*, 37(3), 136-159.

Liu, H. Y., et al. (2001), Constraints from Pb-210 and Be-7 on wet deposition and transport in a global three-dimensional chemical tracer model driven by assimilated meteorological fields, *J. Geophys. Res.*, 106(D11), 12109-12128.

Liu, J. L., et al. (2012), Spatial distribution and speciation of mercury and methyl mercury in the surface water of east river (dongjiang) tributary of pearl river delta, south china, *Environ. Sci. Pollut. Res.*, *19*(1), 105-112.

Loring, D. H., and J. M. Bewers (1978), Geochemical mass balances for mercury in a canadian fjord, *Chem. Geol.*, *22*(4), 309-330.

Mansson, N., et al. (2009), Phasing out cadmium, lead, and mercury, *J. Ind. Ecol.*, *13*(1), 94-111.

Maurice-Bourgoin, L., et al. (2003), Transport, distribution and speciation of mercury in the Amazon River at the confluence of black and white waters of the Negro and Solimoes rivers, *Hydrol. Process.*, *17*(7), 1405-1417.

Muresan, B., et al. (2008), Mercury sources and transformations in a man-perturbed tidal estuary: The Sinnamary Estuary, French Guiana, *Geochim. Cosmochim. Acta*, *72*(22), 5416-5430.

Noh, S., et al. (2013), Influence of salinity intrusion on the speciation and partitioning of mercury in the mekong river delta, *Geochim. Cosmochim. Acta*, *106*, 379-390.

Obrist, D. (2012), Mercury distribution across 14 U.S. Forests. Part II: Patterns of methyl mercury concentrations and areal mass of total and methyl mercury, *Environ. Sci. Technol.*, *46*(11), 5921-5930.

Obrist, D., et al. (2014), Vertical profile measurements of soil air suggest immobilization of gaseous elemental mercury in mineral soil, *Environ. Sci. Technol.*, *48*(4), 2242-2252.

Paraquetti, H. H. M., et al. (2004), Mercury distribution, speciation and flux in the Sepetiba Bay Tributaries, SE Brazil, *Water Res.*, *38*(6), 1439-1448.

Rajar, R., et al. (2007), Mass balance of mercury in the Mediterranean Sea, *Mar. Chem.*, *107*(1), 89-102.

Ram, A., et al. (2003), Mercury in sediments of Ulhas Estuary, *Mar. Pollut. Bull.*, *46*(7), 846-857.

Ramalhosa, E., et al. (2005), Mercury distribution in Douro Estuary (Portugal), *Mar. Pollut. Bull.*, *50*(11), 1218-1222.

Sankar, R., et al. (2010), Seasonal variations in physico-chemical parameters and heavy metals in water and sediments of Uppanar Estuary, Nagapattinam, India, *J.Environ.Biol.*, *31*(5), 681-686.

Schafer, J., et al. (2006), Mercury in the Lot-Garonne River system (France): Sources, fluxes and anthropogenic component, *Appl. Geochem.*, *21*(3), 515-527.

Schuster, P. F., et al. (2011), Mercury export from the Yukon River basin and potential response to a changing climate, *Environ. Sci. Technol.*, *45*(21), 9262-9267.

Shi, J. B., et al. (2010), Mercury profiles in sediments of the Pearl River Estuary and the surrounding coastal area of south China, *Environ. Pollut.*, *158*(5), 1974-1979.

Shi, J. B., et al. (2007), Spatial and temporal variations of mercury in sediments from Victoria Harbour, Hong Kong, *Mar. Pollut. Bull.*, *54*(4), 480-485.

Smith-Downey, N. V., et al. (2010), Anthropogenic impacts on global storage and emissions of mercury from terrestrial soils: Insights from a new global model, *J. Geophys. Res.-Biogeosci.*, *115*, G03008.

Soerensen, A. L., et al. (2010), An improved global model for air-sea exchange of mercury: High concentrations over the North Atlantic, *Environ. Sci. Technol.*, *44*(22), 8574-8580.

Srivastava, R. C. (2003), Guidance and awareness raising materials under new UNEP mercury programs (Indian scenario), edited by C. f. E. P. M. a. Mitigation, Lucknow, India.

Steinberg, N., et al. (2004), Health of the harbor: The first comprehensive look at the state of the NY/NJ Harbor Estuary, *Rep.*, 22 pp, Hudson River Foundation, New York, NY.

Streets, D. G., et al. (2011), All-time releases of mercury to the atmosphere from human activities, *Environ. Sci. Technol.*, *45*(24), 10485-10491.

Sunderland, E. M., and R. P. Mason (2007), Human impacts on open ocean mercury concentrations, *Global Biogeochem. Cycles*, *21*(4), GB4022.

Sunderland, E. M., et al. (2012), Mercury sources and fate in the Gulf of Maine, *Environ. Res.*, *119*, 27-41.

Tong, Y. D., et al. (2013), Behavior of mercury in an urban river and its accumulation in aquatic plants, *Environ. Earth Sci.*, *68*(4), 1089-1097.

Turner, R. R., and S. E. Lindberg (1978), Behavior and transport of mercury in river-reservoir system downstream of inactive chloralkali plant, *Environ. Sci. Technol.*, *12*(8), 918-923.

Varekamp, J. C., et al. (2003), Mercury contamination chronologies from Connecticut wetlands and Long Island Sound sediments, *Environ. Geol.*, *43*(3), 268-282.

Wang, F. Y., et al. (2012), Total and methylated mercury in the Beaufort Sea: The role of local and recent organic remineralization, *Environ. Sci. Technol.*, *46*(21), 11821-11828.

Woitke, P., et al. (2003), Analysis and assessment of heavy metal pollution in suspended solids and sediments of the River Danube, *Chemosphere*, *51*(8), 633-642.

Yi, Y. J., et al. (2011), Ecological risk assessment of heavy metals in sediment and human health risk assessment of heavy metals in fishes in the middle and lower reaches of the yangtze river basin, *Environ. Pollut.*, *159*(10), 2575-2585.

Zelewski, L. M., et al. (2001), Mercury dynamics in Tivoli South Bay, a freshwater tidal mudflat wetland in the Hudson River, *Biogeochemistry*, *52*(1), 93-112.

Zhang, Z. S., et al. (2010), Recovery from mercury contamination in the Second Songhua River, China, *Water Air Soil Pollut.*, *211*(1-4), 219-229.

Zhu, H., et al. (2012), Risk assessment for methylmercury in fish from the Songhua River, China: 30 years after mercury-containing wastewater outfalls were eliminated, *Environ. Monit. Assess.*, *184*(1), 77-88.